Dissertation

submitted to the

Combined Faculty of Natural Sciences and Mathematics

of the Ruperto Carola University Heidelberg, Germany

for the degree of

Doctor of Natural Sciences

Presented by

Ranjith Viswanathan, M.S.

born in Wrexham (U.K.)

Oral examination: 26th November 2019

Optogenetic modulation of Delta reveals the role of Notch signalling dynamics during tissue differentiation

Referees: Dr. Alexander Aulehla

Prof. Dr. Ingrid Lohmann

Summary

Spatio-temporal regulation of signalling pathways plays an important role in generating diverse responses during the development of multicellular organisms. While increasing number studies are uncovering the importance of signalling dynamics in controlling tissue patterning and morphogenesis, the precise role of signal dynamics in transferring information *in vivo* is incompletely understood owing to the lack of methods to manipulate protein activity at the relevant spatio-temporal scales. In this PhD thesis, I employ genome engineering in *Drosophila melanogaster* to generate a functional optogenetic allele of the Notch ligand Delta (opto-Delta), at its endogenous locus. Light mediated activation of opto-Delta disrupts Notch signalling during different developmental stages. Using clonal analysis, I show that optogenetic activation blocks Notch activation through *cis*-inhibition in signal-receiving cells. To investigate how a Notch input is dynamically translated into a differentiation output, I focused on mesectoderm specification during early *Drosophila* embryogenesis. Signal perturbation in combination with quantitative analysis of a live transcriptional reporter of Notch pathway activity reveals different modes of regulation at the tissue and cellular level. While at the tissue-level the duration of Notch signalling determines the probability with which a cellular response will occur, in individual cells Notch activation needs to reach a minimum threshold to generate a response. Taken together these results provide novel insights into the dynamic input-output regulation of Notch signalling, supporting a model in which the Notch receptor is an integrator of (noisy) analog signals that generates a digital switch-like behaviour at the level of target gene expression during tissue differentiation.

In order to further test this model, I attempted to develop an optogenetic system to activate Notch *in vivo* (opto-Notch). Despite showing light-responsive changes in localization, a certain level of Notch is activated even prior to photo-activation, thus necessitating further optimization. Finally, I describe efforts for further characterization of opto-Delta as a tool to spatially perturb signalling, to study Notch signalling during neuroblast delamination, and for adaptation to mammalian cell-culture systems.

Zusammenfassung

Die räumlich-zeitliche Regulation von Signalwegen spielt eine wichtige Rolle bei der Erzeugung unterschiedlicher Zellantworten während der Entwicklung mehrzelliger Organismen. Die Bedeutung des dynamischen Verlaufs von Signalübertragungen für die Steuerung der Musterbildung in Geweben und der Morphogenese allgemein wird durch viele Forschungsstudien belegt; wobei die genaue Rolle der Signaldynamiken für die Informationsübertragung *in vivo* nur unvollständig verstanden ist. Grund dafür ist das Fehlen von Methoden zur Manipulation der Proteinaktivität auf den relevanten räumlich-zeitlichen Skalen. In dieser Doktorarbeit nutze ich Verfahren der Genom-Editierung von *Drosophila melanogaster*, um ein funktionelles optogenetisches Allel des Notch-Liganden Delta (Opto-Delta) auf endogener Ebene zu erzeugen. Die Licht-abhängige Aktivierung von Opto-Delta ermöglicht es den Notch-Signalweg in verschiedenen Entwicklungsstadien zu unterbrechen. Mithilfe klonarer Analysen zeige ich, dass die optogenetische Stimulierung von Opto-Delta die Induktion von Notch durch cis-Inhibition in signalempfangenden Zellen blockiert. Um zu untersuchen, wie Notch-Signalinput dynamisch in eine Differenzierungsausgabe übersetzt wird, habe ich mich auf die Spezifikation des Mesektoderms während der frühen *Drosophila*-Embryogenese konzentriert. Die Licht-induzierte Inhibition des Notch-Signalwegs in Kombination mit einer quantitativen Analyse der Signalaktivität eines Live-Transkriptionsreporters brachte verschiedene Regulationsmodi auf Gewebe- und Zellebene zum Vorschein. Während auf der Ebene des Gewebes die Dauer des Notch-Signalinputs die Wahrscheinlichkeit bestimmt, mit der eine zelluläre Antwort auftritt, muss die Notch-Aktivierung in einzelnen Zellen einen Mindestschwellenwert erreichen, um eine Antwort zu generieren. Zusammengenommen unterstützen diese

Ergebnisse zur dynamischen Input-Output-Regulation von Notch-Signalen ein Modell, in dem der Notch-Rezeptor ein Integrator von (verrauschten) analogen Signalen ist, der ein digitales, schalterartiges Verhalten auf der Ebene der Zielgenexpression während der Gewebedifferenzierung bewirkt.

Um dieses Modell weiter zu untersuchen, habe ich versucht, ein optogenetisches System zur Aktivierung von Notch (Opto-Notch) *in vivo* zu entwickeln. Obwohl Licht-abhängige Änderungen der Proteinlokalisation beobachtet wurden, scheint bereits vor der Lichtaktivierung eine bestimmte Menge von Opto-Notch aktiv zu sein, was weitere Optimierungsschritte der Methode erforderlich macht. Abschließend beschreibe ich die Bemühungen zur weiteren Charakterisierung von Opto-Delta als Instrument zur räumlichen Inhibierung der Notch-Signalübertragung während der Delaminierung von Neuroblasten und zur Adaptierung des Systems in Säugetierzellkultursystemen.

Contents

List of figures

Abbreviations

aa = Amino acid

ADAM = A Disintegrin and Metalloproteinase

AP = Anterior-posterior

APF = After puparium formation

CIB1 = Cryptochrome interacting basic-helix-loop-helix 1

CIBN = N-terminus of CIB1 (aa 1-170)

CNS = Central nervous system

CRY2 = Cryptochrome 2

CSL = CBF1, Suppressor of Hairless, Lag-1

DLL1/4 = Delta like-1/4

Dpp = Decapentaplegic

DV = Dorsal-ventral

EDTA = Ethylene-diamine-tetra-acetate

EGF = Epidermal growth factor

ERK = Extracellular signal regulated kinase

E(Spl) = Enhancer of split

FGF = Fibroblast growth factor

FISH = Fluorescent in-situ hybridization

FRAP = Fluorescence recovery after photobleaching

FRET = Fluorescence/ Förster resonance energy transfer

GAP43 = Growth associated protein 43

GFP = Green fluorescent protein

Hh = Hedgehog

LOV = Light-oxygen-voltage sensing (domain)

LOVTRAP = LOV2 trap and release of protein

Mam = Mastermind

MAPK = Mitogen-activated-protein-kinase

MCP = MS2 coat protein

MZT = Maternal to zygotic transition

NECD = Notch extracellular domain

Neur = Neuralized

NICD = Notch intracellular domain

NLS = Nuclear localization sequence

PCR = Polymerase chain reaction

RFP = Red fluorescent protein

Shh = Sonic Hedgehog

Sim = Single-minded

SOP = Sensory organ precursor

Su(H) = Suppressor of Hairless

TGF-β = Transforming growth factor - β

YFP = Yellow fluorescent protein

Zdk = Zdark

1. **Introduction**

Overview

An organism's ability to respond to stimuli is one of the key facets to its classification as "living". Physical stimuli like light or gravity, and chemical molecules in the environment are sensed, and this information is processed by the organism to maintain its dynamic equilibrium, or homeostasis. The ability to manipulate and track living systems at the micron scale has made us understand that in fact, every cell that makes up an organism acts as an information processing system, interpreting signals arising within themselves or from other cells in the organism. This communication forms the fundamental basis of defining and altering the functional state of the cell and importantly, co-ordinating these decisions in both space and time at the tissue, organ and organism level.

It is the same co-ordination that plays a pioneering role during the course of development of multicellular organisms. **Embryonic development** describes the fascinating process of how the entire complexity of an organism is carved out from a single cell, the fertilized egg. The sequence of events that leads to a uniform ball of cells resulting from zygotic cleavages diversify and pattern into the various kinds of tissues that comprise the adult, has intrigued developmental biologists over the past century. **Morphogenesis** is the term used to broadly describe this process during embryonic development by which cells, tissues and organs are shaped. This encompasses the interplay of various dynamic biological processes including tissue patterning, cell-cell interactions, cell shape changes and cell migration.

Landmark experiments, beginning with simple tissue transplantations to large scale genetic screens in model organisms have been carried out to understand the

principles and identify the factors driving morphogenesis. This has led to the identification of a number of key genes that have been characterised over the years as signalling molecules, belonging to a specific set of signal transduction pathways that are largely conserved across organisms. These signalling pathways that govern and coordinate collective decisions during morphogenesis, require reproducible precise, yet robust communication between cells. In contrast to homeostasis, where signalling pathways play the role of adjusting the state of a cell after measuring the surroundings, during development “they are usually irreversible, pushing forward the developmental program in a ratchet-like mechanism” (Perrimon et al., 2012).

Information processing by cells during development usually culminates in the turning on of a gene expression program through the activity of transcription factors that are downstream of signalling pathways. This determines the fate of the cell that needs to be manifested in the right group of cells within a specific developmental timeframe. Several studies have uncovered the importance of regulation of signalling pathways in space and time in order to accomplish this.

What properties of a signal are cells able to sense and respond to? Do cells “comprehend” absolute levels of signals alone or do they respond to signals that are changing in time? How these dynamics are interpreted to co-ordinate cell fate changes at the cell and tissue level during development is incompletely understood.

In my PhD thesis I have focused on the Notch signalling pathway as a system to investigate signalling dynamics *in vivo*. First, I will discuss recent examples of signalling pathways employing dynamics to pattern tissues *in vivo*, and bring out the need to understand this in the context of Notch, using *Drosophila Melanogaster* embryogenesis as a model system. Next, I will introduce new tools that have made it possible to precisely manipulate and record signalling activities *in vivo*.

1.1 Cell-cell communication as the driving force of development

1.1.1 Concepts

Early in development, cells need information about their positional context with respect to their neighbours in a tissue. A Morphogen is a molecule that can diffuse across a tissue and determine cell fate in a concentration dependent manner. Morphogens are normally produced as a gradient across tissues and can differentiate responding cells into different categories.

Induction refers to the process by which one group of cells changes the properties of a neighbouring group of cells. This phenomenon was first discovered by Hans Spemann and Hilde Mangold in amphibian embryos. When they transplanted a piece of tissue from the dorsal lip region of newt gastrulas to a different region of another gastrula, this tissue not only autonomously maintained its fate but also sequentially induced the fates of the surrounding tissues based on their position. This tissue was named the organizer due to its ability to establish early-on the anterior-posterior (AP) and dorsal-ventral (DV) axes.

This discovery of the inducer led to excitement, trying to purify potential factors secreted by it (from embryonic extracts) that determined the development of the neighbours. However, this was challenging owing to the limitations in experimental techniques at that time.

“Responder” refers to the tissue that is being influenced, and in order to respond, they need to have receptors for the factors secreted from the neighbouring tissue and all the other necessary components in order to activate the pathway. This is called competence.

The type of inducing signal can determine the properties of the responder. Recombining a single kind of epithelial tissue from the chick embryo with different kinds of mesenchymal tissues, Saunders et al. (1957) discovered that the type of structures made by the epithelium, whether feathers or claws, is determined by the region from which the underlying mesenchyme was derived. On the other hand, the identity of the responding tissue can determine how the incoming signal is interpreted. Transplantation of ectoderm regions between newt and frog embryos resulted in the newt developing frog structures and vice versa proving that the genetic make-up of the transplanted ectodermal tissue determines how the inducing signal from the underlying tissue will be manifested. (Spemann and Schotte 1932).

1.1.2 Genetic screens to identify signalling components

In the latter half of the 20th century, the ability to investigate embryonic development from a molecular standpoint revolutionized the field, and gave rise to the identification and characterization of these morphogens. Particularly, the escalation of genetics gave rise to tools to access and manipulate the genome in model systems (Brenner, 1974), *Drosophila melanogaster in primis*. *Drosophila* made it possible to apply genetics to the understanding of development. Indeed, large scale mutagenesis screens enabled the identification of several cell signalling molecules. The most significant of these screens was the Heidelberg mutagenesis screen done in 1979-80 by Eric Wieschaus and Christiane Nusslein-Volhard (Nüsslein-volhard and Wieschaus, 1980). 600 mutants that influenced the embryonic cuticle structure and pattern were identified and could be mapped back to 120 genes. Most of these genes were later characterized as key signalling regulators or transcription factors whose functions were largely conserved among different organisms, until humans. Several

key signalling components were identified from this screen and many subsequent studies have filled in the missing gaps.

1.1.3 Common modes of signalling during development

Over the course of evolution, organisms have opted for signalling pathways that function over a short range to drive developmental patterning and morphogenesis.

Paracrine Signalling

The paracrine class of signalling molecules refer to ligands that are secreted by a cell, or group of cells into the extracellular matrix and can diffuse over a diameter of several cells. The range of diffusion of these molecules generally determines their range of signalling. Binding of these factors to the receptor activates a signal transduction cascade resulting in the modulation of transcription factors or cytoskeletal elements. Common and well characterized examples of this class of signalling molecules include the Fibroblast growth factor (FGF), Hedgehog (Hh), Wnt, and the Transforming growth factor (TGF-β) superfamily. Studies on these pathways have uncovered their roles in various processes during development, a few of which I will very briefly mention below.

FGF is a paracrine factor important in various contexts of morphogenesis like vertebrate limb development and branching of trachea in *Drosophila* (Crossley et al., 1996; Sutherland et al., 1996).

The **TGF- β** family of extracellular signalling molecules include TGF- β, Nodal, Bone Morphogenetic protein (BMP) and play an important role in regulating extracellular matrix (ECM) formation. TGF- β molecules in particular regulate cell proliferation, Nodal determines left and right body axes and BMPs induce mesenchymal cell transformation into bone (Hirokawa et al., 2006; Hogan, 1996; Zhang et al., 2017).

Hh is another important secreted molecule important in the creation of tissue boundaries. It has been best studied during Anterior-Posterior boundary formation in the *Drosophila* wing disc. In vertebrates, Hh patterns the developing neural tube and defines limb digits (Dessaud et al., 2008; Riddle et al., 1993; Strigini and Cohen, 1997). **Wnt** was originally identified in *Drosophila* as Wingless (Wg) and broadly functions as an extracellular growth factor that influences cell proliferation. In the early amphibian embryo, Wnt plays a major role in determining AP and DV axes polarity (Kiecker and Niehrs, 2001).

Juxtacrine signalling

This mode of signalling involves ligands and receptors that are both cell surface bound, thus further reducing the spatial range of signalling when compared to Paracrine factors. Juxtacrine signalling depends on direct cell-cell contact and usually occurs between immediate neighbouring cells, although there is increasing evidence for the role of cellular protrusions or filopodia to mediate longer range signalling.

However, the most commonly occurring juxtacrine pathway across different organisms is the **Notch-Delta** signalling pathway. The principles and mechanisms that this pathway uses will be elaborated in section 1.3.

Besides Notch, the **Ephrin** family of receptors and ligands comprise a juxtacrine pathway that plays a role in cell-cell adhesion and boundary formation (Arvanitis and Davy, 2008). **Semaphorins** are another class of membrane associated ligands that bind to the transmembrane Plexin receptors and provide cues for cell migration and growing axons (Jongbloets and Jeroen Pasterkamp, 2014).

1.2 Dynamics in signalling pathways

Signalling pathways are relatively limited in number and yet they control many diverse processes. While this serves to be an energetically efficient strategy for organisms, how is this “multi-tasking” accomplished?

One solution, as mentioned previously in the case of morphogens, is that cells can sense the concentration of molecules and provide a concentration dependent response. The second way is to respond in a context dependent or combinatorial fashion i.e. the interaction between different signalling pathways or a signalling pathway and a pre-existing factor produce a distinct output from the individual outputs. A third possibility is that rather than just sensing the presence or absence of a signalling input, information can be carried in the form of the dynamic properties of the signal - amplitude, delay, duration, rate of increase decrease or frequency (Fig. 1). With emerging tools and techniques to study developmental processes at a higher spatial and temporal resolutions, it has emerged that dynamic regulation of signalling pathways is a key strategy used by multicellular organisms to generate diverse responses during embryonic patterning, growth, and differentiation (Purvis and Lahav, 2013; Sagner and Briscoe, 2017; Sonnen and Aulehla, 2014).

Below, I will describe different dynamic properties of signals with examples depicting the underlying principles by which cells and tissues process information to give rise to distinct outputs.

1.2.1 Signal amplitude

I will first discuss the different ways by which cells can respond to increasing amplitude (quantity) of signal with time.

Graded response

A Linear or graded signal response is when a cell responds proportionally to the level of input signal increasing in time. In such pathways, the increase in the concentration of receptor or ligand is translated directly into an increase in target gene activation. This is seen in the case of Smad response to gradual increase of activated Activin receptors in the *Xenopus* blastula (Shimizu and Gurdon, 1999), and for Decapentaplegic (Dpp), where its gradient is translated into a gradient of its target pMad in the nucleus (Bollenbach et al., 2008). In such cases, the transfer of information from plasma membrane to nucleus is generally linear without any amplification. A potential downside of linear pathways is that they are very susceptible to noise or random change in concentrations, especially if cells are competent at all times to activate the pathway and depend only on optimal ligand-receptor interactions.

Threshold generation

An alternate method used by signalling pathways is to convert a graded input to an all-or-none or switch like output. In such pathways, the input signal would need to overcome a minimum threshold to generate an output. Mechanistically, such non-linear responses are commonly the manifestation of having either a positive feedback or ultra-sensitivity; where at the threshold level, very small changes in input-signal concentration can result in step changes in activity (Sagner and Briscoe, 2017). In the process of patterning the ventral ectoderm in the *Drosophila* embryo, a gradient of MAPK (Mitogen-activated-protein–kinase) activity is transformed into a sharp switch like response with regards to the degradation of the transcription factor Yan. The phosphorylation-dependent degradation of Yan is balanced by a constant rate of de-phosphorylation, leading to an ultrasensitive system being established (Melen et al.,

2005). In general, step wise digital outputs are more robust to random fluctuations as compared to graded responses.

Fold change

In addition to absolute levels, also fold change in input-signals can be read by cells. This has been observed in the *Drosophila* wing disc, where Dpp gradients are created and control both cell patterning and proliferation in the tissue (Wartlick et al., 2011). Despite this gradient, the proliferation across the disc is homogenous. This is achieved due to the fact that both the concentration and distance over which Dpp spreads, scales with the size of the tissue as it grows (Fig. 2A). Thus the entire gradient is increasing over time across the tissue and therefore at an individual cell level, each cell experiences an increase of Dpp; sensing this increase (by min of 50%) determines the decision to divide.

1.2.2 Signal Duration

Here I will discuss studies that bring out the importance of signal duration determining cell fate, especially in the case of several morphogens where concentration alone was originally thought to be sufficient to generate a response.

In cell culture, a distinct set of genes activated by short duration of ERK (Extracellular signal-regulated kinase) signalling of around 20 min. and a longer duration of 120 min was identified (Toettcher et al., 2013). While the genes expressed from a 20 min. activation are direct ERK targets, the targets post 120 min. are downstream of the JAK-STAT pathway and represent secondary targets of phosphorylated ERK primary targets.

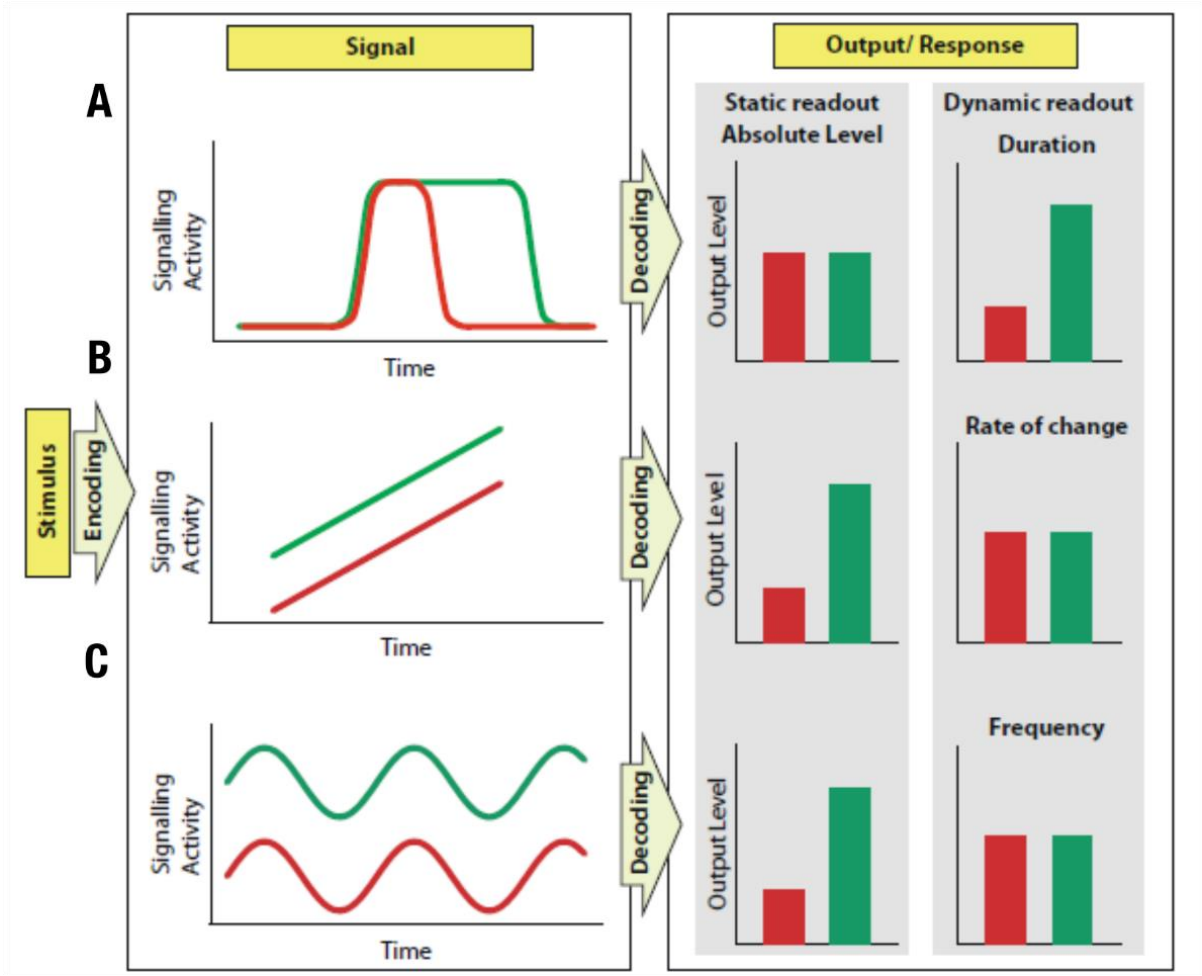

Figure 1: Encoding and decoding of signalling dynamics

(A-C) Examples of dynamic modes of signal delivery and corresponding interpretation by systems responding to either absolute levels (system-1), or dynamic properties of the signal (system-2). When the duration of the signal is varied, keeping the amplitude constant, system-1 produces an identical output, while system-2, where duration determines the output, produces a different response **(A)**. If the slope/ rate of change of signal is constant over time, but the absolute levels are different, system-1 manifests a differential output, while system-2 that interprets the rate of signal delivery "reacts" in the same fashion **(B)**. If the frequency of an oscillating signal is unchanged, but the amplitudes are different, system-1 again decodes the input differentially, while system-2 where frequency is important for output, does not distinguish between both signals **(C)**. Figure adapted with permissions from (Sonnen and Aulehla, 2014) (see Appendix)

While in many contexts, cells respond as long as the signal lasts, in other cases, negative feedback gives rise to a response that is shorter than the stimulus. This is called **adaptation**. In *Xenopus* animal caps it was observed that despite continuous activation of the TGF- β pathway, the transcription factor Smad 4 exhibited transient bursts of nuclear translocation (Warmflash et al., 2012) (Fig. 2B). Experiments in myoblasts cells showed that this kind of adaptive response depends critically on the rate at which ligand concentration changes. Steadily changing the concentration of ligand over an extended period of time results in a diminished effect of signalling, while a rapid increase of ligand concentration over short bursts displays an additive effect in signalling, serving to overcome adaptation (Sorre et al., 2014).

In the developing vertebrate spinal cord, the neural tube DV patterning is determined by the Sonic-hedgehog (Shh) morphogen. Initially all cells are equally sensitive to Shh, but over time, due to adaptation, cells are desensitized and hence continuously increasing Shh levels are required to overcome this. Cells closer to the source of signal do receive higher level of signal, and as a result the duration of signalling is also increased in these cells (Balaskas et al., 2012).

1.2.3 Signal frequency

Frequency of signals can also be used to encode information, as in the case of the MAPK pathway, where inducing ERK activation at different frequencies (ranging from 4 min to 2hr) strongly correlated with the proliferation rate of cells (Toettcher et al., 2013).

Input signals can also exhibit periodic activity, as in the case of **oscillatory** signals. In such cases, both the frequency and period of oscillations can be used to encode information. In cell culture, the degree of DNA damage (double-stranded breaks) is

encoded in the number of p53 oscillations. This information is essential for the cell to make a decision between cell cycle arrest and death (Batchelor et al., 2008).

During mouse embryonic development, the patterning of somites is determined by oscillatory signals involving the Notch, FGF and Wnt pathways (Fig. 2C). The time period of the oscillatory gene expression of these signalling targets determines when the next somite will form, and the Notch pathway plays an important role in synchronising these oscillations (Sonnen et al., 2018).

In conclusion, the examples discussed above demonstrate that signalling dynamics plays an important instructive role in creating complex patterns. These dynamics also serve to increase the precision and robustness of developmental processes in order to minimize abnormalities.

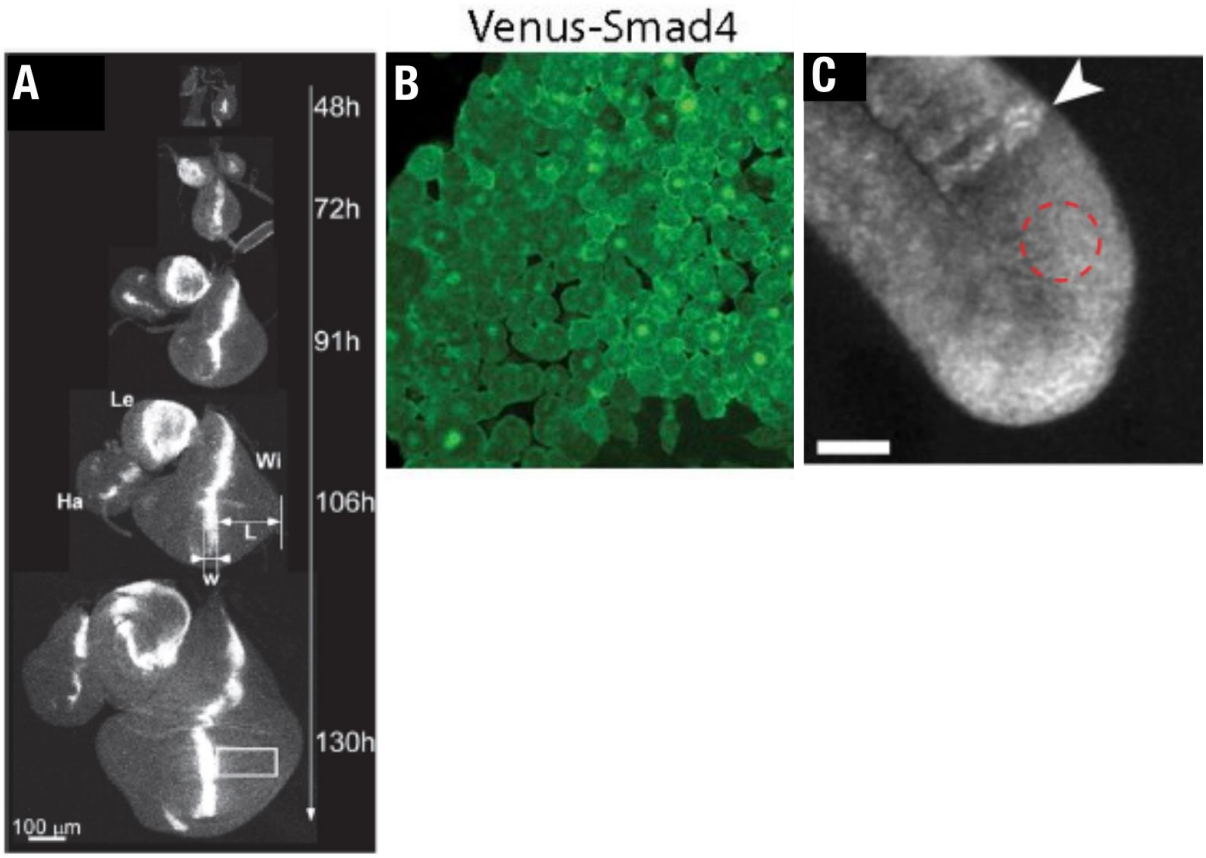

Figure 2: Examples of signalling dynamics during development

(A) Snapshots of Wing (Wi), leg (Le), and haltere (Ha) discs from *Drosophila* larvae during the time-course of their growth, expressing fluorescently tagged Dpp (Dpp-GFP). Bright regions represent the source of the Dpp signal that diffuses over the entire disc. The gradient of Dpp scales with the size of the discs, resulting in homogenous growth.
(B) Animal cap explant from a *Xenopus* embryo injected with Venus-Smad4 mRNA, showing heterogenous nuclear localization of Smad-4 protein (downstream of TGF- β signalling). Following single cells over time, a pulsatile mode of Smad-4 nuclear localization was observed, further investigation suggesting that this could be necessary in order to overcome adaptation.
(C) Mouse pre-somitic mesoderm (PSM) expressing a readout of Wnt signalling (Axin2). Oscillations of Notch, Wnt and FGF signalling collectively give rise to the segmentation of the mesoderm.
Figure panels **(D)**, **(E)** and **(F)** adapted with permission from (Wartlick et al., 2011) (see Appendix), (Warmflash et al., 2012) and (Sonnen et al., 2018) respectively.

1.3 Notch signalling

In this thesis, I will further explore signalling dynamics using the Notch pathway as a paradigm. This section provides an overview of the Notch pathway regulation, and strategies to modulate its activity.

Notch signalling plays a major role in determining cell fate decisions across many metazoan species and regulates fundamental processes ranging from neurogenesis to somite segmentation during development. Notch was first discovered in *Drosophila* following phenotypic observations in embryos that contained certain X-chromosome deficiencies (Poulson, 1937, 1940). Also readily apparent were the haplo-insufficient phenotypes in the adult flies that included the characteristic Notching at the wing margin, thus giving rise to the nomenclature of the protein.

1.3.1 Notch activation mechanism

As mentioned in section 1.1.3, Notch exhibits a juxtacrine mode of signalling, distinctively acting via cell-cell contact and thus providing a mode to transmit short-range signals across cells. Notch is a large transmembrane receptor activated by binding to its ligand Delta on the surface of neighbouring cells. Notch and its ligands are both transmembrane proteins that bind to each other through their extracellular EGF-like repeats (Fig. 3A). In *Drosophila*, there is one Notch receptor and two ligands (Delta and Serrate) that are used depending on the context. In mammals there are at least 4 Notch proteins (Notch 1-4) and 5 ligands - Delta-like (1,3 and 4) and Jagged (1 and 2).

The Notch receptor is synthesized as a precursor which is then processed in the Golgi-apparatus into two subunits – one polypeptide containing the extracellular domain, which is linked to another polypeptide containing both a transmembrane and intracellular domain (S1 cleavage). The general mechanism for the activation of the canonical Notch signalling pathway is as follows: Binding of Notch to its ligand Delta on the adjacent cell surface (in *trans*) results in a conformational change in the Notch structure, inducing two proteolytic events. The first one releases the extracellular domain of Notch and is catalysed by an ADAM metalloprotease which is associated with the plasma membrane (S2 cleavage). The second proteolytic-cleavage is induced by the γ-secretase complex and this leads to the release of the Notch intra-cellular domain (NICD) (Artavanis-Tsakonas et al., 1999; Bray, 2006; Kopan and Ilagan, 2009).

NICD then translocates to the nucleus where it interacts with the DNA binding CSL proteins (Suppressor of Hairless (Su(H)) in case of *Drosophila* /CBF1/LAG1) in combination with coactivators like Mastermind (Mam) to regulate gene expression in

a context-specific manner. The CSL genes were initially identified as repressors, but the binding of NICD switches the activity of the CSL proteins from repressor to activator. Notch targets that have been best studied are the BHLH transcription factors belonging to the HES/HEY family of genes. Of them, the Enhancer of split (E(Spl)) gene complex in *Drosophila* and HES1 in mouse are best known. The several Notch targets mediate processes like proliferation, apoptosis, cell fate, other signalling pathways, cell architecture etc. (Bray and Gomez-Lamarca, 2018).

In addition to ligand-receptor binding, endocytosis of Notch ligands in the signal sending cell (mediated by the E3 Ubiquitin ligase Neuralized/ Mindbomb) is important for this activation event. This results in the *trans*-endocytosis of the Notch extra-cellular domain (NECD) along with Delta in the signal-sending cell (Chitnis, 2006; Le, 2006). Studies in *vitro* have shown that the processing of Notch after binding Delta in *trans* requires a mechanical pulling force that is presumably induced by endocytosis of the Notch bound ligand (Gordon et al., 2015; Luca et al., 2017). Testing the requirement of a mechanical force in vivo has remained challenging; however, recent studies have tested this using chimeric ligand receptor combinations containing a force sensor domain, providing strong evidence for the mechanical force model (Langridge and Struhl, 2017).

From the above mentioned mechanism, potential ways to regulate/manipulate Notch signalling are at the level of ligand-receptor binding, ligand/ receptor trafficking and at the level of NICD nuclear entry regulation.

1.3.2 Modes of Notch functionality

A commonly used mode of patterning by Notch is where the signal-sending cell inhibits its neighbours from adopting a particular fate. This is known as **Lateral inhibition** (Fig.

3B). Lateral inhibition has been best studied in *Drosophila* during neurogenesis, first in the embryonic neurectoderm, and then in the adult Notum during peripheral neurogenesis (sensory bristle development) (Hartenstein and Campos-Ortega, 1984; Heitzler and Simpson, 1991). In both tissues, initially, there are multiple groups of cells that are equipotent for neural differentiation, called proneural clusters. Stochastic variations in Notch and Delta levels, that are further amplified by feedback, biases the directionality of signalling within the cluster. One cell becomes the signal sending cell, and the surrounding cells receive the Notch signal, thus resulting in cells with two distinct fates.

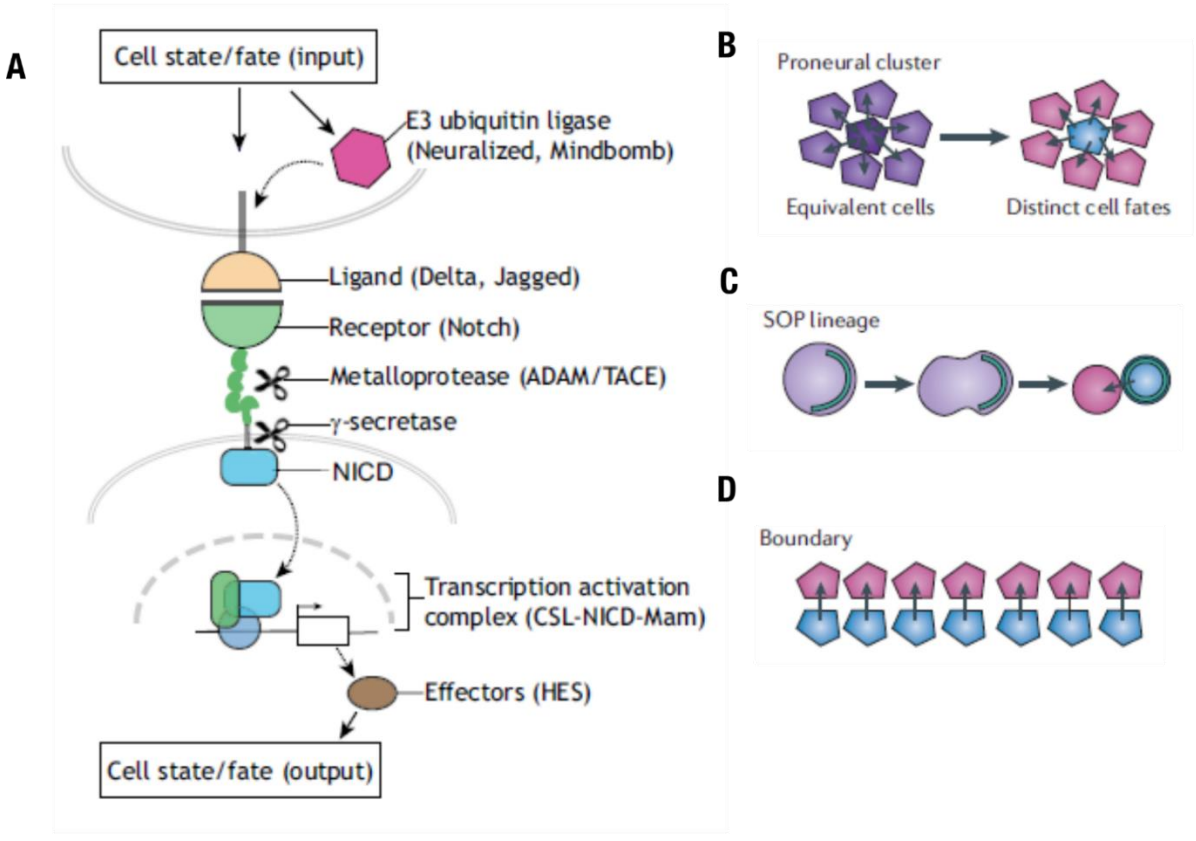

Figure 3: Notch signalling mechanism and modes of activation

(A) Schematic representing the molecular components of the Notch signalling pathway and its mechanism of activation. The signal-sending cell expressing the ligand, Delta (above) and signal-receiving cell expressing the Notch receptor (below) are shown. Activation of

signalling involves (i) binding of Notch and Delta via their extracellular domains and (ii) pulling force induced by the activation of Delta endocytosis (by the E3 ubiquitin ligase Neuralized/ Mindbomb). This induces a series of proteolytic cleavages of Notch – first one induced by the ADAM metalloprotease in its extracellular domain and the second one induced by γ-secretase in the intracellular domain. The resulting cleaved NICD fragment translocates to the nucleus and induces transcription of target genes in cooperation with CSL molecules and Mam coactivators.

(B-D) Modes of Notch functionality in different tissue contexts. Lateral inhibition **(B)** – stochastic differences in Notch and Delta expression in an initially equivalent group of cells results in one cell in the cluster becoming signal-sending and the surrounding receiving the Notch signal, and thereby adopting a differential cell fate. Notch regulating lineage decisions **(C)** – asymmetric divisions of stem cells e.g. SOP cells give rise to differential inheritance of Notch regulatory molecules in the daughter cells, thus influencing the directionality of signalling between them and further determining fate decisions. Notch signalling between two populations of cells **(D)** gives rise to boundary formation between them by inducing a distinct cell-fate at the interface.

Figure panel **(A)** was adapted with permission from (Henrique and Schweisguth, 2019) and panels **(B-D)** were adapted with permission from (Bray, 2006) (see Appendix).

In the neurectoderm, the signal-sending cell becomes the delaminating neuroblast and the other surrounding cells in the cluster that receive the Notch signal remain epithelial cells. In the adult notum, the signal-sending cell becomes the sensory organ precursor (SOP) while the surrounding cells that receive the Notch signal are repressed from SOP fate (by repressing proneural genes like Achate-scute) and become epidermal instead (Heitzler and Simpson, 1991). Notch signalling further plays an instructive role during asymmetric cell divisions (Fig. 3C), activating Notch in one daughter cell and not the other, thus resulting in distinct cell lineages. Both the delaminated neuroblasts and the SOPs undergo Notch dependent asymmetric divisions giving rise to cell lineages of the *Drosophila* CNS and the bristles (Schweisguth, 2015).

The final mode of signalling is instructive in nature (Fig. 3D), where Notch signalling between two cell types that are initially equivalent in nature, gives rise to a third cell

type at the interface. E.g. Mesectoderm specification in the early *Drosophila* embryo (elaborated in section 1.5) and D-V boundary specification in the wing disc (Becam and Milán, 2008).

1.3.3 *Cis*-inhibition

Apart from activation of Notch in *trans* (in the neighbouring cell) as described above, Delta has also been shown to inhibit Notch cell-autonomously in *cis* (Fig. 4). While this phenomenon has been demonstrated across different species from *C.elegans* to mammals (del Álamo et al., 2011; Becam et al., 2010) , it was first identified during D-V boundary formation in the *Drosophila* wing disc (Micchelli et al., 1997). Overexpression and deletion studies have identified Delta to inhibit the processing of Notch in the same cell, and this is dependent on the interaction of their extracellular domains. Changing the relative amounts of Notch and Delta in cell-culture has shown that cells exhibit a sharp threshold switch between receiving/signalling/non-receiving states that can influence the strength and the direction of signalling (Sprinzak et al., 2010). Overall, cis inhibition has been a difficult process to study *in vivo*, as traditional loss of function experiments affects both cis and trans interactions.

Although mechanistically still unclear, inhibition from cis interactions could result from the titration of Notch by competing for the same extracellular *trans*-binding domain, or by actively downregulating Notch, inducing degradation or internalization. The Glycosyl-transferase, Fringe, which is present both in vertebrates and mammals can modulate the *cis*-interaction ability of Notch by post-translational modifications (LeBon et al., 2014). Additionally, in vertebrates, the type of ligand (DLL1/4) can influence the ability to cis inhibit Notch (Franklin et al.; Itoh et al., 2003).

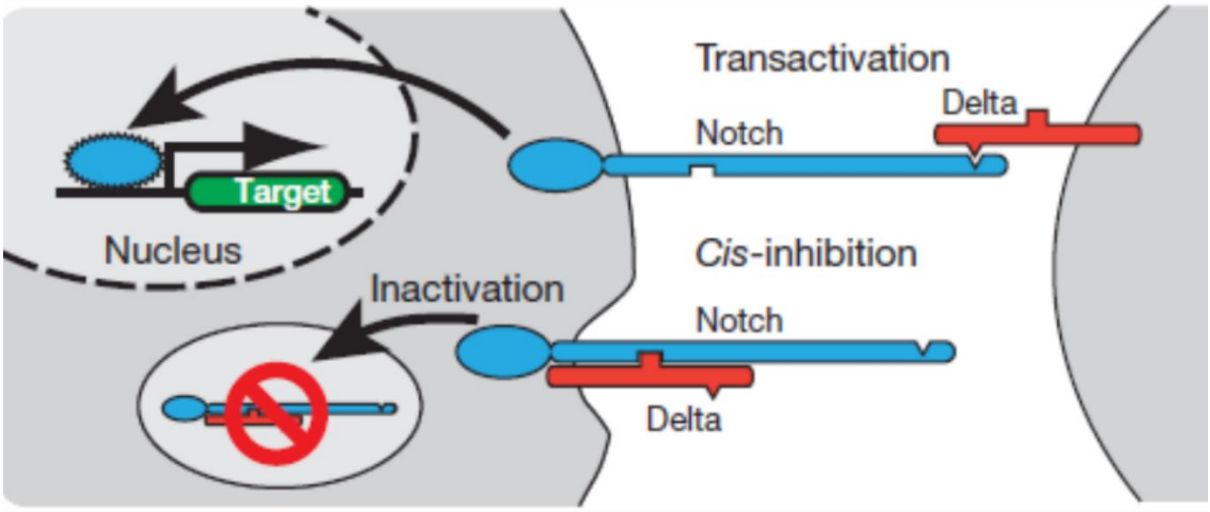

Figure 4: Notch-Delta interactions – *trans* activation and *cis* inhibition

Notch and Delta can undergo productive interactions *in trans* (between neighbouring cells) giving rise to signalling activation, or bind *in cis* (in the same cell) to result in an inhibition of Notch activation in that cell. Figure adapted with permission from (Sprinzak et al., 2010) (see Appendix)

Endogenous *cis*-inhibition has often been found to be associated with lateral inhibition, eg. during *Drosophila* neurogenesis and ommatidium formation in the eye (Miller et al., 2009). Mathematical modelling studies have predicted that *cis*-inhibition could play a role in minimizing errors and compensate for normal feedback dynamics that take longer periods of time (Corson et al., 2017).

1.4 Notch dynamics for activation relatively unexplored

While several studies have focused on the mechanisms controlling Notch activation by ligand endocytosis, knowledge about the activation of Notch targets by cleaved NICD and the dynamics involved remains limited. Lack of signal amplification between Notch intra-cellular domain (NICD) generation and target gene activation, in addition to the fact that the Notch receptor cannot be re-used subsequent to an active signalling event, suggest a direct transfer of information from the plasma membrane to the

nucleus. Moreover, once cleaved, NICD molecules move into the nucleus within few minutes. This has been confirmed by multiple fluorescent tagging techniques to visualise Notch entry in the nucleus, in mammalian cell culture (Ilagan et al., 2011; Kawahashi and Hayashi, 2010) . Using calcium chelation via EDTA as a technique to rapidly induce the proteolytic cleavage that releases NICD, a linear relationship between Notch activation and nuclear entry has been shown. After 20 min., 50 percent of the maximal Notch levels was observed in the nucleus (Kawahashi and Hayashi, 2010). Moreover, in *Drosophila* cell culture, a pulse of 5 min. was sufficient to generate an NICD fragment that co-immunoprecipitated with Su(H) (Housden et al., 2013).

The speed of nuclear entry implies need to study the response on a faster timescale in order to capture immediate transcriptional changes and the regulatory logic of how target genes are turned on. In cell culture, dynamics of Notch signalling was investigated by analyzing genome-wide transcriptional profiles of active genes following a pulse of Notch activation (Housden et al., 2013). The activation of these Notch targets was followed over the course of several minutes. Around 150 genes were differentially expressed upon Notch activation, some showing early upregulation, reaching a peak around 20 minutes, others late upregulation and few being downregulated. In summary, a feed-forward loop in Notch activation was proposed to explain this behavior and reiterates the need to investigate the dynamics of the pathway.

In the *Drosophila* wing disc, using a temperature sensitive Notch allele, preliminary insights could be gained into the dose sensitivity of Notch dependent processes, although the perturbation was in the time-range of 24 to 48 hours, using temperature sensitive alleles. Low levels of Notch were found to be sufficient to maintain the DV boundary, however with regard to Notch target genes activated at the boundary, some

genes had a higher threshold than others (Cut more than Wg) (Becam and Milán, 2008). In human hematopoetic precursor cells, the density of Notch ligands is important in determining fate outcome (Dallas et al., 2005).

In light of these observations, several aspects of Notch signalling remain poorly understood in an endogenous context *in vivo*. Once Notch is cleaved and enters the nucleus, how does it activate gene expression? A quantitative study of the input-output relationship is needed to understand whether dynamically changing levels of Notch or the duration of the signal are important in determining target gene activation. How these dynamics could influence processes at the tissue level, for instance during boundary formation or lateral inhibition is another outstanding question.

1.5 *Drosophila melanogaster* embryogenesis as a model system to study Notch

Drosophila provides an excellent system to study mechanisms governing development due to its fast lifespan, small chromosome number and the wide repertoire of genetic manipulations that can be carried out with relative ease.

As mentioned in the previous section, Notch and Delta were first identified in *Drosophila* from dominant mutations that gave rise to characteristic phenotypes in the adult wing morphology. Embryos that are homozygous deficient for Notch (and/or) Delta do not hatch into larvae. Notch signalling plays a key role in neurogenesis during embryonic development and mutants in any of the upstream activating components in the pathway give rise to neural tissue at expense of ventral epidermis, severely compromising ventral cuticle secretion (Nüsslein-volhard and Wieschaus, 1980; Poulson, 1937).

Notch signalling has been extensively studied in various processes including SOP specification in the pupal Notum (See section 1.3.2), bristle cell-lineage specification (Heitzler and Simpson, 1991), DV boundary formation in the wing disc (Becam and Milán, 2008) and intestinal stem cell differentiation (Ohlstein and Spradling, 2007). In the context of this thesis, I will focus on greater detail on Notch signalling during mesectoderm specification in the early embryo.

1.5.1 Early embryonic development

Upon fertilization of the *Drosophila* egg, the zygote nucleus undergoes several rounds of rapid and synchronous mitotic divisions in a common cytoplasm, resulting in a syncytial blastoderm (Foe and Alberts, 1983). These nuclear divisions are characterized by consecutive S and M phases of the cell cycle, with the absence of a G phase. By the 10^{th} cycle of nuclear division, most of the nuclei migrate to the periphery of the egg and undergo three more division cycles as a syncytium. During the interphase of the following nuclear division cycle (cycle 14), cellularization occurs. Cellularization is the process during which the embryonic cell membrane ingresses between the nuclei at the periphery, resulting in a cellular blastoderm of approximately 6000 cells surrounding a central yolk (Mazumdar and Mazumdar, 2002). Cellularization lasts for approximately 50 minutes at 25 C and occurs in two phases. There is an initial slow phase, during which the cell membrane invaginates between the cortical nuclei and grows inwards in a process mediated by microtubules and actin-filaments. Once the cellularization front reaches the base of the nuclei, the fast phase begins, during which the rate of ingression increases and the actomyosin contractile network organizes into interconnected rings that eventually constrict to form the base of the cells. The end of cellularization coincides with the beginning of gastrulation

movements in the early embryo, when the different germ layers start to be segregated. A series of cell shape changes in the ventral cells eventually results in the invagination of the presumptive mesoderm, creating the ventral furrow (Sweeton et al., 1991).

There are two sets of genes responsible for patterning the embryo - maternal and zygotic. Maternal genes are expressed in the female during oogenesis and form the components of embryonic patterning that are already present in the egg. Zygotic genes are transcribed in the early embryo from cycle 10 onwards.

Cycle 14 is also the stage when Zygotic gene transcription is significantly increased and the maternal mRNAs are concomitantly degraded. This is referred to as the maternal to Zygotic transition (MZT) (De Renzis et al., 2007). The main factors regulating this precisely timed process of MZT are the DNA/Cytoplasm (n/c) ratio, and proteins Smaug and Zelda. While the exact mechanisms by which the embryo measures the n/c ratio are still under investigation, the proteins Smaug and Zelda which are encoded by maternal mRNA, function by degrading maternal mRNAs and activating the zygotic genome respectively (Benoit et al., 2009; Harrison et al., 2011). These zygotic genes determine the spatiotemporal patterning of the blastodermal embryo along both the DV and AP axes. Many of these genes that pattern the *Drosophila* body plan were identified from the Heidelberg mutagenesis screen (Nüsslein-volhard and Wieschaus, 1980) mentioned in section 1.1.2, based on observed phenotypes of cuticle patterning in the embryo and other defects during morphogenesis.

1.5.2 AP patterning

AP polarity is predetermined and initiated by maternal gene transcripts that are localized to different regions of the egg/oocyte, most important of them being, *bicoid* and *nanos* which define anterior and posterior identity respectively. The proteins encoded by these transcripts later activate a series of zygotic genes that determine the formation of different segments along this axis – these are gap genes (eg. Giant, Knirps), pair rule genes (eg. Even-skipped, Hairy), segment polarity genes (eg. Hh, Wg) and homeotic genes (eg. Bithorax, Antennapedia) (van Eeden and St Johnston, 1999).

1.5.3 DV patterning

Many of the genes corresponding to the patterning along the DV axis were identified from early gastrulation defects in embryos. The Dorsal protein which is encoded by maternally deposited mRNAs in the oocyte plays a pioneering role in determining and establishing the DV axis. Dorsal acts as both a morphogen and transcription factor; although deposited everywhere, its nuclear translocation is tightly regulated in a ventral to dorsal gradient by Toll signalling (Reeves and Stathopoulos, 2009). Thus, Dorsal enters the nucleus only in ventral cells to turn on ventral fate determining genes (Fig. 5B), with mutations giving rise to entirely dorsalized phenotype evident from the cuticular exoskeleton.

The concentration of Dorsal in the nucleus determines the fate of cells in the early blastodermal embryo. Consequently, the embryo is divided into the following domains – presumptive mesoderm, mesectoderm, neurectoderm, dorsal ectoderm and amnioserosa. The 16 ventral most cells with the highest dorsal concentration become

the mesoderm that later gives rise to muscles and other internal organs. The zygotic genes Snail and Twist are important targets of Dorsal and specify mesodermal fate and are important for initiating gastrulation movements (Leptin, 1991). Snail mainly acts as a repressor of many ectodermal genes, while Twist activates mesoderm specific genes, and thus act in synchrony. Intermediate nuclear levels of Dorsal in the lateral ectoderm induce genes like Sim and rhomboid that along with other inputs, define the single-cell wide mesectoderm and the adjoining neurectoderm. These target genes are repressed ventrally by Snail. This tissue gives rise to the cells comprising the CNS/ ventral nerve cord and the epidermis that can be identified in the cuticle. Absence of nuclear Dorsal in the dorsal side of the embryo allows the expression of genes such as Dpp and Zen, which enable dorsal fates of cells that give rise to the amnioserosa tissue (Morisato and Anderson, 1995) (Fig. 5A).

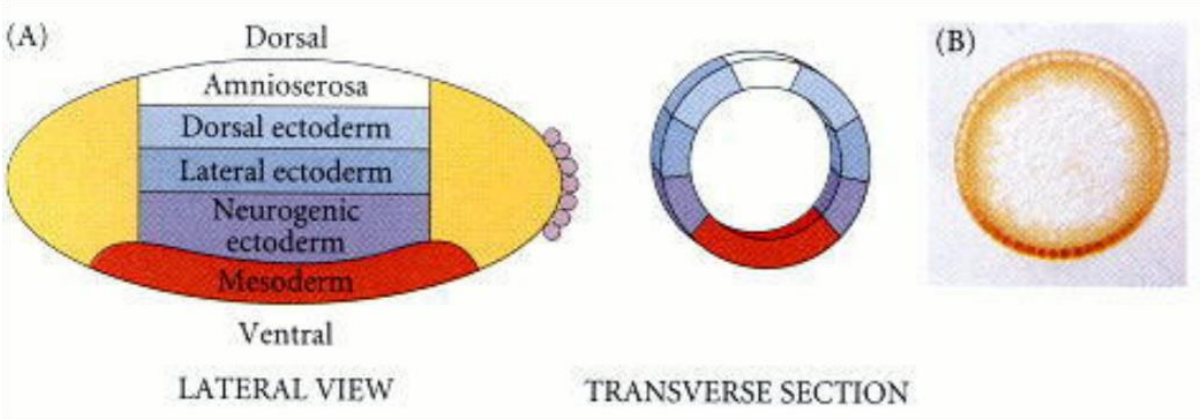

Figure 5: Patterning of the early *Drosophila* embryo along the DV axis

(A) Cell fates along the DV axis in an embryo at nuclear cycle 14. The ventral-most cells receive the highest concentration of the Dorsal protein in the nucleus (antibody-staining in **(B)**) and become the mesoderm. Lateral cells that receive intermediate Dorsal become the neurectoderm, while further Dorsal cells that receive almost no Dorsal activation adopt lateral ectoderm, dorsal ectoderm and amnioserosa fates. Figure adapted from *Gilbert, S.F.,* Developmental Biology. *10th edition.*

1.5.4 Notch signalling during mesectoderm specification

Mesectoderm specification during cellularization provides a convenient system to study Notch signalling owing to the precise onset of its activation and the short duration of signalling (1 hour). In the early embryo, prior to cellularization, Notch and Delta are both maternally encoded and ubiquitously distributed at the plasma membrane. The maternal contribution is thought to be sufficient to perform most of their roles in early embryogenesis (Cowden and Levine, 2002). Notch signalling is important for the activation of mesectodermal genes, specifically of interest in this study is the notch-dependent zygotic transcription of Single-minded (Sim), whose expression is restricted to single cell wide stripes flanking either side of the mesoderm (Cowden and Levine, 2002; Morel and Schweisguth, 2000). Notch signalling is activated right at the beginning of cellularization leading to all the mesectodermal cells expressing *sim* prior to the onset of gastrulation. How is this extremely precise spatial and temporal activation of *sim* achieved?

Zygotic activation of majority of the genes starts at the beginning of cellularization and this provides the opportunity for regulation of signalling and its precise activation. The two zygotic genes, Snail and Neuralized (Neur) play critical roles in activating signalling and positioning Notch activity in single rows of cells. The transcription factor Snail, as mentioned previously, is required for mesoderm specification and its expression is tightly restricted to cells that internalize during ventral-furrow formation. Snail specifies the boundary at which Notch signalling occurs by the following mechanism. First, it autonomously represses Notch targets in the mesoderm. Second, it non-autonomously relieves the Su(H) dependent repression of Sim in the mesectoderm by the activation of Notch (Ip et al., 1992; Morel et al., 2003).

This non-autonomous activation of Notch is achieved indirectly via the activation of another essential zygotic gene, Neur. Neur ecodes a RING E3 ubiquitin ligase that is essential for Delta trafficking. Neur marks Delta for internalization by ubiquitination and targets it to endocytic vesicles starting few minutes after the onset of cellularization. The activity of Neur is strictly restricted to the mesoderm due to the presence of inhibitors (belonging to the Bearded family of proteins) in the ectoderm, which are directly repressed by Snail specifically in the mesoderm (Bardin and Schweisguth, 2006; De Renzis et al., 2006). This results in the mesoderm-specific endocytosis of Delta along with *trans*-endocytosis of the Notch extra cellular domain (NECD), leading to the activation of Notch in the immediately neighbouring cells comprising the mesectoderm (Fig. 6). Previous *in situ* hybridization data has shown that despite Notch activation shortly after the onset of cellularization, *sim transc*ripts are only detected approximately 40 min. into cellularization (Cowden and Levine, 2002; Morel and Schweisguth, 2000). The reason for this delay in *sim* expression is unclear.

Apart from the activation by Notch, both Dorsal and its target gene Twist act as co-acivators of Sim in the mesectoderm – Sim contains both Dorsal and twist binding sites in its 5' regulatory region (Kasai et al., 1998). As both Dorsal and Twist domains extend few cells wider than the mesoderm boundary marked by Snail, in gain-of-function mutants expressing Notch ubiquitously, *sim* expression is extended to a 3-4 cell wide domain flanking the mesoderm (Cowden and Levine, 2002).

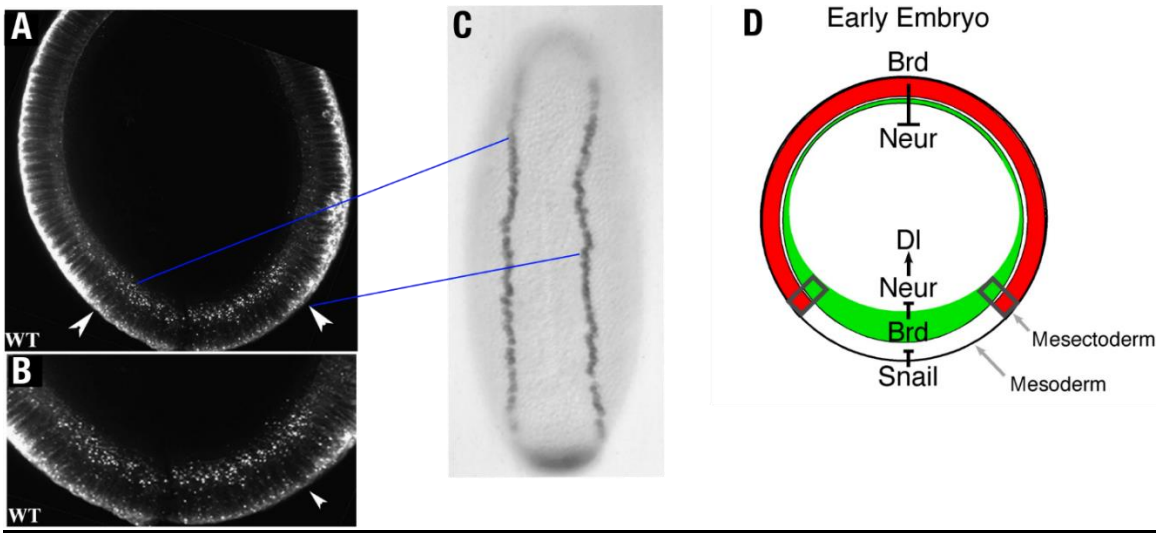

Figure 6: Notch activation in the mesoderm and restriction of *sim* to single-cell wide mesectoderm.

(A-B) Transverse section of an embryo at the end of cellularization and immunostained for Delta, showing polarized trafficking of Delta along the D-V axis (top to bottom). Magnified inset **(B)** showing Delta localized to intracellular vesicles in the mesodermal cells (between the arrows in (A)).

(C) Ventral view of the embryo. Mesoderm restricted trafficking of Delta results in Notch activation in single rows of cells flanking the mesoderm (mesectoderm) and the expression of Notch target-gene *sim*.

(D) Schematic representing the factors influencing the positioning of Notch signalling in the embryo. Neuralized (Neur) that activates Delta endocytosis, is inhibited by the Bearded (Brd) family of proteins in the ectoderm (red). Mesodermal transcription factor Snail relieves this repression, resulting in Delta endocytosis and the precise activation of Notch. *sim* expression is inhibited by Snail in the mesoderm, restricting its expression in response to Notch activation in the mesectoderm.

Figure panels **(A)**, **(B)** were adapted with permission from (De Renzis et al., 2006), panel **(D)** was adapted with permission from (Bardin and Schweisguth, 2006). (see Appendix)

Post gastrulation, both rows of *sim* expressing cells merge together to form the ventral midline cells. Sim encodes a transcription factor that is a key master-regulator of other genes that specify central nervous system (CNS) ventral midline cell fate. These cells later give rise to midline neurons and glia (Kasai et al., 1998).

Apart from Sim, the genes M5 and M8 are other direct targets of Notch in the mesectoderm. These targets belong to the E(Spl) family of genes and encode transcriptional repressors that suppress neurogenesis (Lecourtois and Schweisguth, 1995).

1.6 Tools to manipulate signalling

Signalling pathways can operate over timescales of few seconds to several days depending on the tissue and the organism. Choosing the appropriate time scale for studying processes is essential to capture all dynamic events taking place downstream of signal activation. For example, processes such as ion transport and calcium signalling can take seconds, protein production can take several minutes to hours and changes in cell fate can even take place over several days (Doupé and Perrimon, 2014; Purvis and Lahav, 2013). Recent studies in cell culture have shown that signalling dynamics on the timescale of a few seconds to minutes can be sufficient to generate distinct responses (Toettcher et al., 2013). This necessitates the use of appropriate tools to first manipulate signalling pathways in a dynamic fashion and simultaneous techniques to visualize their immediate activity. Due to limitations in tools to manipulate signals *in vivo* at the relevant spatio-temporal scale, it has been challenging to study the impact of signal dynamics. Much of our current understanding *in vivo* is from studies where signalling has been perturbed over relatively long timescales. Common current methods for signalling pathway activation or inactivation include mutations, knockout or knockdown approaches, and tissue-specific expression tools like the GAL4/UAS system based genetic approaches (Duffy, 2002). While classical mutations work in a black or white fashion, only providing information whether a gene plays a role in a particular process or not, the other mentioned

methods take several minutes or hours to operate making it extremely difficult to identify the exact time-point of activation or inhibition of the pathway.

While temperature-sensitive alleles that exist for several genes in *Drosophila* provide a superior mode of manipulation compared to the above mentioned techniques in terms of specificity, it still occurs over a timescale of several minutes, and does not allow spatial perturbation (López-Schier and St. Johnston, 2001).

Recent methods including microfluidics make it possible to administer chemicals or drugs to cells or tissues in culture in a dynamic fashion (Sonnen et al., 2018). However, this still remains a challenge *in vivo* where potentially invasive techniques like injections are required, in addition to the common challenges of using chemicals, like non-specificity and diffusibility.

1.6.1 Optogenetics as a precise manipulation tool

Optogenetics is a tool combining optics and genetics, that, making use of small protein tags that change their conformation specifically when exposed to light, allows the manipulation of proteins of interest that are fused to them. Optogenetics was initially developed as a tool to control neuronal function by activating or inhibiting photosensitive ion channels and thereby individual neurons (Boyden et al., 2005). Recent studies have successfully applied various optogenetic systems to regulate signal transduction and morphogenetic processes during animal development (Guglielmi et al., 2016; Izquierdo et al., 2018; Johnson et al., 2017; Sako et al., 2016). Light, representing an ideal stimulus that can be manipulated dynamically, provides us with an excellent tool to acutely perturb signalling with sub-cellular specificity and precision on the seconds to minutes scale during development. It allows a tunable

control over protein activity by modulating the frequency or extent of protein interactions/activity by controlling the duration or power of the light input.

This can facilitate the uncovering of dynamic behaviours that were cryptic previously. In non-neuronal contexts, optogenetic systems are generally based on photoreceptor domains that upon a light stimulus undergo dimerization/oligomerization or uncaging. These photosensitive domains have been derived from orthogonal systems like plants or bacteria, enabling their use in animals without interfering with the endogenous protein machinery. Once the appropriate optogenetic tag is fused to the protein-of-interest, light can be used to either change the intracellular-localization, binding partners or oligomerization state of the protein, thus affecting its function.

I will provide an overview of two commonly used photoreceptor proteins/ domains that have been exploited create various optogenetic tools – Cryptochromes (CRY) and the Light-oxygen-voltage-sensing domain (LOV).

Cryptochrome (CRY2)

CRY2 is a photoreceptor derived from *Arabidopsis thaliana* and it responds to wavelengths in the blue region of the visual spectrum. It requires the molecule Flavin adenine dinucleotide (FAD) as a cofactor, which is naturally present in most animals, and upon photoactivation, undergoes photoisomerization. In this activated state, CRY2 can either bind to its partner, CIBN, the N-terminal fragment of the protein CIB1 (Kennedy et al., 2010), or homo-oligomerize with itself (Bugaj et al., 2013) (Fig. 7A, B). The former property is useful to control the localization of a target protein fused with CRY2 by anchoring CIBN at an intracellular location. This has been recently used to synthetically control gastrulation movements in the early *Drosophila* embryo and uncover new principles that were previously unknown (Izquierdo et al., 2018). The use

of two-photon illumination for activating CRY2 has given rise to the possibility of manipulating proteins with sub-cellular precision (Guglielmi et al., 2015).

The homo-oligomerization property of CRY2 is especially enhanced when proteins are already distributed at higher spatial density in the plasma-membrane or in cellular organelles. Positive regulation can be brought about by locally increasing protein concentration, while in other cases, this can result in inhibition sterically blocking protein-protein interactions.

Light-oxygen-voltage-sensing (LOV) domain

The LOV photoreceptor domain is found in a large number of organisms ranging from bacteria to plants. Upon blue light illumination, covalent bond formation between an amino-acid in the LOV core domain and the Flavin cofactor triggers a conformational change resulting in the unfolding of its C-terminal J-alpha helix (Pudasaini et al., 2015). This has been exploited to unmask catalytic domains or signal-peptides conditionally and reversibly upon photoactivation and has resulted in the development of several optogenetic caging/ uncaging systems that result in changing the protein's localization or activity (Niopek et al., 2014a; Wu et al., 2009) (Fig. 7C).

LOV domains have also been exploited to make hetero-dimerizing systems (iLIDs) using which one can tune the binding and dissociation kinetics using different available mutants for the LOV domain (Guntas et al., 2015; Strickland et al., 2012). This tool has been employed to study signalling in vivo (Johnson et al., 2017).

Recently, one of the first optogenetic tools for photoinduced protein dissociation was developed, called LOVTRAP (LOV2 trap and release of protein) (Wang et al., 2016). LOVTRAP has been employed successfully to induce cell edge protrusion and retraction by restricting the access of key signalling molecules to the cell edge.

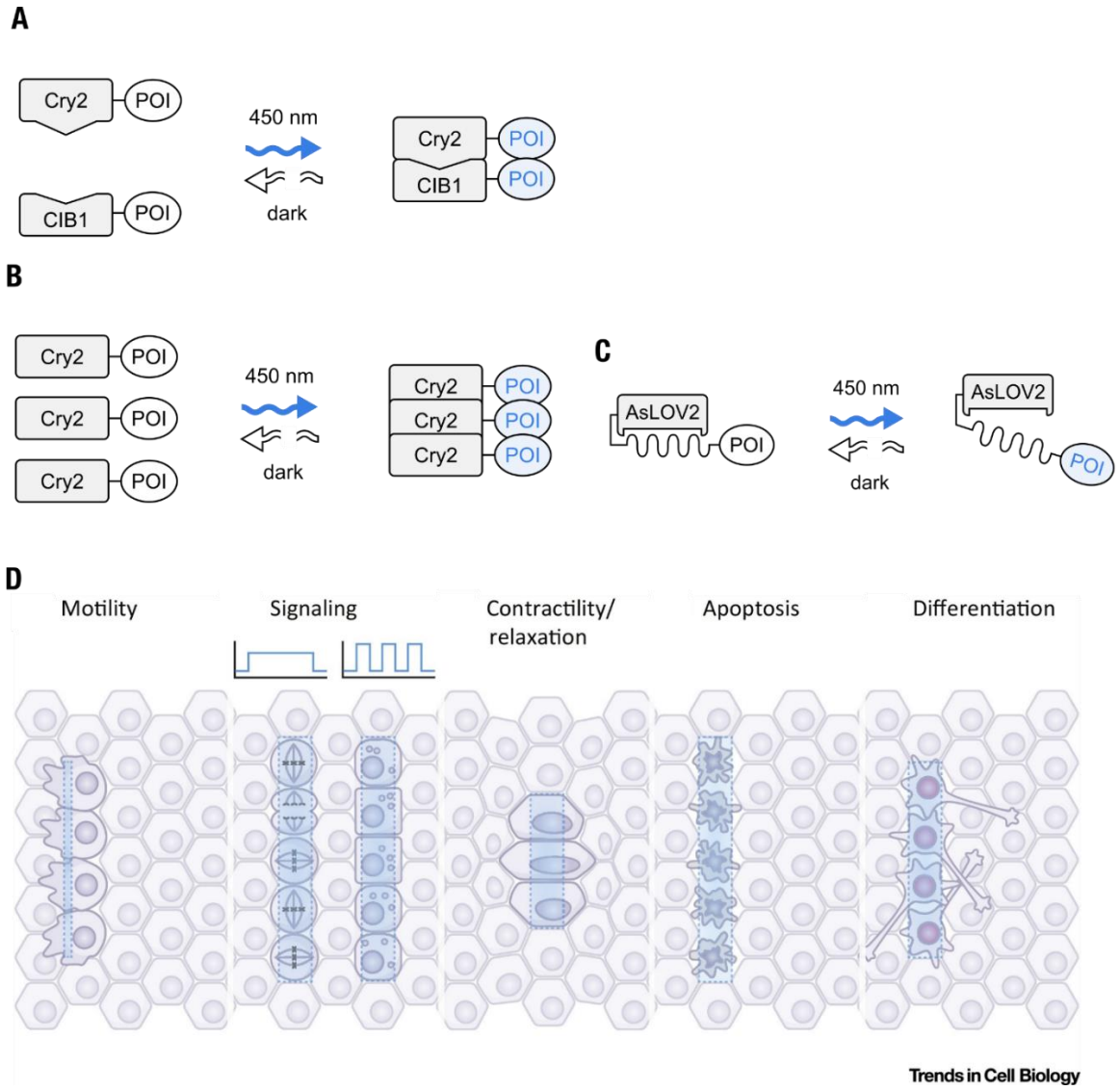

Figure 7: Optogenetic systems and their application to control cellular processes with light

(A) Schematic representing the CRY2-CIB1 heterodimerization system. Two protein interacting partners fused with CRY2 and CIB1 interact upon blue light illumination via CRY2-CIB1 dimerization.

(B) Schematic representing CRY2-CRY2 homo-oligomerization. A protein-of-interest fused to CRY2 can form homomeric clusters as a result of CRY-CRY2 interactions upon photo-activation, especially when expressed alone.

(C) Schematic representing the conformational change of the AsLOV2 domain upon photo-activation. A protein-of-interest fused to the C-terminal J-alpha helix of the LOV2 domain is caged in the dark owing to the closed conformation, and is released upon blue light photo-activation.

(D) Application of optogenetics to control cellular functions by patterned illumination of tissues. Optogenetic activation can be applied to drive behaviours like cell migration,

modulate signalling, induce/inhibit acto-myosin contractions, activate programmed cell death or differentiation, and understand them in a tissue-wide context.
Figure panels **(A-C)** were adapted from https://www.optobase.org/ (Kolar et al., 2018) and panel **(D)** from (Guglielmi et al., 2016).

This tool makes use of two components - the LOV2 light sensor domain from Avena Sativa Phototropin 1 and a small protein called Zdark (Zdk) that is based on the Z domain of the immunoglobulin-binding Staphylococcal protein A. Zdk is able to selectively bind to the dark state of the LOV2 domain. Hence the strategy used was to anchor one of these components at an intracellular location where the protein of interest would not function, and fuse the protein of interest with the other component. In the dark, the protein is sequestered from its region of activity and upon photoactivation with blue light, it is released to its site of action. The fast activation kinetics (few seconds) and reversibility kinetics (< 1 min.) make it a potentially useful tool for in vivo applications.

1.7 Methods to readout dynamic signalling activity

Apart from perturbation tools, there is need for fast and quantitative reporters as a readout of signalling dynamics. Traditional techniques have been to use fluorescent-tagged protein reporters in order to get a quantitative readout or combine them with techniques like FRET. The downside of this technique is the long time period taken for protein-folding and maturation of the fluorophore, whereby primary effects can be missed (Doupé and Perrimon, 2014). The use of destabilised fluorescent reporters of YFP or luciferace was efficient to study dynamics of signalling oscillations in the mouse embryo, however, this compromised the sensitivity (Masamizu et al., 2006).

Tracking transcriptional responses provides possibly the quickest way to monitor downstream signalling activity and delineate immediate responses. While quantitative RT-PCR and RNA seq. techniques have been used to track changes in few minutes scale, in an in vivo context, assigning cell types to these different responses is extremely difficult (Housden et al., 2013). A quantitative measure of immediate transcription within nuclear loci can be provided using Fluorescent-in-situ-hybridization (FISH) coupled with high-resolution imaging (Gaspar and Ephrussi). However, dynamic information is lost, as this technique is for fixed samples.

1.7.1 Live transcription reporters

As an immediate readout for signalling, a fluorescent-based tool for detection of nascent mRNA has been developed, thus serving as a real-time transcriptional reporter.

This system is based on the interaction between a fluorescently MS2 coat protein (MCP) and the phage MS2 stem loops incorporated in the 5' or 3' UTR of the mRNA of interest (Weil et al., 2010) (Fig. 8). MCP-GFP interacts with the nascent MS2 tagged transcripts to produce bright spots of fluorescence in the nuclei. Overall, this enables an immediate recording of transcriptional events in addition to providing a quantitative measure of signalling activity, carrying information about whether the nucleus is actively transcribing and the amount of transcript being produced at that particular instant.

This technique has been previously used in oocytes to study transport of maternal mRNA (Halstead et al., 2015) and recently in many studies to study transcriptional dynamics and enhancer properties especially in the context of the early *Drosophila* embryo (Bothma et al., 2014, 2015).

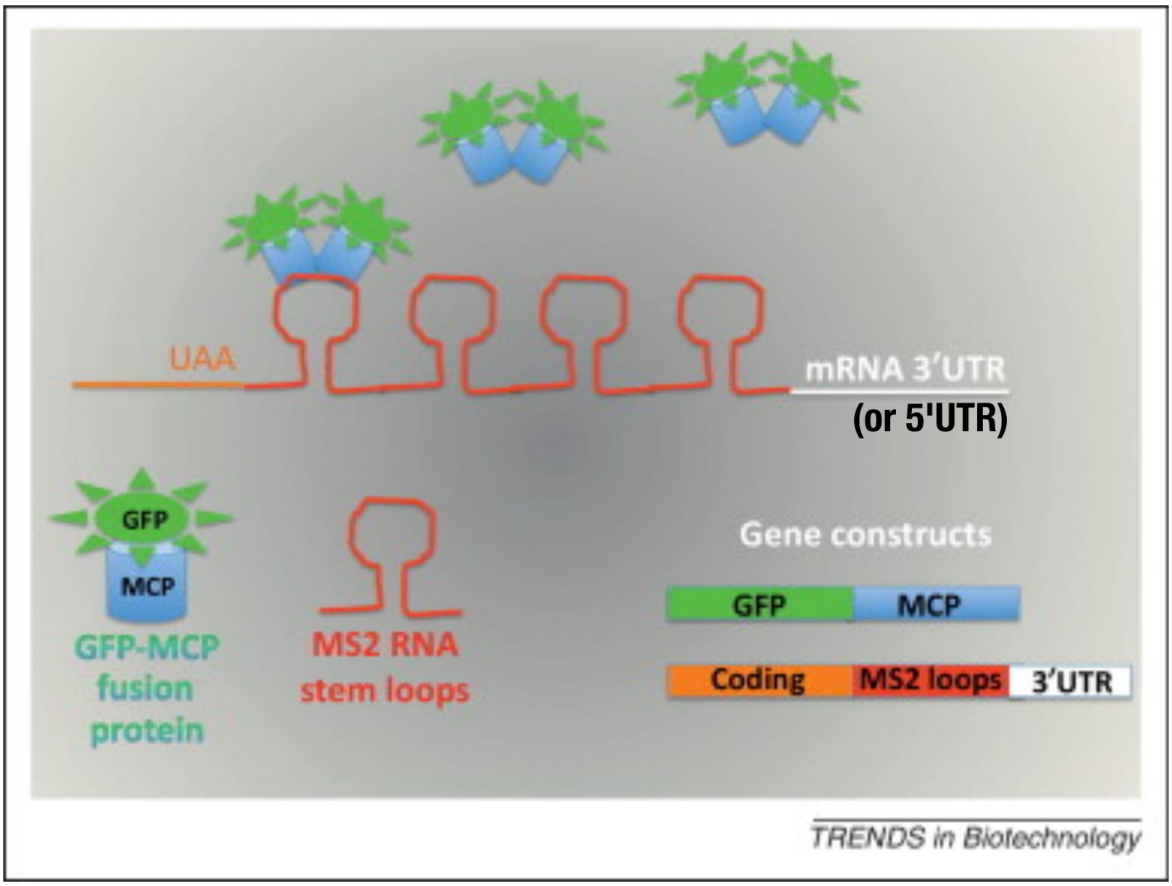

Figure 8: Real time quantitative transcriptional reporter.

Schematic representation of the MCP-MS2 system for visualizing live transcription of mRNA. This system consists of two components – the mRNA to be visualized, tagged with MS2 stem loop repeats at its 5'or 3'end, and fluorescently labelled MCP protein (eg. MCP-GFP) that specifically binds to the MS2 RNA stem loops. This results in the ability to visualize nascent transcripts as bright spots of fluorescence in the nucleus.

Figure adapted with permission from (Dictenberg, 2012) (see Appendix).

2. Aim

Increasing number studies are shedding light on the importance of dynamic regulation of signalling pathways in encoding information to control complex motifs of patterning, growth and morphogenesis during development. Inability to manipulate protein activity with high spatio-temporal precision has made it difficult to study dynamic input-output relationships of signalling pathways. How dynamic information is utilized to interpret and co-ordinate cell fate changes at the cell and tissue level during development is incompletely understood.

In this thesis I describe the experiments I have conducted to study what kind of information is encoded into a dynamic signalling system in *vivo* during organismal development. I have developed tools to manipulate signalling components and track gene expression changes with sub-minute temporal precision and cellular resolution. In particular I focused on activation of the Notch signalling pathway, which is seemingly simplistic with linear transfer of information from the plasma membrane to the nucleus within minutes. I develop real-time, quantitative approaches to perturb endogenous Notch signalling and monitor transcriptional responses of target genes during mesectoderm specification using the early *Drosophila* embryo as a model system. I addressed the following questions: do Notch targets exhibit a linear or threshold response to increasing amounts of signal? Is Notch required in a continuous manner over time or are there specific intervals of signalling necessary to activate targets genes? Is the competence of cells to generate a response determined by the cumulative amount of processed Notch?

3. Results

3A. Results – part 1

3A.1 Opto-Delta - a tool to inhibit Notch signalling by light induced delta clustering

3A.1.1 Tagging of the endogenous Delta locus

In order to investigate the dynamic aspects of Notch signalling, I developed an optogenetic tool to acutely block signalling for definite periods of time during development. I focused on the Notch ligand Delta, which is the most upstream component of the pathway, with the aim to regulate its endogenous localization and function at the plasma membrane and thus affect Notch activation.

For this, I collaborated with a colleague in the lab, Aleksander Necakov to generate an endogenously tagged, functional optogenetic allele of Delta (opto-Delta). The following strategy was used to generate a Delta landing line that could be used to insert multiple tags. A ϕC31 recombinase-landing site was introduced in the Delta locus, replacing a large part of the sequence coding for Delta. The resulting line, which was heterozygous for the Delta mutation, acted as an acceptor line to systematically screen for the insertion of donor constructs carrying a cognate *attB* recombination sequence (Huang et al., 2009) (Fig. 9A). Using sequence conservation and linear motif analysis, an intra-molecular poly-alanine rich region in the intracellular domain of Delta (aa 701) was located, which was neither conserved nor predicted to reside in a known folding domain (Dinkel et al., 2016). This was identified as a potential site for tagging, as the insertion of an intramolecular GFP tag in this region resulted in fully viable

Delta::GFP homozygous flies, with one copy of Delta::GFP capable of rescuing a Delta deficiency in *trans*. The same strategy was used to design opto-Delta constructs.

3A.1.2 Optogenetic system employed

The Chrypotochrome based CRY2/CIB1 heterodimerizing system was employed in order to optogentically tag Delta. This system had already been successfully exploited by our lab to control protein-protein interactions during *Drosophila* morphogenesis.

As mentioned in section 1.6.1, upon blue light photo-activation, apart from being able to bind to its partner CIB1, CRY2 undergoes homo-oligomerization, particularly when expressed on its own (Bugaj et al., 2013). Delta::CRY2 could thus potentially serve as a single component based optogenetic system to induce clustering of Delta in the membrane and potentially interfere with the stoichiometry of endogenous Delta/Notch complexes or the conformation of Delta molecules at the plasma membrane.

A series of CRY2 tagged constructs were generated, either with a CRY2 tag alone (CRY2-PHR, residues 1-498) (Delta::CRY2), or a CRY2 tag fused to EGFP (Delta::CRY2::GFP) or tag-RFP (Delta::CRY2::RFP). Additionally, a CRY2 variant with an enhanced capability for oligomerization, CRY2-olig (Delta::CRY2-olig) (Taslimi et al., 2014), and CIBN (a CIB1 construct without the C-terminal nuclear localizing signal (Delta::CIBN) were also used to generate constructs (Fig. 9A-C). These constructs were injected into the Delta landing line described in the previous section and the generated lines were screened for viable homozygous flies when raised without light exposure. Of all the constructs, only Delta::CRY2 and Delta::CIBN gave rise to fully viable and fertile homozygous flies, while Delta::CRY2::GFP, Delta::CRY2::RFP, and Delta::CRY2-olig homozygous flies were less frequent and exhibited lesser fertility.

This could be due to the addition of two large tags (~ 35 kDa each) that could either affect the protein folding or increase the dark state activity of the CRY2-olig tag.

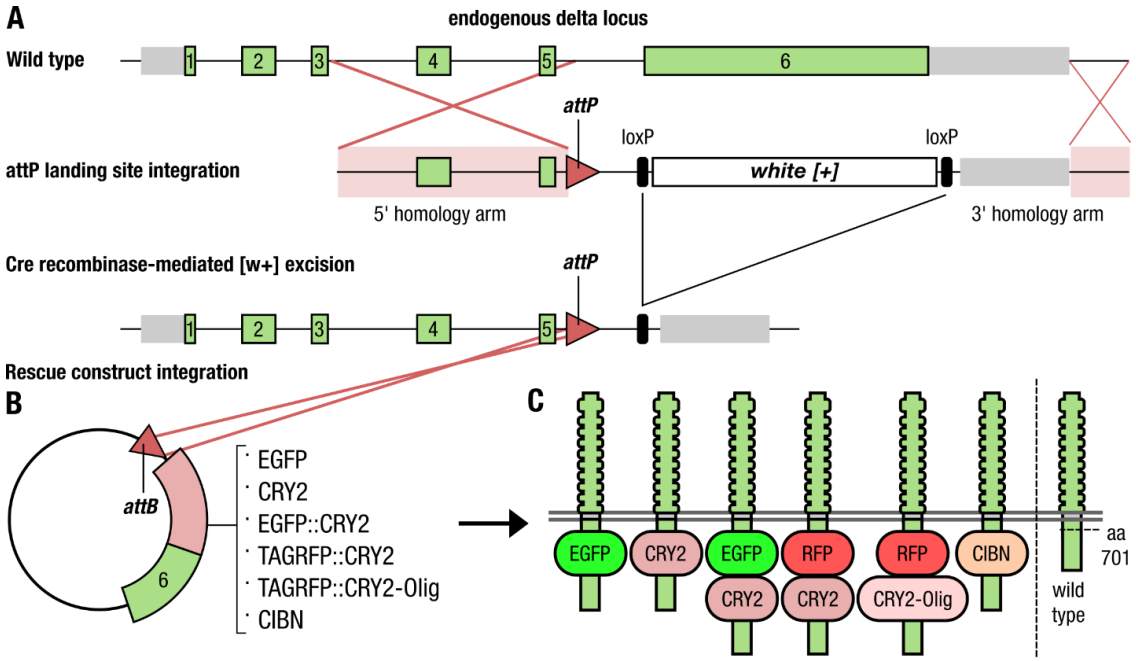

Figure 9: Endogenous optogenetic tagging of Delta

(A-C) Schematic illustrating the strategy used to generate a functional optogenetic-tagged allele of the Notch ligand Delta. **(A)** Gene structure of the Delta locus, green and grey bars represent exons and 5'/3' UTRs, respectively. Exons 1 to 6 are shown in green, 5' and 3' in grey, homology arms are highlighted in pink, and recombination sites are indicated by red lines. Homologous recombination was used to replace a large portion of the Delta locus between the intron preceding exon 6 to a region downstream of the transcriptional stop site, through knock-in of an attP landing site and a loxP-flanked mini-white cassette. attP knock-in founder lines were identified as red-eyed transformants. Cre recombinase was subsequently used to remove the mini-white cassette, resulting in white-eyed flies. Delta-attP white-eyed founder lines were then transformed with attB rescue construct vectors carrying an attB recombinase binding site upstream of the genomic Delta sequence **(B)**, along with incorporated sequences coding for a variety of tags inserted into an 11 amino acid polyalanine sequence in the intracellular domain of Delta (amino acid 701). **(C)** position of the different tags with respect to the Delta protein sequence and its orientation in the plasma membrane.

This figure (including legend) was generated by Aleksander Necakov and is part of the submitted manuscript “Optogenetic inhibition of Delta reveals digital Notch signalling output during tissue differentiation” (see Appendix)

3A.1.3 Characterization of light-induced phenotypes during development

Rearing Delta::CRY2 homozygous (opto-Delta) flies in ambient light conditions made them develop severe phenotypes that were characteristic of deficient Notch signalling. These phenotypes were evident during larval and pupal development (Fig. 10A-N) and included a loss of wing vein margins, a characteristic Delta wing phenotype (Klein and Arias, 1998) (Fig. 10A-D), increased density of bristles in the adult notum (Mummery-Widmer et al., 2009) (Fig. 10E-H), and modified eye morphology (Cagan and Ready, 1989) (Fig. 2I-L). Consistently, constant illumination under a dissecting microscope resulted in lack of embryo hatching and a bald embryonic cuticle phenotype, which is a hallmark of deficient Notch signalling (Nüsslein-volhard and Wieschaus, 1980; Poulson, 1937)(Poulson, 1937)(Fig. 10M-N). During embryogenesis, compromised Notch signalling results in an increased number of cells with neuronal cell fate as compared to ectodermal cells. As the ectodermal cells are responsible for cuticle secretion, the phenotype observed is a lack of cuticle, while the other structures like anal plate and mouth hooks remain unaffected (Nüsslein-volhard and Wieschaus, 1980). Furthermore, opto-Delta flies grown under light had comparatively severe wing, eye and cuticle phenotypes than their Delta heterozygous counterparts, suggesting that Delta activity was compromised to an extent of 50% or more (Fig. 10O-W).

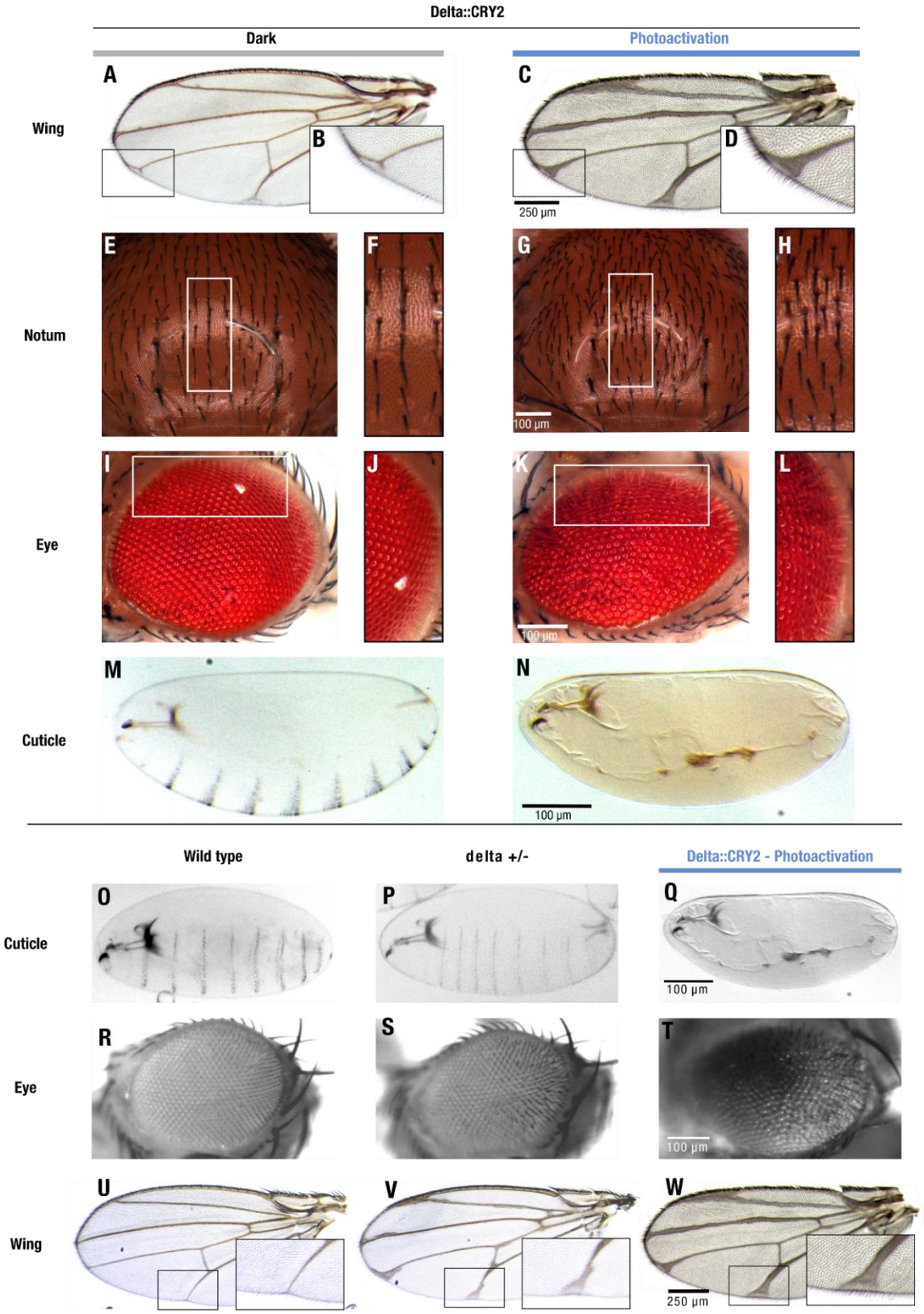

Figure 10: opto-Delta activation results in inhibition of Notch signalling during different developmental stages.

(A-N) Flies homozygous for Delta::CRY2 are viable and fertile, and exhibit light-gated control of Notch signalling during development. Homozygous Delta::CRY2 flies raised in the

dark exhibit only a mild Delta phenotype in the terminal tips of the wing **(A, B**-magnified view**)**. Otherwise, these flies exhibit normal patterning and morphology in tissues including the notum **(E, F**-magnified view**)**, the eye **(I, J**-magnified view**)**, and the embryo **(M)**. In contrast, Delta::CRY2 flies reared in the light exhibit Delta loss-of-function phenotypes, which include thickening of the wing veins **(C, D** -magnified view**)**, an increase in microchaeta in the notum **(G, H**-magnified view**)**, disorganization of the ommatidia **(K, L**-magnified view**)**, and loss of denticle belt patterning in the embryo **(N)**. Scale bars, 250 μm in **F** and 100 μm in **G**, **K**, **N**.

(O-W) Benchmarking of light-induced loss-of-function phenotypes in Delta::CRY2 flies. Delta::CRY2 flies reared in the light exhibit more severe Delta loss-of-function phenotypes compared to Delta heterozygotes. This is evident from the loss of denticle belt patterning in the embryonic cuticle **(Q)**, disorganization of the ommatidia **(T)**, and thickening of the wing veins **(W)** when compared to the Delta heterozygous counterparts where the denticle belt patterning is unaffected **(P)**, and the ommatidia **(S)** and wing venation **(V)** phenotypes are milder. Corresponding wildtype cuticle, eye and wing are depicted in panels **(O)**, **(R)** and **(U)** respectively. This suggests that the activity of Delta is compromised by at least more than 50% in Delta::CRY2 flies upon photo-activation. Scale bars, 100 μm in **(Q)** and **(T)**, and 250 μm in **(W)**.

This figure (including legend) was generated by me and is part of the submitted manuscript "Optogenetic inhibition of Delta reveals digital Notch signalling output during tissue differentiation" (see Appendix)

3A.1.4 Characterizing the mechanism of Notch signalling inhibition by opto-Delta

In order to characterize the mechanisms behind the loss of opto-Delta activity upon photo-activation, I recorded the dynamics of Delta and correspondingly, Notch activation in the early embryo. During early embryogenesis, Delta is uniformly distributed at the plasma membrane and undergoes mesoderm specific endocytosis that is activated by Neuralized during early cycle 14 (Bardin and Schweisguth, 2006; De Renzis et al., 2006). As detailed in section 1.5.4, this gives rise to the activation of Notch in the mesectoderm and resulting in the expression of target gene single-minded (*sim*) in single stripes of cells adjoining the ventral mesoderm (Cowden and

Levine, 2002). In order to observe the light-responsive behaviour of opto-Delta, I imaged embryos heterozygous for Delta::CRY2::GFP (Delta::CRY2::GFP) as a representative for Delta::CRY2.

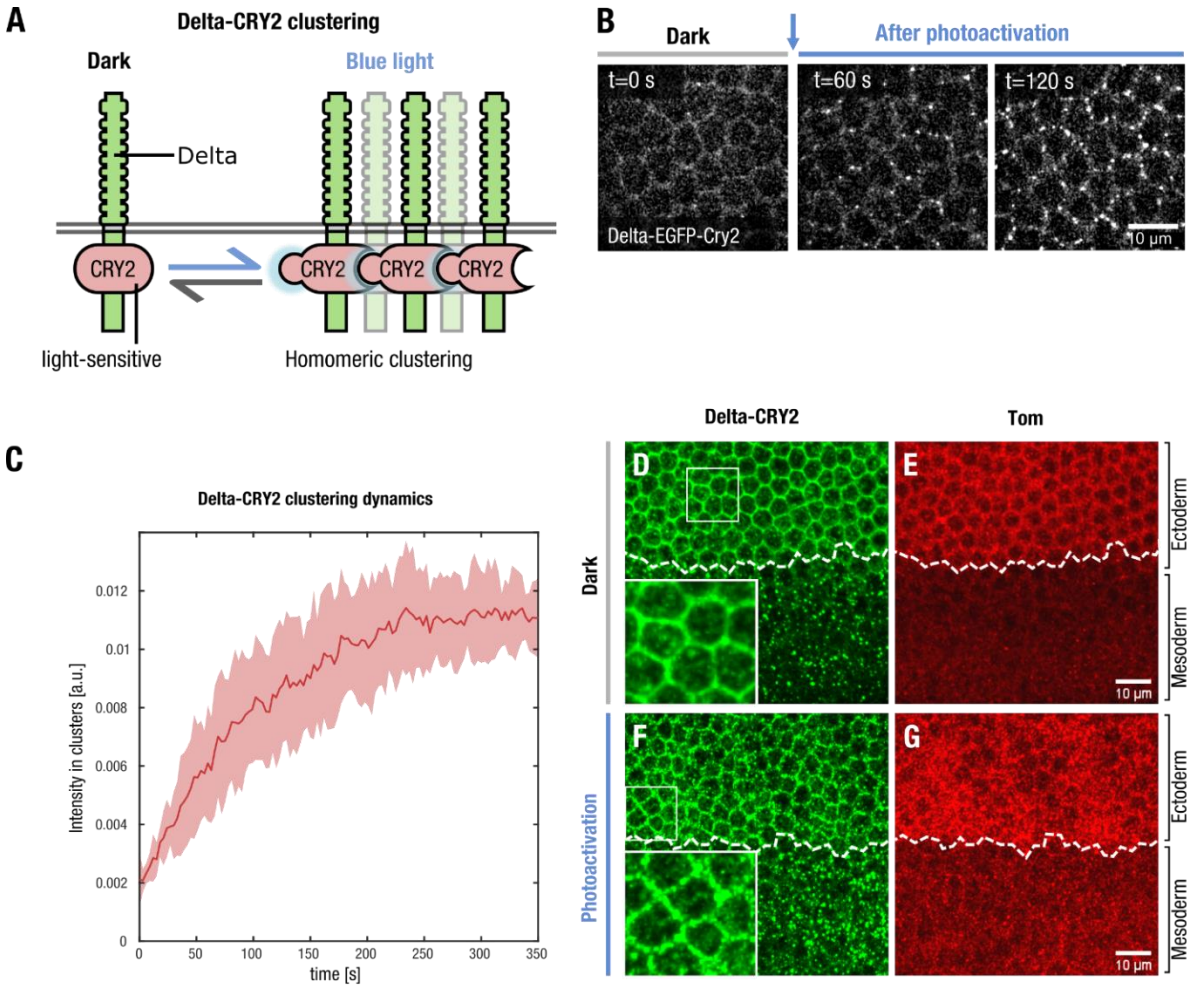

Figure 11: opto-Delta undergoes rapid plasma membrane light-induced oligmerization.

(A) Schematic illustrating the oligomerization of opto-Delta molecules at the plasma membrane upon photo-activation with blue light.

(B) Snapshots from confocal live imaging movies of Delta::GFP::CRY2 embryos (ectoderm stage 5) at the onset of photo-activation (T_0) or after 60 s and 120 s at 2 s intervals (λ= 488 nm, 0.6 mW). Scale bar, 10 µm.

(C) The kinetics of light-induced opto-Delta clustering were quantified in the ectoderm of Delta::EGFP::CRY2 embryos. Data was collected using confocal live imaging at 2 s intervals

(λ= 488 nm, 0.6 mW) and the relative intensity of Delta::GFP::CRY2 clusters in three embryos (n=3, 100 cells) was quantified over time using a custom-built image analysis pipeline developed in Cell profiler. Relative intensity of Delta clusters is shown over time (red line), with standard deviation between replicates highlighted in pink.
(D-G) Immunostaining of Delta::CRY2 embryos using an anti-Delta antibody (green) at the end of cellularization in embryos fixed in the dark **(D-E)** or after batch photo-activation as described in Material and Methods (**F-G)**. Panels display max. intensity z-projections of 10 slices at a z-interval of 0.7 μm. Magnified insets in **(D, F)** show the localization of Delta::CRY2 in the ectoderm in the dark **(D)** and after photo-activation **(F)**. Embryos were co-stained with an anti-Tom antibody **(E, G)** in order to mark the ectoderm-mesoderm boundary. Delta::CRY2 protein clustered in the ectoderm and was normally internalized in the mesoderm.
This figure (including legend) was generated by me and is part of the submitted manuscript "Optogenetic inhibition of Delta reveals digital Notch signalling output during tissue differentiation" (see Appendix). Panel **(C)** was generated by me in collaboration with Rohit Krishnan Harish.

While in the initial frame of acquisition using the 488 nm laser, a uniform localization in the plasma membrane was observed (<1 s), after few acquisition time-points ($t_{½}$ ~40 s) (Fig. 11A-C) Delta::CRY2::GFP displayed rapid reorganization into plasma membrane clusters. These Delta clusters underwent normal internalization in the mesoderm, and were retained on the ectodermal plasma membrane (Fig. 11D-G), indicating that neuralized dependant ubiquitination and Delta endocytosis were unaffected.

To further confirm this result, I quantified Delta plasma membrane levels in opto-Delta embryos, and this showed a ~70% decrease in the mesoderm with respect to the ectoderm in both the dark and photo-activated conditions (Fig. 12A-C). Quantification of the plasma membrane to cytoplasmic ratio of Delta in the mesoderm also displayed no significant change between the dark and photo-

activated conditions (Fig. 12D). I also imaged the trafficking of opto-Delta in embryos expressing the early endosome marker Rab5, and this revealed a ~75% colocalization between Delta and Rab-5 positive vesicles in wildtype and opto-Delta (both dark and photo-activated) embryos (Fig. 12E-H). In summary, these results show evidence that Delta clustering does not affect the normal mechanisms underlying Delta trafficking (ubiquitination and internalization) in the mesoderm.

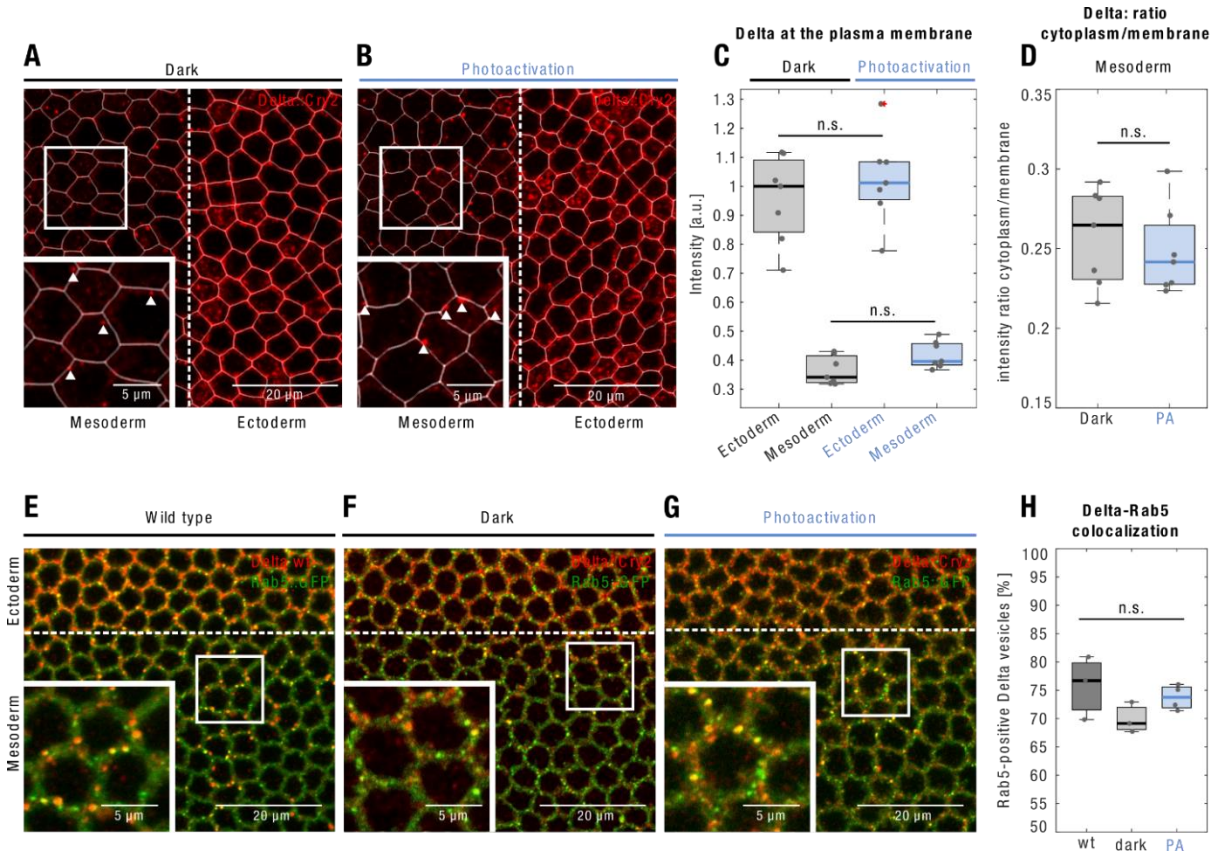

Figure 12: Light induced Delta clustering does not affect Delta trafficking in the mesoderm.

(A-C) Plasma membrane segmentation of Delta::CRY2 embryos immunostained with anti-Delta (red) and anti-Cadherin (used for plasma membrane segmentation, white) antibodies at the end of cellularization, in embryos fixed in the dark **(A)** or after batch photo-activation **(B)**. Panels display single confocal zslices. Magnified insets in **(A, B)** show Delta cytoplasmic vesicles in the mesoderm that are excluded from the plasma membrane segmentation. Plot **(C)** shows the quantification of Delta plasma membrane levels in the ectoderm and mesoderm in both dark and photo-activated conditions. In both cases, Delta plasma membrane levels

were depleted by ~70% in the mesoderm compared to the ectoderm. No significant difference was observed when comparing ectodermal or mesodermal Delta plasma membrane levels with or without photoactivation, indicating that Delta was normally depleted in both conditions. N= 7 embryos for both dark and photo-activation, n.s. represents no statistically significant difference in a 2-sample t-test. Scale bars, 20 μm **(A, B)**

(D) Plot depicting the cytoplasm to membrane ratio of Delta in the mesoderm, both in the dark and upon photo-activation. No significant difference was observed between both conditions. N= 7 embryos for both dark and photoactivation, n= ~40 cells/embryo. n.s. represents no statistically significant difference in a 2-sample t-test.

(E-H) The extent of colocalization of Delta-positive vesicles with the early endosomal marker Rab5 did not change upon light induced Delta-clustering. Single confocal z-slices of Rab5::GFP **(E)**, Rab5::GFP in a Delta::CRY2 homozygous background embryos either fixed in the dark **(F)** or after batch photo-activation **(G)**. In all panels Delta was visualized by immunostaining using an anti-Delta antibody (red). The endogenous GFP signal was used to visualize Rab5 (green). Magnified insets in all three panels show co-localization between Delta positive vesicles and Rab5 **(E-G)**. Plot **(H)** shows the extent of colocalization of Delta and Rab5 positive vesicles. ~75% of Delta-positive vesicles colocalized with Rab5, and this value did not significantly differ from wildtype, Delta::CRY2 (photo-activated), or Delta::CRY2 (Dark) conditions. N=4 embryos for photo-activation and N=3 embryos for wild type and dark conditions. n.s. represents no statistically significant difference in a 2-sample t-test. Scale bars, 20 μm **(E-G)**

This figure (including legend) was generated by me and is part of the submitted manuscript “Optogenetic inhibition of Delta reveals digital Notch signalling output during tissue differentiation” (see Appendix). Panels **(C)**, **(D)** and **(H)** were generated by Daniel Krueger.

Combining opto-Delta with endogenously tagged Notch::YFP demonstrated that Notch also segregated into clusters in the ectoderm upon photo-activation (Fig. 13A). The rate of clustering increased as the number of opto-Delta alleles was doubled (heterozygous vs homozygous, Fig. 13A, B) presumably due to the higher density of opto-Delta molecules in the plasma membrane. Furthermore, immunostaining showed that both Notch and Delta colocalized in the ectodermal clusters indicating that Notch and Delta were indeed engaged. (Fig 13C-F)

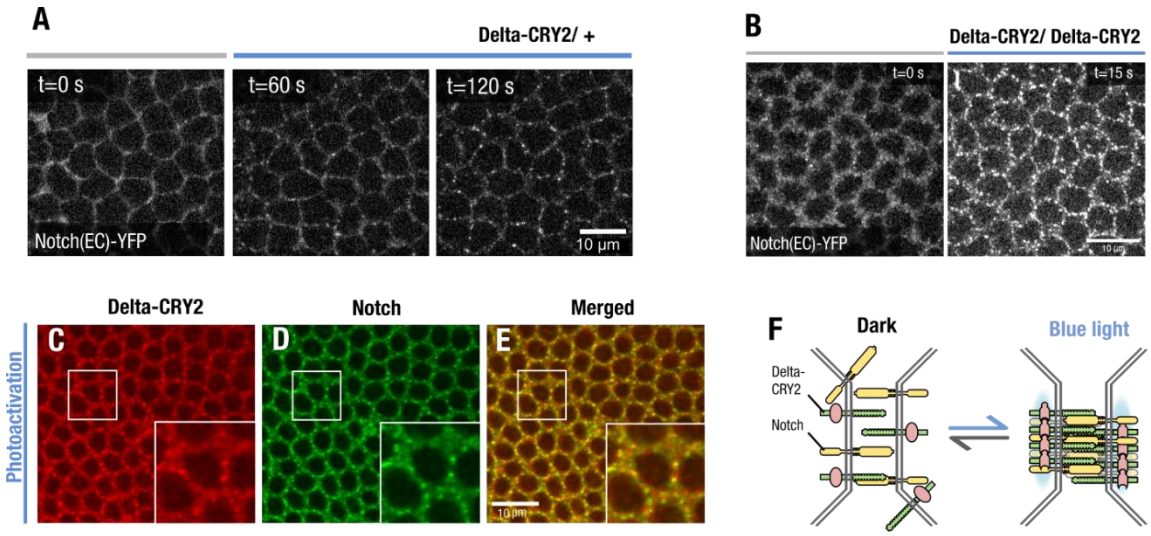

Figure 13: Notch clusters in response to photo-activation of opto-Delta

(A) Sum of slice z-projection of 4 slices at 0.4 µm z-interval of cellularizing embryos expressing endogenously tagged Notch::YFP imaged using an argon laser (λ= 514 nm) in a Delta::CRY2 heterozygous background at the onset of photoactivation (T0), after 60 s and 120 s. Embryos were photo-activated once for 5 s before the. 60 s and 120 s acquisition (stack size of z = 10 µm, λ= 488 nm, 0.6 mW). Scale bar, 10 µm.

(B) Notch clustering in a Delta::CRY2 homozygous background. Single confocal z-slices of cellularizing embryos expressing endogenously tagged Notch::YFP imaged using an argon laser (λ= 514 nm) in a Delta::CRY2 homozygous background before and after photo-activation with a stack of size z = 10 µm for a duration of 5 s (λ= 488 nm, 0.6 mW). Note that Notch clustering in Delta::CRY2 homozygous background is faster than in Delta::CRY2 heterozygous. This is probably due to the higher density of the Delta::CRY2 molecules. Scale bar, 10 µm.

(C-E) Delta::CRY2 clusters in the ectoderm contain Notch. Immunostaining of embryos expressing Notch::YFP in a Delta::CRY2 homozygous background. Delta **(C)**, Notch **(D)**, overlay **(E)** after batch-photo-activation (λ= 488 nm), as described in the methods. Panels display max. intensity z-projections of 3 slices at a z-interval of 0.7 µm. Magnified insets show ectodermal clusters of Delta::CRY2 at the plasma membrane (A) co-clustering of Notch (B), and the merged image in (C). Scale bar, 10 µm.

(F) Schematic illustration of the redistribution of Notch into clusters.

This figure (including legend) was generated by me and is part of the submitted manuscript “Optogenetic inhibition of Delta reveals digital Notch signalling output during tissue differentiation” (see Appendix).

The extracellular domain of Notch (NECD) is trans-endocytosed along with Delta in the mesoderm starting at the onset of cycle 14 (see section 1.5.4). Staining opto-Delta embryos with anti-Notch extra-cellular domain (NECD) showed a decreased production of cytoplasmic NECD vesicles (Fig. 14A-D) upon photo-activation. Staining and quantifying NICD levels revealed a ~30% higher retention of Notch at the plasma membrane when photo-activated (Fig. 14E-I). Together, these data point towards a defect in Delta induced Notch trans-endocytosis suggesting that the signal-sending ability of opto-Delta is affected upon photo-activation.

Detection of Notch target gene, *sim* expression by RNA *in situ* hybridization in photo-activated opto-Delta embryos confirmed that Notch signalling was strongly inhibited (Fig 14J-K). However, since opto-Delta co-cluster with Notch in the signal-receiving mesectoderm cells, and given that we still observe few cytoplasmic NECD vesicles in the mesoderm upon illumination, there exists the possibility that opto-Delta clusters inhibit signalling by repressing Notch activity *in cis*. Cis-interactions between Notch and Delta in signal receiving cells as an inhibitory mechanism for signalling has been studied in various tissue contexts as described in section 1.3.3.

Due to the fact that in the embryo, cells are all tightly packed in a continuous fashion, it is technically extremely challenging to activate opto-Delta only on the surface of the signal sending cells or signal receiving cells, and hence difficult to distinguish between *cis* versus *trans* inhibition.

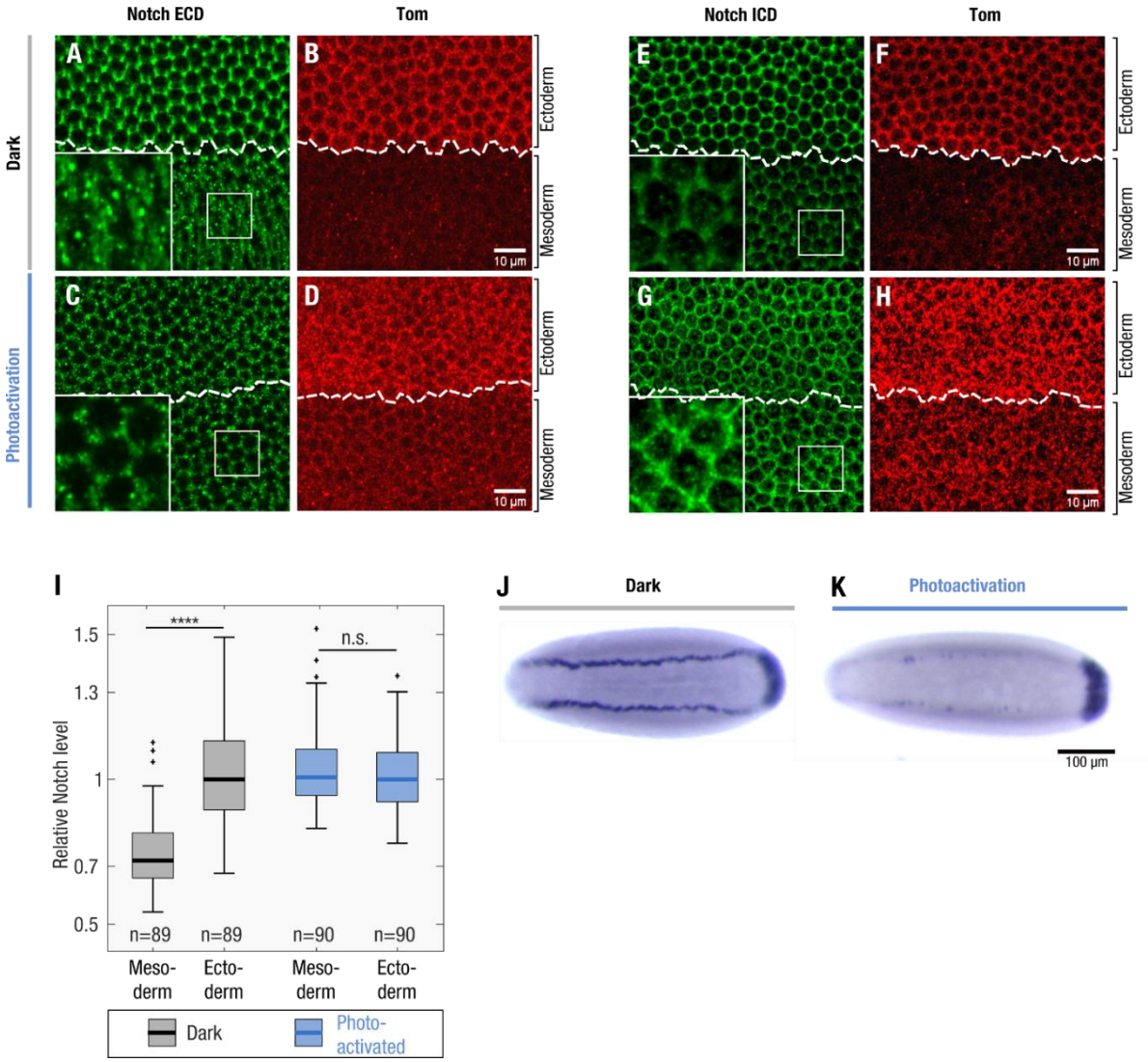

Figure 14: Optogenetic activation inhibits Notch processing in the mesoderm and signalling activation in the mesectoderm

(A-I) Light-induced Delta::CRY2 clustering inhibits Notch processing in the mesoderm. Immunostaining for Notch Extracellular Domain (NECD) **(A, C)** or Notch Intracellular Domain (NICD) **(E, G)** at the end of cellularization in Delta::CRY2 embryos fixed in the dark or batch photo-activated as described in Material and Methods. Co-staining with an anti-Tom antibody **(B,D,F,H)** was used to mark the ectoderm-mesoderm boundary. In the dark, normal processing of Notch in the mesoderm results in the depletion of Notch (both NECD and NICD) from the plasma membrane, and accumulation of cytoplasmic NECD vesicles, magnified insets in **(A,E)**. Photo-activation caused reduced number of NECD vesicles, arrows in magnified inset **(C)** and increased retention of Notch in the mesoderm, magnified insets in **(C,G)** as also demonstrated by the box plot in **(I)** showing quantification of NICD plasma membrane levels. NICD Interface intensity values were normalized to the median NICD value present in the ectoderm for each embryo. (N = 3 embryos; n= number of

interfaces with n_{Dark}= 89 n_{PA} = 90. ****p < 0.0001, two-sample t-test. n.s. indicates no statistical significant differences). Scale bars, 10 μm.

(J-K) In situ hybridization against *sim* in Delta::CRY2 embryos fixed in the dark (J) or after batch photo-activated started at the onset of cycle 14 as described in Material and Methods showing lack of *sim* transcription in the mesectodermal cells **(K)**. Embryos are aligned anterior to the left and ventral side facing up. Scale bar,100 μm.

This figure (including legend) was generated by me and is part of the submitted manuscript "Optogenetic inhibition of Delta reveals digital Notch signalling output during tissue differentiation" (see Appendix).

In order to uncover this, I decided to use the pupal notum as an experimental tissue since it offers the possibility to perform clonal analysis as opposed to the embryo. In the notum, Notch employs the mode of lateral inhibition (see section 1.3.2) for patterning sensory organ precursor (SOP) cells that give rise to bristles in the adult. In groups of cells known as proneural clusters, the cell that is signal sending adopts sensory organ precursor (SOP) fate, while the neighbouring cells where Notch is activated become epidermal and were inhibited from SOP fate (Fig. 15A). Opto-Delta pupae when exposed to light right after pupal formation exhibit an increased density of SOPs (~ 40% more), consistent with previous studies showing impaired Notch signalling in this tissue (Fig. 15B, C) (Couturier et al., 2012).

To disentangle whether opto-Delta clustering was responsible for signal-sending or signal-receiving defects, using the the FLP/FRT technique, mitotic clones of cells homozygous for opto-Delta were generated in a wildtype background. The FLP recombinase was expressed in the notum tissue under the control of the Ubx promoter, and clones homozygous for opto-Delta were identified by the lack of nuclear-RFP expression (Fig. 16A). I focussed on cells at the boundary between the opto-Delta homozygous clones and the surrounding wild-type tissue, and using an

SOP marker (neur>iRFP-nls), scored for signal sending and signal receiving activity (Fig. 16B-F).

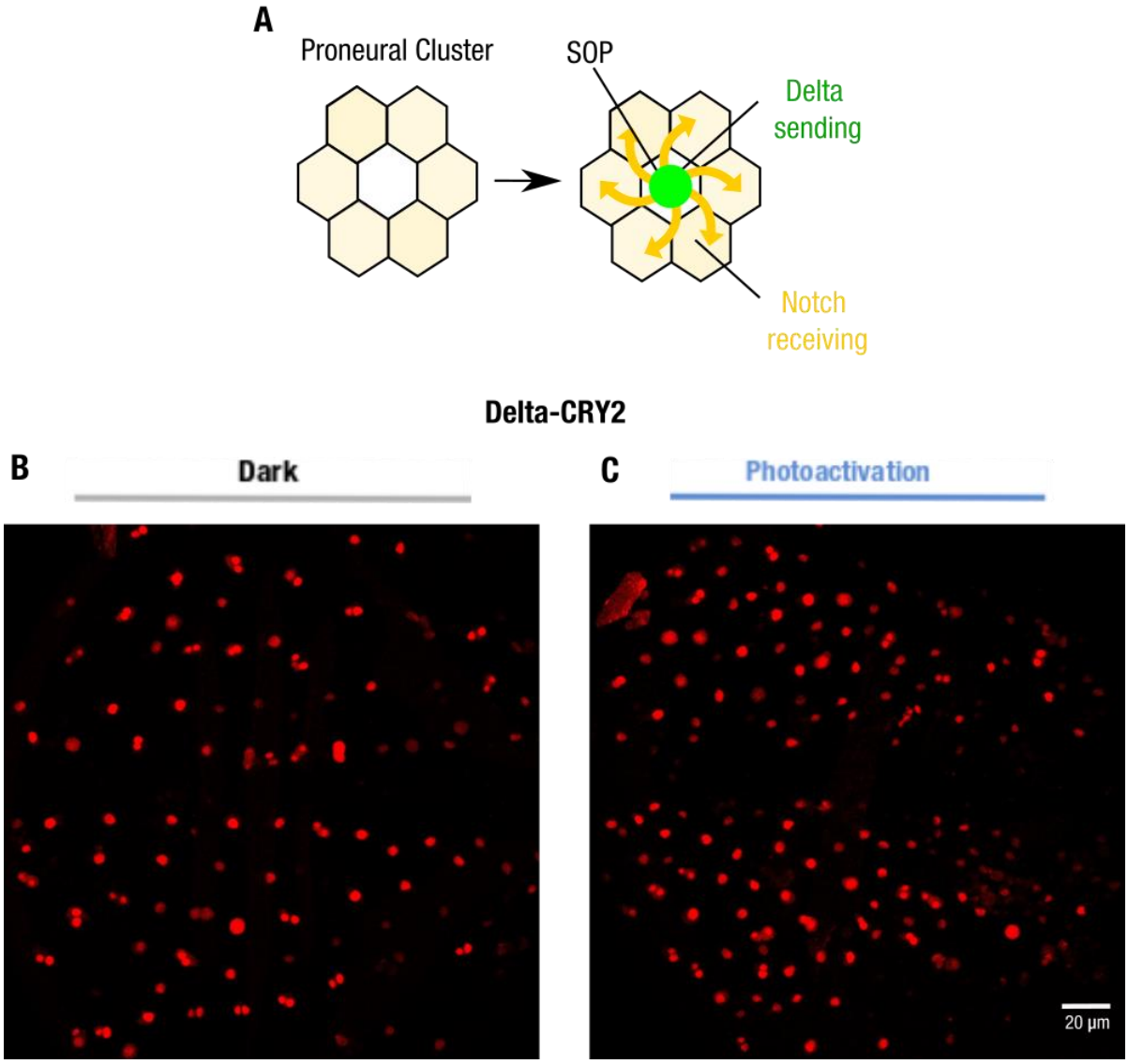

Figure 15: opto-Delta activation in the pupal notum affects SOP patterning.

(A) Selection of Sensory organ precursor cells (SOPs) in proneural clusters by the process of lateral inhibition, wherein signal-sending SOPs inhibit the surrounding signal receiving cells from SOP fate.

(B, C) Maximum intensity z-projections of the pupal nota expressing Delta::CRY2 and reared in the dark **(B)** or light **(C)** until 16 hrs APF. Upon photo-activation, there was a disruption of SOP patterning along defined rows, and an increased density of SOPs specified in the tissue (by ~40%). Scale bar, 20 µm.

This figure (including legend) was generated by me and is part of the submitted manuscript "Optogenetic inhibition of Delta reveals digital Notch signalling output during tissue differentiation" (see Appendix). Panels **(B)** and **(C)** were generated by me in collaboration with Mateusz Trilinski.

In a wild-type pupa, there is an equal probability (50%) of finding an SOP cell on either the opto-Delta side or wild-type side of the clone boundary (Couturier et al., 2012; Heitzler and Simpson, 1991). Any defects in signalling or receiving will be reflected in a change in this percentage across the boundary. Upon quantification of all the clone-boundary SOPs post 18h of pupa formation (APF), I observed that in photo-activated opto-Delta pupae, ~ 90% (94.6 ± 2.6) of SOPs were located inside the opto-Delta clones (Fig. 8B, F). In pupae reared in the dark, only a slightly greater (62.5 ± 5.6) percentage was observed compared to the expected value of 50%, indicating a random pattern (Fig. 16C, F).

This result indicates that opto-Delta cells upon photo-activation have an increased chance of adopting SOP fate compared to their wild-type neighbours, suggesting that they have a reduced capacity to process and activate Notch i.e. opto-Delta clustering interferes with the activation of Notch signalling by *cis* inhibition. Additionally, the neighbouring wild-type cells outside the opto-Delta clone boundary always adopted a non-SOP fate, indicating that they were able to receive Notch signal and that opto-Delta cells are signalling competent. In summary, I concluded that photo-activation of opto-Delta, to a significantly greater extent affected signal receiving in *cis*, rather than signal activation in *trans*.

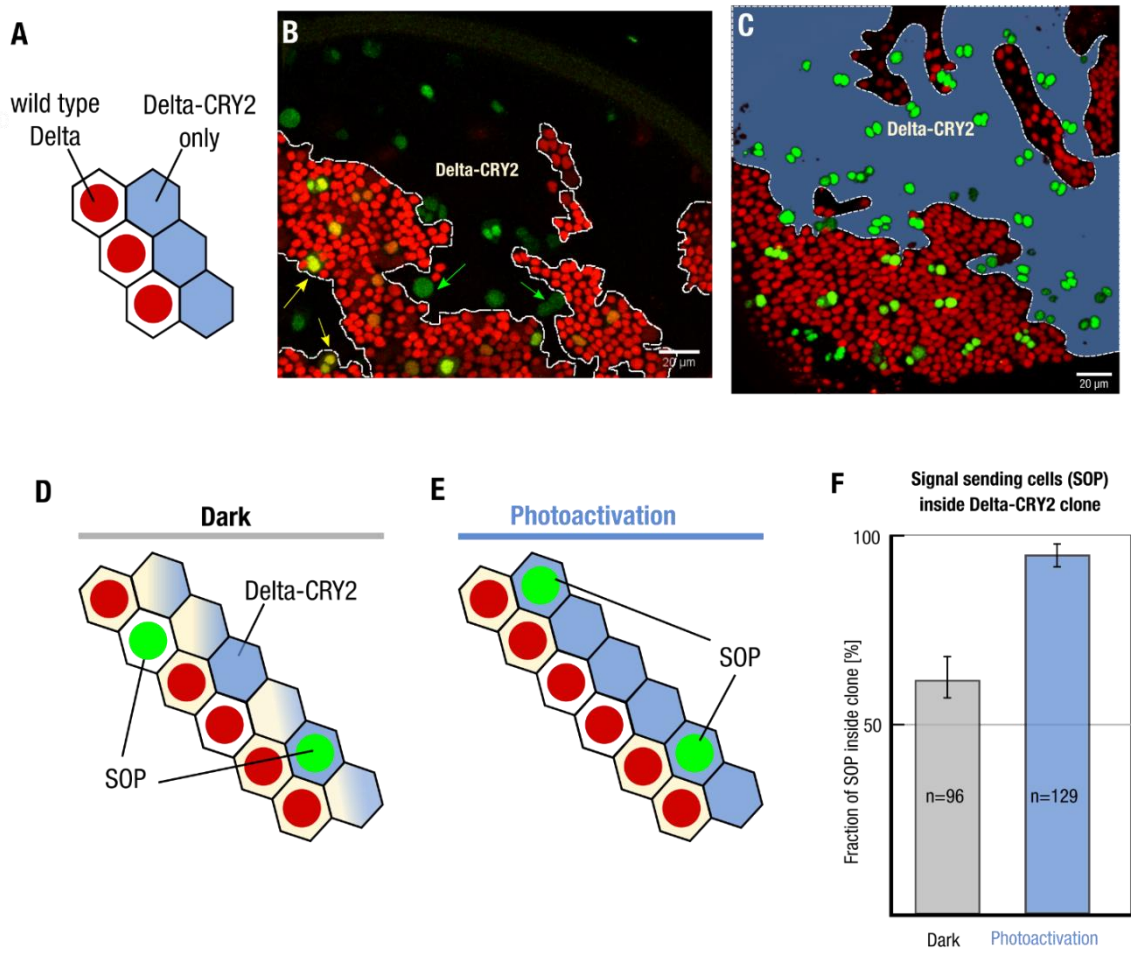

Figure 16: Clonal analysis in the pupal notum reveals that opto-Delta inhibits Notch in the signal-receiving cells.

(A-C) Clonal analysis in the pupal notum to distinguish whether signal-sending or signal-receiving is impaired upon optogenetic activation. Schematic illustration depicting the clone boundary between Delta::CRY2 cells (nls-RFP negative) and WT cells (nls-RFP positive) **(A)**. Control (non-photo-activated) **(B)** and photo-activated **(C)** nota at 18 h after puparium formation showing Delta::CRY2 clones in blue and dashed lines depicting the clone borders where the number of SOPs (green) are scored. In **(B)**, yellow arrows indicate examples of SOPs inside the wild-type clone and green arrows show SOPs scored inside the Delta::CRY2 clone Scale bar, 20 µm.

(D-F) Analysis of SOP fate decisions across Delta-CRY2/wild-type clone borders. The bar plot **(F)** shows the percentage of SOPs located inside Delta::CRY2 clones out of the total number of SOPs scored at the border, in either dark or photo-activated conditions. In a wild type case, there is a 50% chance for an SOP to be present on either side of the boundary, schematic in **(D)**. In the dark, 62.5% of SOPs are present on the side of the Delta::CRY2 clone. This proportion significantly increased to 94.6% in photo-activated pupae, schematic

(E), suggesting a strong signal receiving deficiency of Delta::CRY2 cells (N = 3 pupae; n_{SOP} = 96 (dark) ; N = 5 pupae; n_{SOP} =126 (photo-activation). n_{SOP} signifies total number of SOPs at clone boundary. Error bars indicate standard deviation between different pupae. SOPs formed inside the Delta::CRY2 clones are able to inhibit their neighboring cells on the wild-type side from adopting SOP fate, thus showing their signal-sending competence.
This figure (including legend) was generated by me and is part of the submitted manuscript "Optogenetic inhibition of Delta reveals digital Notch signalling output during tissue differentiation" (see Appendix). Panels **(B)** and **(C)** were generated by me in collaboration with Mateusz Trilinski.

3A.1.5 Investigating the input-output dynamics of Notch signalling during embryonic mesectoderm specification

Having characterized how opto-Delta activation inhibits Notch signalling upon photo-activation, I used it as a tool to characterize the input-output relationship of Notch signalling. I focussed on mesectoderm specification in the early embryo, when Notch signalling is activated during the course of cellularization resulting in the expression of target gene *sim*. In combination with opto-Delta, as a readout of signalling, I used a *sim* transgene that was generated based on the MS2-MCP system (Garcia et al., 2013) (*sim*-MS2) in order to monitor its live transcription upon Notch activation (Fig. 17A). MCP::GFP binds to nascent *sim*-MS2 *trans*cripts to generate fluorescent spots in the nuclei that enables both a quantitative and instantaneous measure of signalling activity. Using a specially generated image analysis pipeline (in collaboration with Pierre Neveu) it was possible to successfully segment and track these *sim* spots over time and quantify the dynamics in *sim* expression by measuring spot intensities.
Consistent with previous data that were generated by *in situ* hybridization, despite Delta endocytosis and NECD trans-endocytosis starting few minutes post the onset of cellularization, *sim trans*cripts were detected only ~30 min after the onset of cellularization (Cowden and Levine, 2002; Morel and Schweisguth, 2000). Live

imaging of *sim*-MS2 onset also revealed a gradual increase in the number of nuclei expressing *sim* and after 10 min, almost all nuclei in the mesoectoderm expressed *sim* (Fig. 17B-F). The reason for this time delay in *sim* expression is unclear. Nuclei may not be competent to express *sim* during early cycle 14 because additional factors may be necessary and these become available only late in cellularization. The alternate possibility is that Notch activation needs to build up to reach a critical threshold level in order to activate *sim*. As the delay is the time when Notch activation occurs, this provided the opportunity to use opto-Delta to perturb signalling in a graded fashion during this period and track *sim* transcription in the tissue in order to distinguish between the models proposed above.

Opto-Delta embryos expressing the MCP-MS2 *sim* module were photo-activated either from the beginning of cellularization (0 min), or after 5 min, 10 min, 15 min 20 min, or 25 min (0/ 5/ 10/ 15/ 20/ 25 min of signalling) (Fig. 18A-F). In order to get a quantitative measure of transcribing nuclei over time, I measured the increase in the number of sim-transcribing nuclei in the tissue at high temporal resolution (30 sec) from the onset of transcription until onset of gastrulation (Fig. 18C).

To precisely measure the tissue wide sim activation rates and onset times, the average curves for the different conditions were adjusted to the equation N_{max} (1-exp(-*k* (t-t_0)) where N_{max} is the maximum number of mesectodermal nucelei that can be activated, *k* is the tissue level activation rate (rate of increase in the number of sim transcribing nuclei) and t_0, the delay in onset of transcription with respect to the control (Fig. 19A). N_{max} was taken as constant and only two parameters *k* and t_0 were adjusted for each embryo.

The results show a graded response at the level of the tissue. The longer the photo-activation time, the lesser the tissue-level activation rate of *sim* expression (k), slowing

down from ~0.2 min^{-1} per µm for individual nuclei in the control to 0.05 min^{-1} per µm in the case where photoactivation was throughout the duration of cellularization (Fig. 18D).

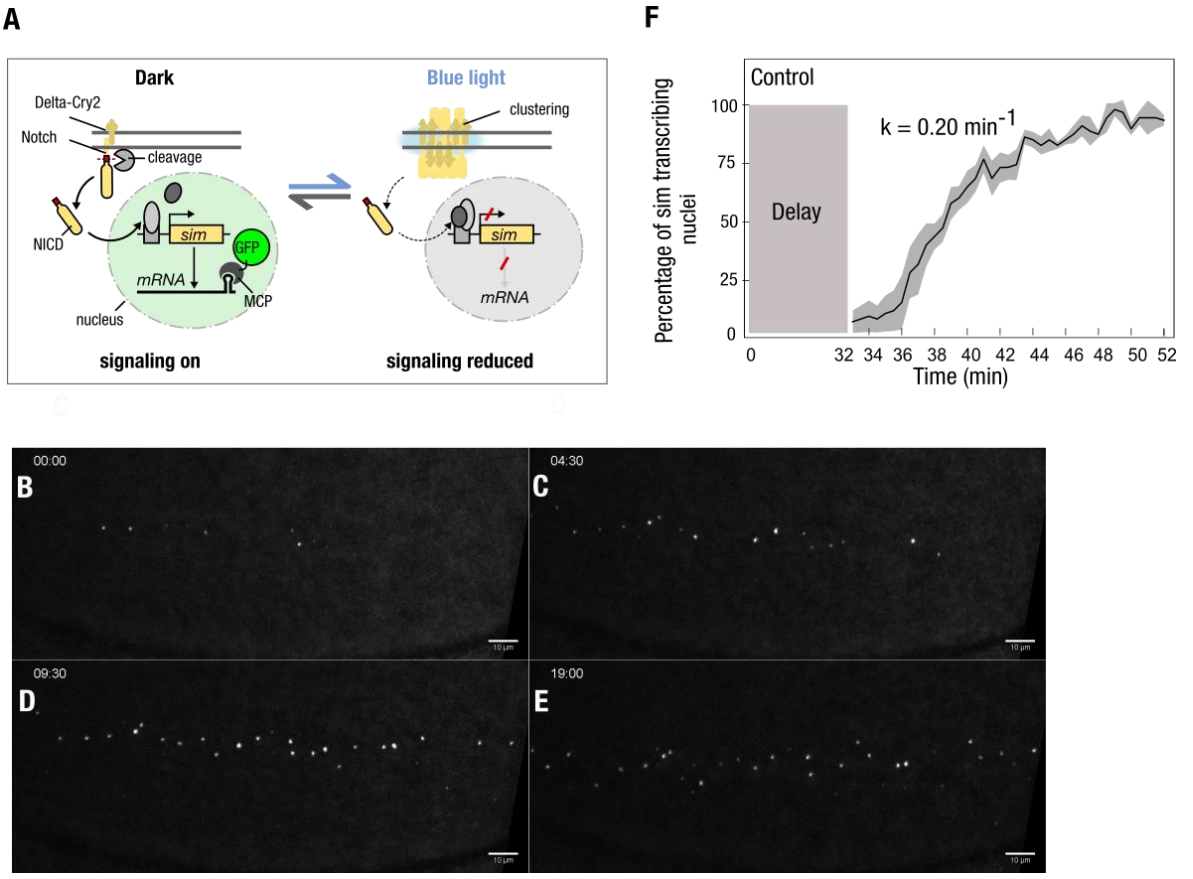

Figure 17: Live tracking of sim transcription reveals gradual activation of nuclei after a delay.

(A) Schematic illustrating the use of light induced Delta::CRY2 clustering in combination with the MCP-MS2 live transcriptional reporter of *sim* expression.

(B-E) Snapshots from a recorded confocal movie over the course of nuclear cycle 14, depicting maximum intensity z-projections of a representative control embryo expressing MCP-GFP and *sim*-MS2. **(B)** represents the onset of sim expression and **(E)** represents the time-point just prior to the onset of ventral furrow formation. Scale bar, 10 µm.

(F) Graph illustrating the gradual onset of s*im* transcription in mesectodermal nuclei during the time-course of nuclear cycle 14 in embryos expressing MCP-GFP and *sim*-MS2. Following a delay of approx. 30 min, *sim* spots began to appear stochastically in the tissue and increased at the rate of 0.2 spots min-1. The rate is calculated by fitting the averaged

curve as shown in Figure 11. Shaded area represents standard error of mean, N = 3 embryos.
This figure (including legend) was generated by me and is part of the submitted manuscript "Optogenetic inhibition of Delta reveals digital Notch signalling output during tissue differentiation" (see Appendix). Panels **(F)** was generated by Pierre Neveu.

20 min of signalling represented the minimum time needed for all nuclei to have an equal probability of turning on *sim* with the same rate as the control embryos. Overall, this experiment also indicates that Notch signalling is continuous during the course of cellularization.

In addition, a significant delay (~10 min) was observed with regard to the onset of sim expression for all the photo-activation conditions ranging from 0 min to 20 min of signalling, suggesting that the timing of sim onset is Notch dependent (Fig. 18E). Genetically reducing Notch levels by 50% using a heterozygous Notch mutant line ($Notch^{55e11}$) resulted in a similar significant delay of sim onset, further validating the results obtained using opto-Delta (Fig. 19B-C). In summary, these results indicate that opto-Delta photo-activation manifests in changes in the activation kinetics of *sim* expression, that are compatible with reduced levels of Notch activity.

As opposed to this gradual mode of *sim* activation at the tissue level, at the level of individual nuclei a contrasting behaviour was observed. *sim* spots were either present or absent and once on, their intensity remained relatively stable, fluctuating around the mean value right from the time point they came on till the onset of gastrulation. Over time, the spot intensity varied by ~20%, a number that was smaller than the variation of ~75% in spot intensity for a given time point (Fig. 18F). This result was further confirmed by fluorescent *in situ* hybridization of wildtype embryos fixed at different timepoints across cellularization (Fig. 19D-I).

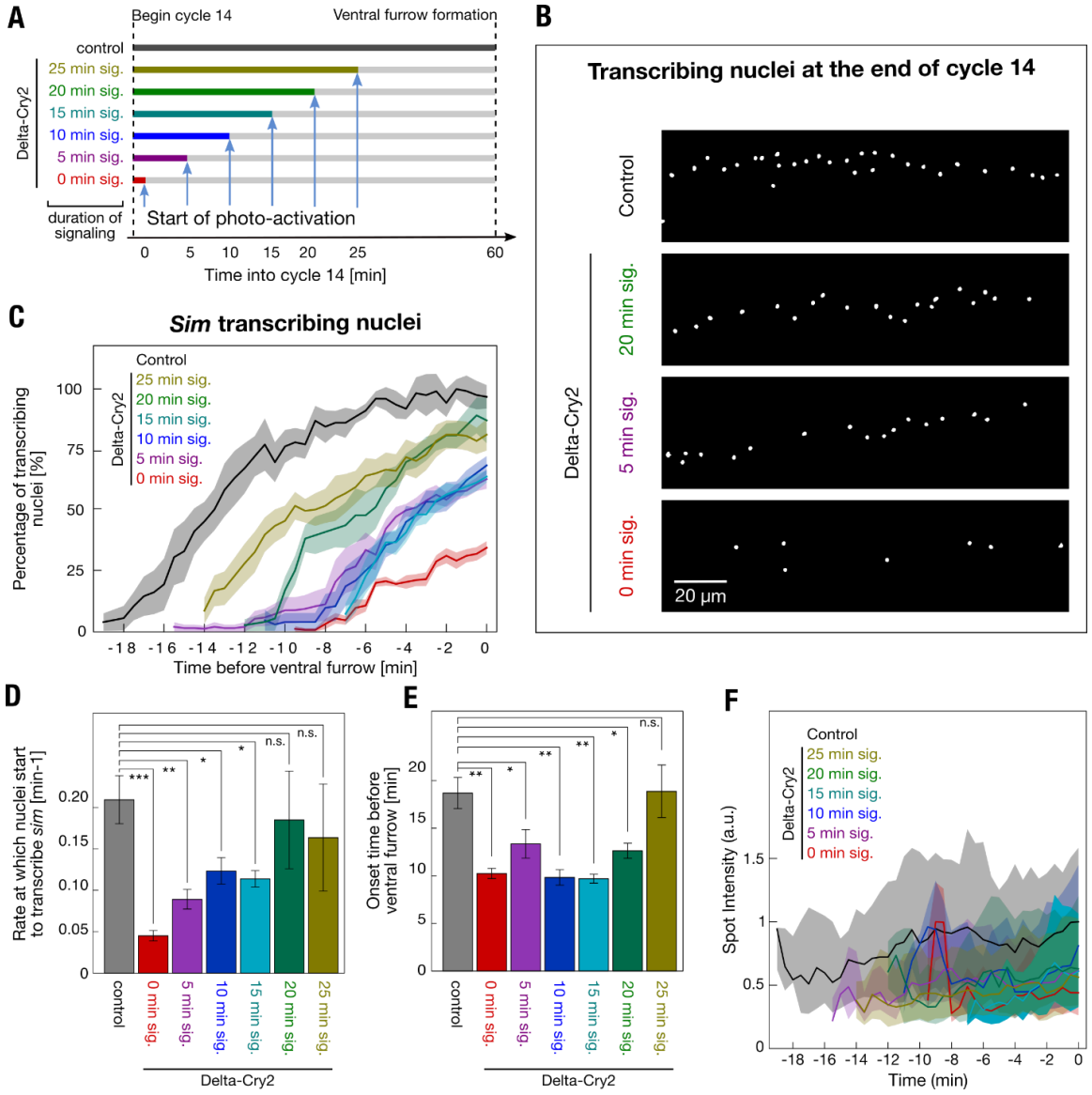

Figure 18: Optogenetic inhibition of Notch signalling reveals time-integrated digital regulation of target gene expression.

(A) Schematic representing the optogenetic experiments presented in (B-F) where different periods of signalling were allowed from the onset of cycle 14 (0/5/10/15/20/25 min) prior to beginning of photo-activation in embryos expressing Delta::CRY2, MCP-GFP and *sim*-MS2. **(B)** Segmentation of MCP-GFP positive nuclear spots from confocal movies at the final time-points acquired prior to ventral furrow formation in either control (non-Delta::CRY2) embryos which were photo-activated for 60 min or Delta::CRY2 embryos in which signalling was allowed for either 20 min, 5 min, 0 min. Scale bar, 20 µm.

(C) Plot depicting the percentage of *sim* transcribing nuclei over time (with respect to control embryos) during the different time-periods of photo-activation. The onset of ventral furrow

formation is considered as t = 0 min. N = 5 embryos for control, 0 min sig. and 15 min sig.; N = 6 embryos for 10 min sig. and 20 min. sig.; N = 7 embryos for 5 min. sig. and 25 min. sig. Shaded area represents standard error of mean.

(D) Bar plot showing the gradual increase in the rate at which mesectodermal nuclei start to turn on *sim* (*sim* spot density/min) as the duration of signaling increases from 0 min to 25 min as depicted in **(A)**. The dataset used for quantification is the same as that used in **(C)**. *p ≤ 0.05, **p ≤ 0.01, ***p ≤ 0.001, n.s. represents no statistically significant difference in a 2-sample t-test. Error bars denote standard error of mean.

(E) Bar plot showing that onset *sim* transcription is significantly delayed compared to control embryos as the duration of signalling is increased from 0 min to 20 min. After 25 min of signalling there is no significant delay. The dataset used for quantification is the same as that used in **(C)**. *p ≤ 0.05, **p ≤ 0.01, ***p≤ 0.001, n.s. represents no statistically significant difference in a 2-sample t-test. Error bars denote standard error of mean.

(F) Graph showing that gradually increasing the time-period of active signaling from 0 min to 25 min does not change the mean spot intensity of *sim* transcripts compared to controls. There was only a 20% variation in spot intensity over time, a value that was smaller than the ~75% variation in spot intensity for a given time point. The dataset used for quantification is the same as that used in **(E)**. Shaded areas represent the interquartile range.

This figure (including legend) was generated by me and is part of the submitted manuscript "Optogenetic inhibition of Delta reveals digital Notch signalling output during tissue differentiation" (see Appendix). Plots in panels **(C-F)** were generated by Pierre Neveu.

This result indicates that the cumulative amount of activated Notch determines the competence to express *sim* in mesectodermal nuclei.

When the duration of signalling was gradually increased from 5 min to 25 min by photo-activation, despite the increase in the number of *sim* nuclear dots, their mean nuclear intensity from the time point they first became detectable until the end point of imaging did not change significantly (Fig. 18F). This result supports a digital mode of signalling activation by Notch.

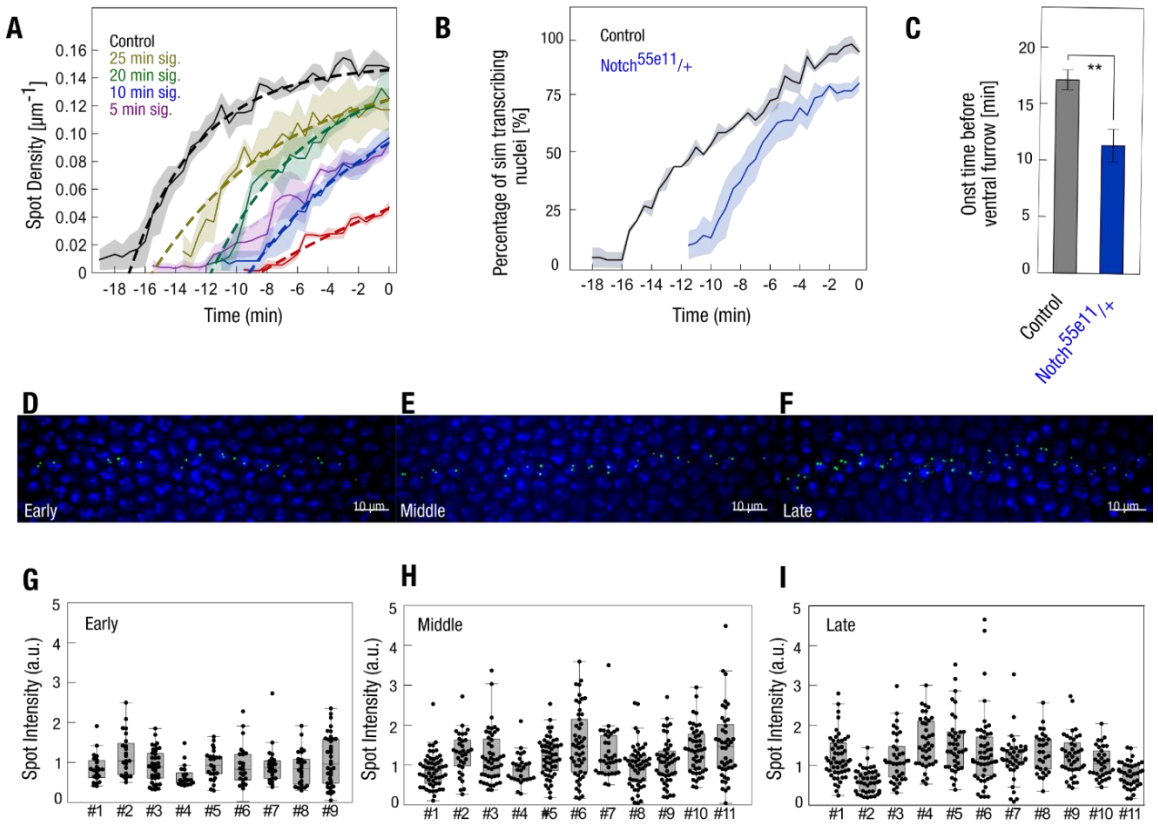

Figure 19: Quantification of sim transcription during mesectoderm specification.

(A) Fitting of *sim* spot-density curves for estimation of activation rates and delays. The average spot density curves (number of sim spots/ unit length of embryo, µm-1) for each condition (control/ 25 min/ 20 min/ 15 min/ 10 min/ 5 min/ 0 min signaling) corresponding to Fig. 4E were adjusted by Nmax (1-exp(-*k* (t-t0)), where Nmax is the maximum number of spots that can be activated (i.e. the number of nuclei in the mesectoderm), *k* is rate at which mesectodermal nuclei start to transcribe *sim* and t0, the delay in the onset of spot appearance with respect to the control. Nmax was taken as constant and only two parameters *k* and t0 were adjusted for each curve.

(B-C) Reducing the copy-number of Notch results in a delay of *sim* transcription.

Plot depicting the percentage of *sim* transcribing nuclei over time in embryos carrying one mutant allele of Notch, Notch55e11 compared to controls **(B)**. Bar plot showing that onset of *sim* spot detection in Notch55e11 heterozygous embryos is significantly delayed compared to controls **(C)**. The onset of ventral furrow formation is considered as t = 0 min. N = 3 embryos for both conditions. **p ≤0.01, two-sample t-test. Shaded area and error bars represent standard error of mean.

(D-I) Fluorescence-in-situ-hybridization of *sim* transcription. Representative maximum-intensity z-projections depicting nascent *sim* transcripts (green) in the mesectoderm in wild-

type (w1118) embryos staged as early **(D)**, middle **(E)** and late **(F)** during cellularization, as described in the methods section. Nuclei were stained with DAPI (blue). **(G-I)** Scatter plots showing the quantification of nascent *sim* transcripts across wild-type embryos during early (G), middle (H) and late cellularization (I). There was only a 25% variation in sim spot intensity between time points, a value that was smaller than the ~40% variation in sim spot intensity within single embryos.
This figure (including legend) was generated by me and is part of the submitted manuscript "Optogenetic inhibition of Delta reveals digital Notch signalling output during tissue differentiation" (see Appendix). Plots in panels **(A-C)** and **(G-I)** were generated by Pierre Neveu.

The distinct relationship of Notch input on *sim* output at the cell and tissue level can be summarized as follows. At the individual cell level, the results suggest a switch like mechanism where the cumulative amount of Notch activation determines the competence of mesoectodermal nuclei to express *sim*, indicating the existence of a minimum threshold as opposed to a graded input output relationship as described for other signalling systems (as introduced in section 1.2.1). Above this threshold, changing notch activity does not affect *sim* expression. On the other hand, at the tissue level, the level of Notch input determines the frequency of turning on mesectodermal nuclei, thus exhibiting an analog mode of regulation. Finally, the timing of *sim* onset is also Notch dependent and this contributes to the delay between Notch activation during early cellularization and *sim* expression. Cumulatively, this suggests a model where the Notch signal is integrated over time in a digital fashion during tissue differentiation.

3A.2 Generation of an optogenetic tool to activate Notch signalling - opto-Notch

Given the existence of a threshold for Notch target activation, I was interested in understanding the minimum amount of Notch activation required to overcome it. Is a continuous mode of signalling necessary for *sim* activation or can the entire signal be delivered in a single pulse/ pulses? For this, I needed a direct control over the Notch input and hence I decided to develop a tool to activate Notch signalling *in vivo* by directly controlling the nuclear entry of the Notch intra-cellular domain (NICD). I decided to employ the optogenetic dissociation system, LOVTRAP in order to control NICD sequestration and release (Wang et al., 2016). LOVTRAP is a two component system consisting of a small peptide called Zdark (Zdk) that binds to the photosensitive LOV2 domain in the dark and is released upon photo-activation. Given the advantages of its fast kinetics (in the seconds scale), reversible mode of action, and tunable activation, this system seemed ideal to dynamically control NICD.

The strategy employed was as follows: The LOV2 domain was fused to a mitochondrial localization sequence (Mito-LOV2) to serve as the anchor, and NICD (aa 1790-2703) was tagged with the peptide Zdk1 (Zdk1-NICD). I generated fly lines expressing these two constructs and then genetically combined them to check for sequestration and release of NICD upon photo-activation (Fig. 20A, B).

I first tested whether the Zdk1-NICD construct functionally reconstitutes a Notch gain of function phenotype in the embryo. Imaging the fluorescently tagged version of the protein, mCherry-Zdk1-NICD (opto-Notch) confirmed that the subcellular localization of NICD was nuclear. These embryos did not hatch into larvae, consistent with previous studies.

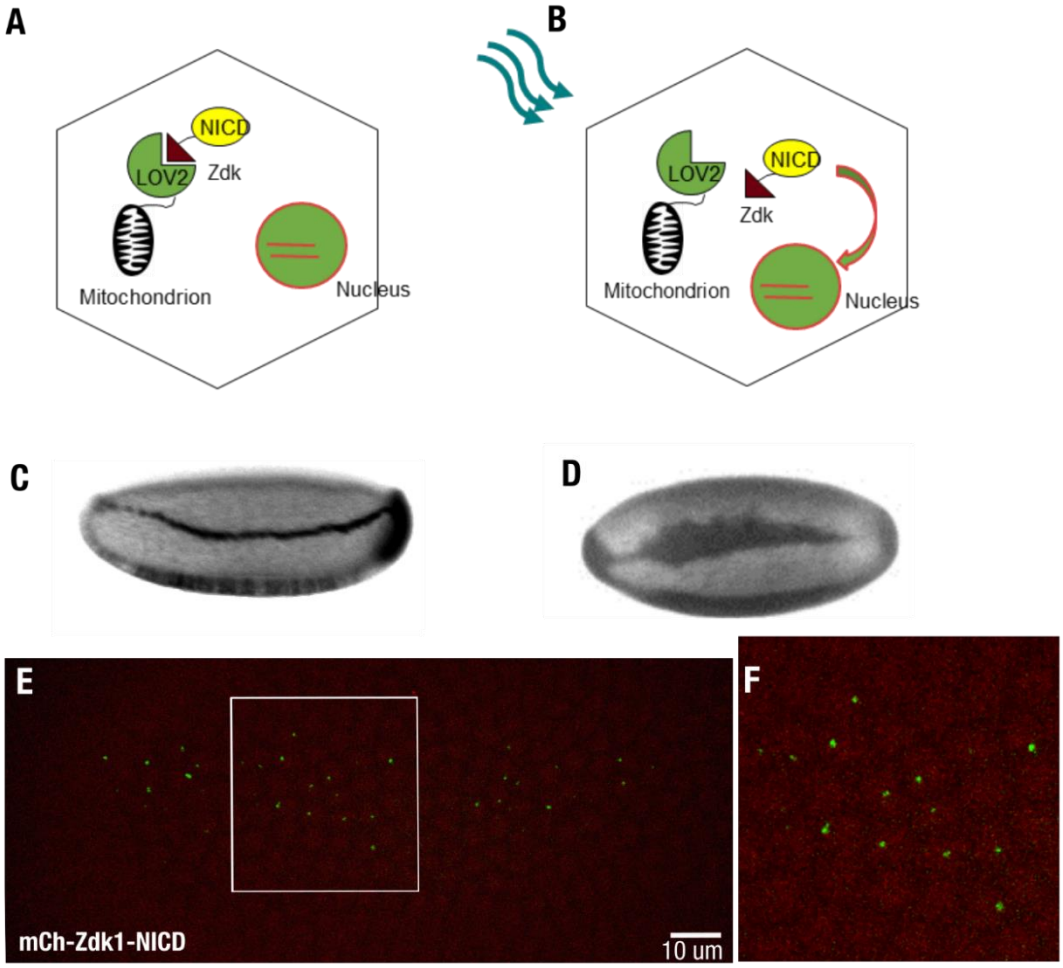

Figure 20: Optogenetic approach to activate Notch signalling and characterization of opto-Notch.

(A, B) The LOV2 domain is tagged with eGFP and is localized to the mitochondrial membrane using a drosophila mitochondrial targeting sequence (Tom-20). This serves as the anchor for NICD that is tagged to the LOV-2 binding peptide Zdk1. In the dark, Zdk1-NICD interacts with Mito-LOV2, to be sequestered at the mitochondria **(A)**, and upon blue light photo-activation is released to activate its transcriptional targets in the nucleus.
(C-F) Testing the functionality of mCherry::Zdk1::NICD. Both in-situ hybridization for *sim* **(D)** and using the live MCP-*sim*MS2 reporter (**E**, Magnified region **(F)**) showed an expansion of *sim* expression to 3-4 rows of cells as opposed to the single row in wildtype controls **(C)**, indicating a Notch gain of function. Scale bar, 10 µm.

Both in-*situ* hybridization against *sim* and combining opto-Notch with the MCP-*sim*-MS2 system for live imaging showed a clear expansion of the domain of *sim* expression to a 3-4 rows of cells representing the characteristic Notch gain of function phenotype (Fig. 20C-F). I then imaged embryos expressing both the anchor, Mito-LOV2 and opto-Notch without photo-activation in order to observe its localization. In the early embryo, during the mitotic phase of the nuclear division cycles 10-12, opto-Notch co-localized with the mitochondrial anchor, suggesting interaction in the dark (here dark refers to non-blue light photo-activated). Upon photo-activation with the 488 nm laser, after 30 s, opto-Notch was released from the mitochondria (Fig. 21A-F) and 2 min. post photo-activation, appeared to localize to the mitochondria again, showing the reversible nature of the tool (Fig. 21G). These results indicated the functionality of this tool *in vivo*.

However, despite being imaged without photo-activation though the nuclear division cycles 10 to 14, opto-Notch was distributed in two pools – mitochondrial during the mitotic phase and nuclear, as soon as the nuclear membrane assembled prior to the onset of interphase. As the embryo developed from cycle 10 to 14, the mitochondrial pool gradually decreased, and by cycle 14 and thereafter, the opto-Notch was almost entirely nuclear (Fig. 22A-E). This could be because NICD molecules enter the nucleus and potentially associate with other factors to get trapped incrementally over time. As cycle 14 is the stage during which I am interested in activating opto-Notch to study ectopic *sim* expression, the tool in its existing state was unusable.

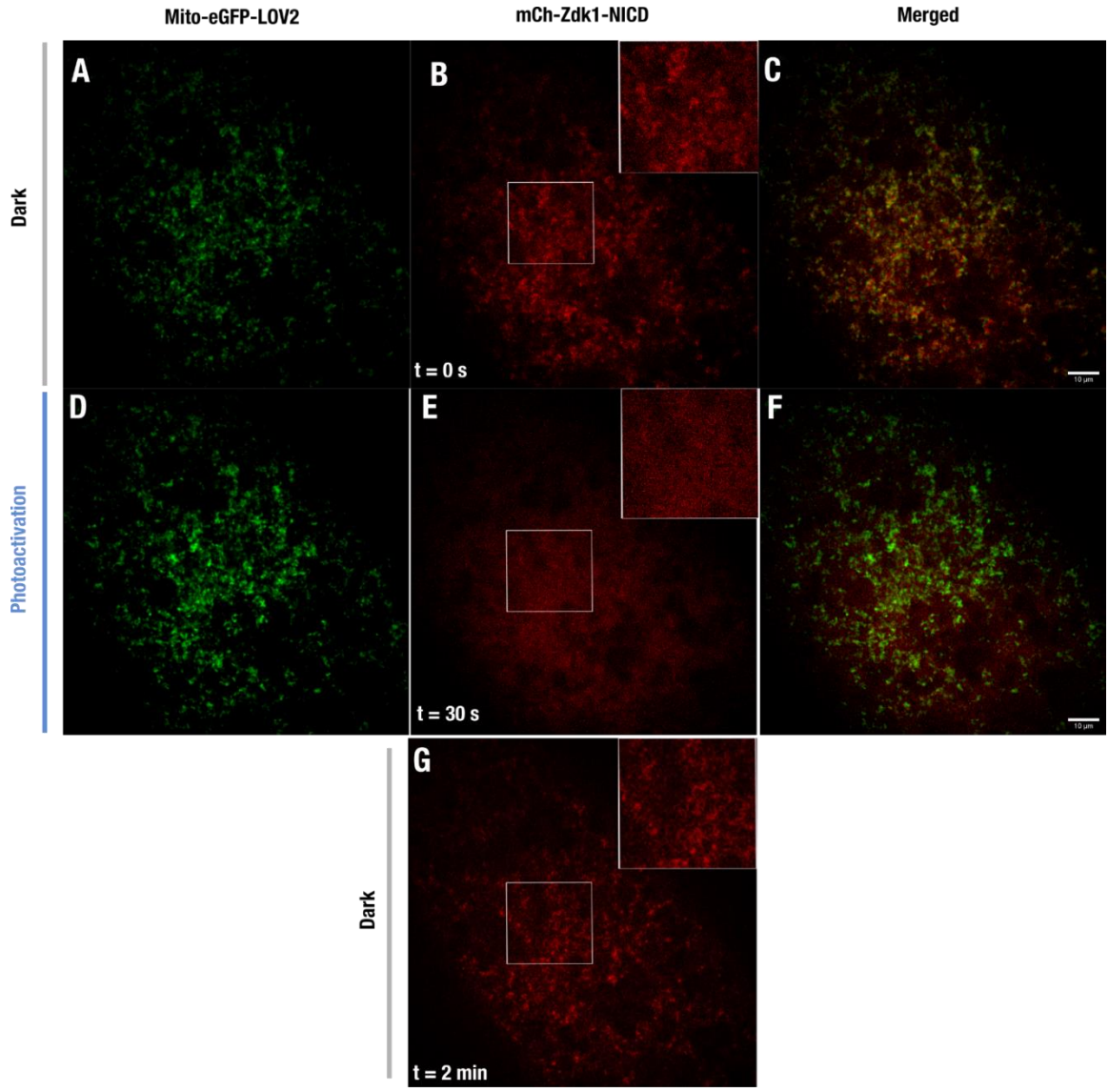

Figure 21: Characterizing the tool to activate Notch.

(A-G) Maximum intensity z-projections of embryos co-expressing Mito::EGFP::LOV2 **(A, D)** and mCherry::Zdk1::NICD **(B, E, G)** and imaged prior to photo-activation **(A-C)**, immediately after photo-activation with three z-stacks (λ= 488 nm, 0.6 mW) lasting 8 s each **(D-F),** or 2 min. after photo-activation **(G)**. Magnified inset in **(B)** and colocalization with Mito-GFP-LOV2 in **(C)** indicate mitochondrial sequestration of mCherry::Zdk1::NICD in the dark. Photo-activation results in subsequent release into the cytoplasm after 30 s (Magnified inset in **(E)**). Placing the embryo in the dark for 2 min. post photo-activation results in re-localization of mCherry::Zdk1::NICD to the mitochondria, indicating reversibility of the tool **(G)**. Scale bar, 10 µm.

To overcome this issue, I decided to add a constitutive Nuclear Export Sequence (Smad4 NES) to opto-Notch in an attempt to ensure that the protein that enters the nucleus in the dark is actively extruded back to the cytoplasm. This resulted in an increase in the cytoplasmic fraction of opto-Notch during the stages of cellularization and beyond, and there was a significant pool that was bound to the mitochondria.

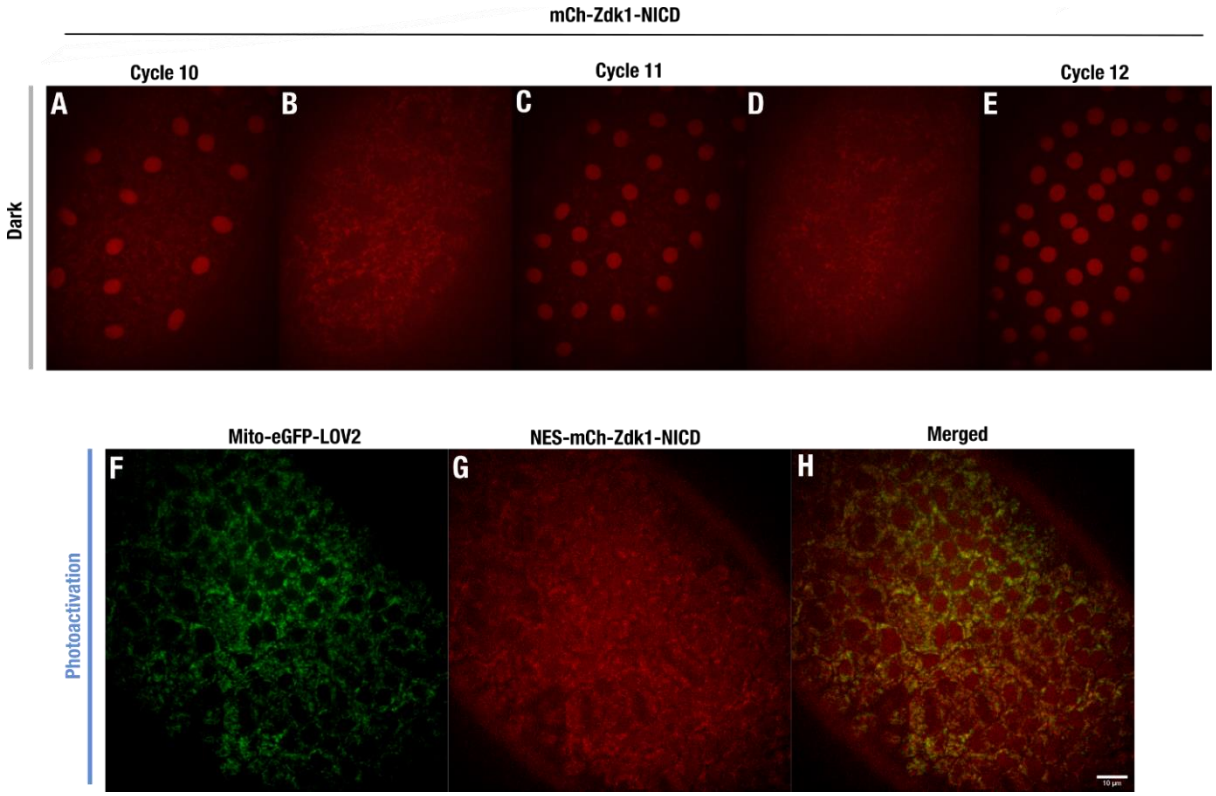

Figure 22: Pitfalls of opto-Notch and effort towards optimization.

(A-E) Maximum intensity z-projection of an embryo co-expressing Mito::EGFP::LOV2 and mCherry::Zdk1::NICD, imaged without photo-activation through nuclear division cycles 10 to 12. mCherry::Zdk1::NICD localized to the nucleus during the interphase of each nuclear division cycle, indicating dark state activity.

(F-H) Addition of a nuclear export sequence (NES) to mCherry::Zdk1::NICD in order to counter dark state activity. Maximum intensity z-projection of an embryo co-expressing Mito::EGFP::LOV2 **(F)** and NES-mCherry::Zdk1::NICD **(G)** during nuclear cycle 14. While the addition of NES increases the cytoplasmic fraction, there still exists a significant nuclear fraction **(H)**, necessitating further optimization.

However there still existed a fraction of opto-Notch that was visible in the nucleus in the dark suggesting that the endogenous NLS of Notch was overpowering the NES (Fig. 22F-H). Currently, experiments are underway towards further optimizing this tool, and these have yielded some promising results. However, since the results are preliminary, they are beyond the scope of this thesis and I will briefly discuss the approaches used in the ‘Discussion’ chapter.

3B. Results – part 2

In this section I describe the further characterization of opto-Delta as a tool – to spatially perturb signalling, to study Notch driven neuroblast delamination and to induce *cis* complexes of Notch and Delta in mammalian cell culture.

3.1.6 Spatially localized inhibition of Notch signalling using opto-Delta

Optogenetics also offers the unique advantage of enabling perturbations over space by restricting the region of photo-activation and I therefore attempted to achieve spatial control over Notch signalling. By employing a two-photon based activation protocol in cellularizing embryos (Guglielmi et al., 2015), I managed to induce Delta-clustering with sub-cellular precision (Fig. 23A). I could show that Delta clustered only in the area of illumination while neighboring non-illuminated cells displayed uniform Delta localization at the plasma membrane. I then tested if this results in loss of signalling by photoactivating embryos locally in a 6-7 wide stripe during the entire course of cellularization and again using the MCP-MS2 system to visualize *sim* transcription. I used MCP::mCherry instead of MCP::GFP as the 2-photon illumination protocol caused significant bleaching of sim spots in non-opto Delta controls. The experiment resulted in a spatially precise inhibition of *sim* transcription matching the localized region of activation (Fig. 23B) and proves that opto-Delta can be used as a tool to spatially perturb Notch signalling.

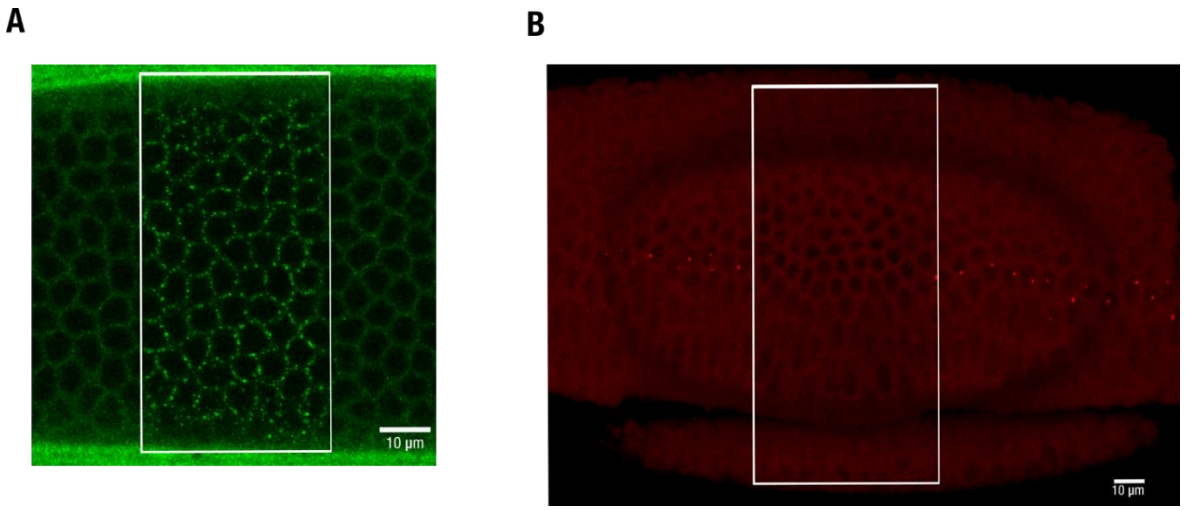

Figure 23: 2-photon mediated local activation of opto-Delta results in spatial inhibition of signalling.

(A) Patterned 2-photon based activation in a defined region (white box) on cellularizing embryos expressing Delta::GFP::CRY2 results in delta clustering, spatially restricted to the region of activation.

(B) Maximum intensity z-projection of an embryo at the onset of ventral furrow formation, expressing MCP::mCherry, *sim*-MS2 and Delta::CRY2. Periodic 2-photon based photo-activation was performed in a defined region (white box) from the onset of cycle 14 (see Methods) and this resulted in the localized inhibition of sim expression in the region of activation. Scale bar, 10 µm.

3.1.7 Using opto-Delta to study neuroblast delamination in the embryonic neurectoderm

As another readout of Notch signalling in the early embryo, I managed to image over time the Notch-dependent process of neuroblast delamination. Neuroblast delamination is a process that begins around 30 mins post ventral furrow formation in the neuroectoderm tissue (that represents a row of 8-9 cells wide from the ventral midline). Clusters of cells in the neuroectoderm express a set of proneural genes and all have the potential of becoming neuroblasts. By the process of lateral inhibition mediated by Notch signalling, one cell in the proneural cluster (the signal sending cell)

becomes the delaminating neuroblast and the other surrounding cells in the cluster that receive the Notch signal remain epithelial cells (Hartenstein and Campos-Ortega, 1984) (see section 1.3.2). Previous studies have shown that in embryos with lowered Notch signalling activity (DelaRNAi or NotchRNAi embryos), clusters of cells adopt neuroblast fate, and eventually all undergo delamination (An et al., 2017; Simões et al., 2017). To test if the opto-Delta embryos also behaved in a similar fashion, I generated lines where I combined opto-Delta with a membrane marker GAP43-mcherry in order to visualize and quantify cell shape changes (Fig. 24A, C). Photoactivation was started immediately after ventral furrow formation and the embryos were imaged over the course of an hour to observe the cell delamination behaviour. Consistent with the observation in the Delta/Notch RNAi embryos, I observed clusters of cells (3-6 in number) that gradually reduced their apical area and eventually delaminated either simultaneously or in a sequential fashion (Fig. 24B, D).

I quantified the decrease in the apical surface area over time, and observed that the rate at which the group of cells delaminated was slower than the normal single cell delamination in the wildtype by approximately a factor of 2, which is also consistent with previous studies. This experiment further confirms the role of Opto-Delta as a loss of function allele in different tissue contexts during *Drosophila* development.

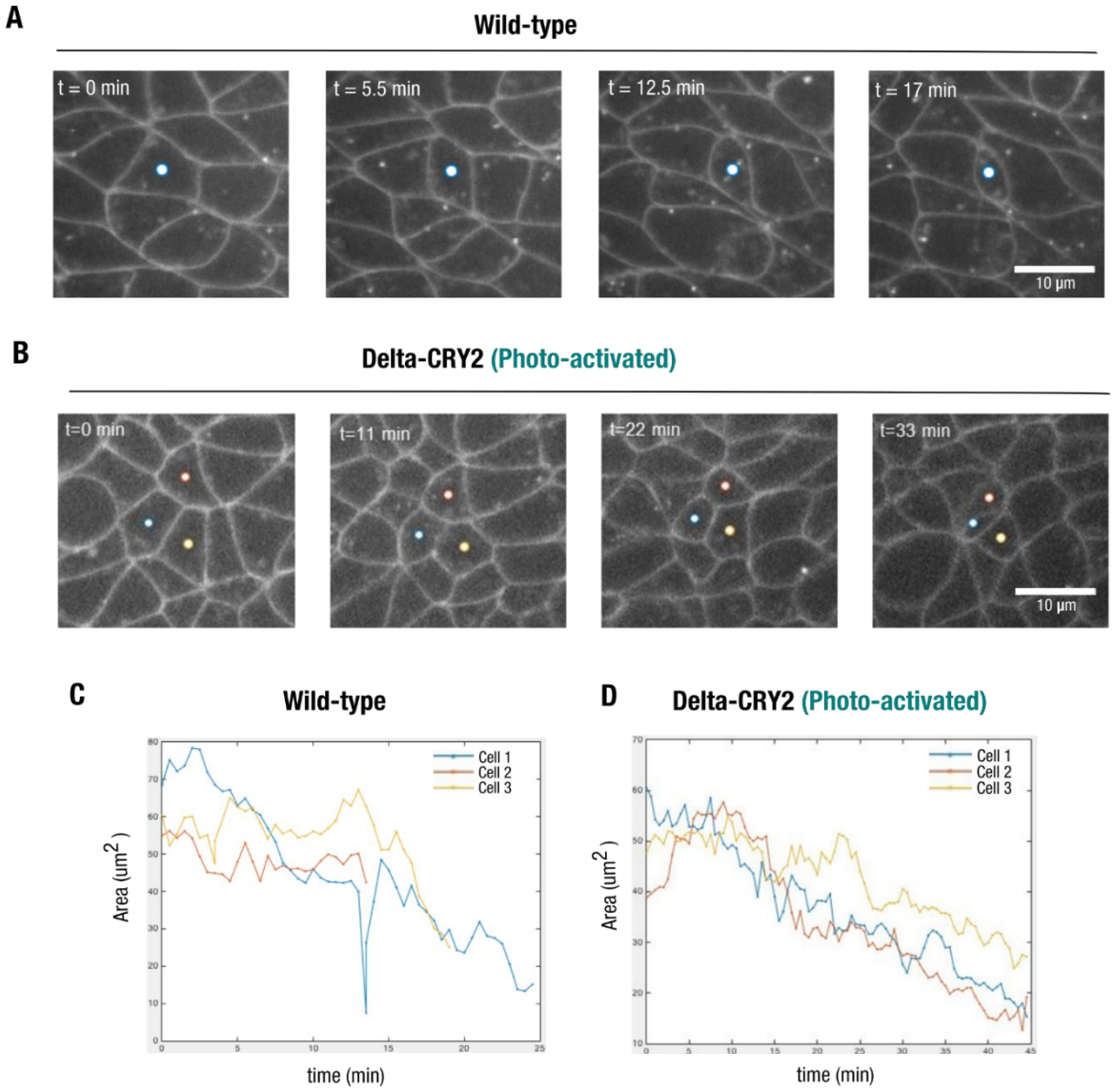

Figure 24: opto-Delta activation affects neuroblast delamination in the neurogenic ectoderm

(A) Single plane confocal snapshots of wildtype embryos expressing a membrane marker (gap43::mCherry), showing the time-course of neuroblast delamination in the embryonic neurectoderm. The apical area of the delaminating neuroblast undergoes gradual reduction over a period of ~20 min. as quantified in **(C)**. Scale bar, 10 µm.

(B) Single plane confocal snapshots of embryos expressing Delta::CRY2 and a membrane marker (gap43::mCherry). Photo-activation for a duration of 5 s (λ= 488 nm, 0.6 mW) and at a frequency of 1 min. over the period of an hour, resulted in the delamination of clusters of neuroblasts in the tissue. The apical area of the delaminating group of neuroblasts undergo gradual reduction over a period of ~40 min. (slower than the wildtype) as quantified in **(C)**. Scale bar, 10 µm. Panels **(C)** and **(D)** were generated by Emiliano Izquierdo.

3.1.8 Characterization of opto-Delta as a tool in mammalian cell culture

In order explore if opto-Delta based clustering could be used as a tool across species, and to further establish its mode of functionality, I decided to use mammalian cell culture as a system. For this, I generated a Mouse Delta-like 1 construct tagged with CRY2 (DLL1::mCherry::CRY2) which was then expressed in HeLa cells. Imaging the cells 48 hrs after transfection, I observed uniform distribution of Delta (DLL1::mCherry::CRY2) on the plasma membrane, that upon photo-activation underwent rapid clustering (t = 40 s, Fig. 25A, B). I then generated a Mouse Notch-1 construct (Notch-1::YFP) with the goal of co-expressing it in HeLa cells along with DLL1::mCherry::CRY2, in order observe the change in distribution of Notch upon light-induced Delta clustering. Possibly due to the addition of a YFP tag (~27 kDa) to an already large Notch protein (>270 kDa), Notch-1::YFP underwent faulty biosynthesis and a major portion accumulated in intracellular structures rather than at the plasma membrane. As an alternative strategy, I decided to fuse Notch extracellularly with a Myc tag which is smaller in size (~1.2 kDa), and visualize the protein using antibody staining against Myc post photo-activation and fixation. I adapted a protocol (Hinners et al., 1999) to specifically stain Notch at the plasma membrane in order to be able to distinguish membrane clusters from intracellular vesicles in close proximity to the membrane. Imaging isolated cells fixed in the dark, both Notch and Delta exhibited a relatively uniform plasma membrane distribution (Fig. 25C-E).

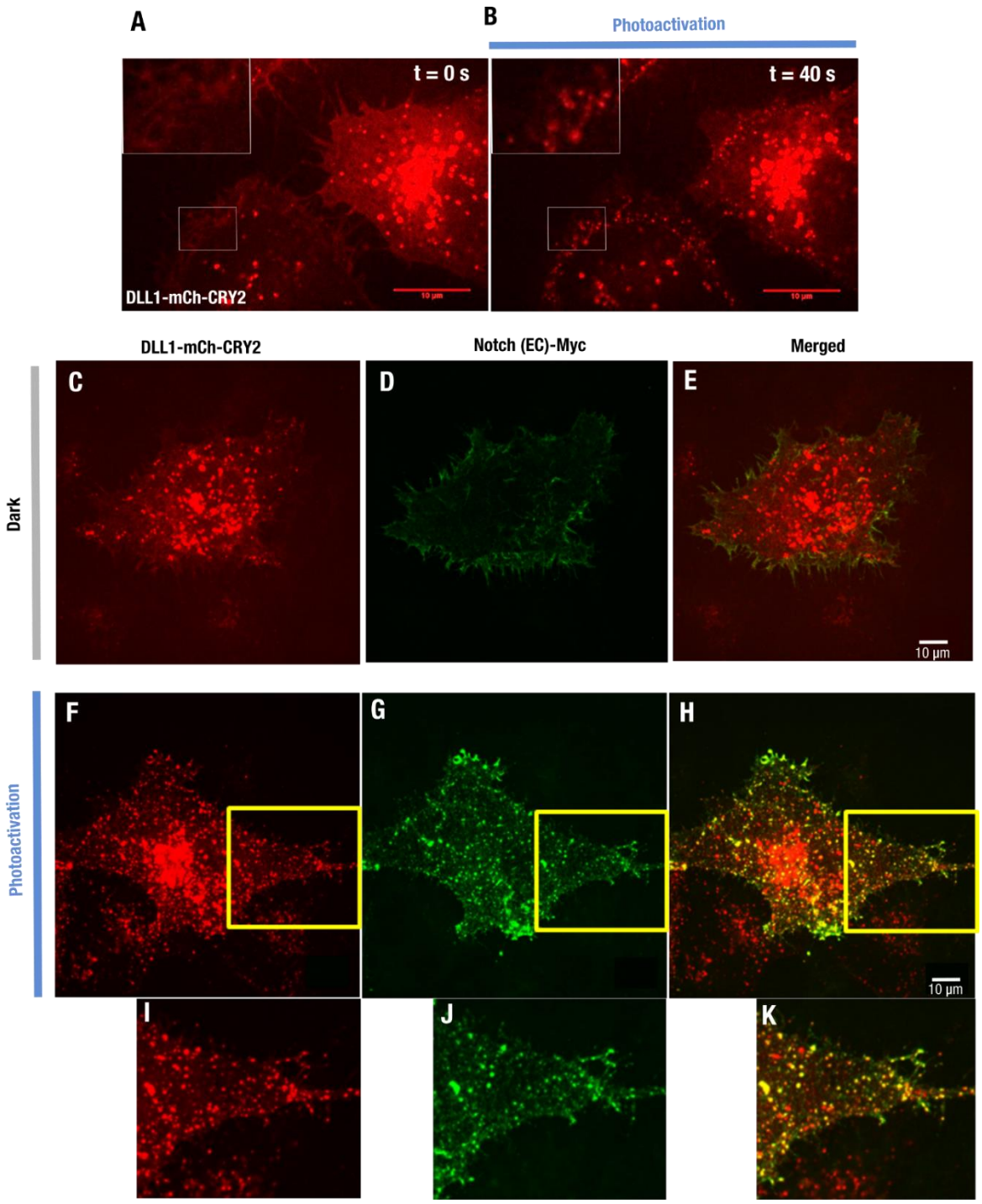

Figure 25: opto-Delta undergoes light induced clustering in mammalian cells and engages Notch in cis

(A,B) Confocal images of a HeLa cell expressing DLL1::mCherry::CRY2 showing uniform distribution of plasma membrane Delta before photo-activation **(A)** and distributing into clusters after four rounds of photo-activation **(B,** t = 40 s**)** with z-stacks (λ= 488 nm, 0.6 mW) lasting 5 s each. Scale bar, 10 µm.

(C-K) Immunostaining for extracellular Notch in HeLa cells co-expressing DLL1::mCherry::CRY2 and Notch-Myc, fixed in the dark **(C-E)** or after photo-activation **(F-**

H). Magnified insets **(I-K)** show plasma membrane clusters of Delta **(I)** co-clustering with Notch **(J)** and the merged image in **(K)**. Scale bar, 10 µm.

Upon photo-activation, Notch appeared clustered on the plasma membrane and exhibited a co-localization with Delta clusters, suggesting that activated DLL1::mCherry::CRY2 is capable of binding Notch::Extra::Myc in *cis* (Fig. 25F-K). Whether Notch-Delta co-clustering results in lack of signalling in the context of mammalian cells remains to be tested. This can be understood by co-transfecting these cells with reporters of Notch activity.

In summary I have demonstrated the use of opto-Delta as a tool to induce Delta clustering and interactions with Notch receptors *in cis* and potentially its utility as a tool to inhibit Notch signalling in mammalian cells/tissues.

4. Discussion

As part of this thesis, I have developed one of the first endogenously tagged optogenetic tools to perturb signalling *in vivo*, replacing the endogenous allele with a light responsive one. I have shown that rearing opto-Delta flies in the light results in Notch/Delta loss of function phenotypes during different stages of *Drosophila* development, suggesting that it can be used as a tool to acutely inhibit signalling. Characterization in cellularizing embryos revealed that opto-Delta undergoes rapid light-induced clustering at the plasma membrane, but still exhibited normal trafficking in the mesoderm. Notch showed decreased trans-endocytosis and increased retention at the plasma membrane, suggesting impaired binding of Delta clusters to Notch in *trans.* However, since Notch clusters formed in the signal receiving mesectodermal cells, it was equally plausible that signalling was affected due to binding of Delta clusters in *cis*. In order to distinguish these two scenarios, I turned to the pupal notum tissue, and clonal analysis revealed a strong bias towards the impaired signal receiving capacity of Notch in cells expressing opto-Delta under photo-activated conditions, compared to the signal sending ability of Delta, which was relatively unaffected. This led to the conclusion that light-induced clusters of opto-Delta bind Notch in *cis* and this results in signalling inhibition.

4.1 Notch exhibits a time-integrated switch-like mode of activation during mesectoderm specification

In order to study the dynamic input-output relationship of Notch and its targets, I focussed on the process of mesectoderm specification in the cellularizing *Drosophila* embryo. The opto-Delta tool was combined with a live transcriptional reporter for target

gene *sim* (based on the MS2-MCP system) in order to visualize nascent transcription upon Notch activation in real time.

In summary, the results show two different relationships between Notch input and *sim* output. At the cellular level, as the levels of Notch increase over the course of cellularization, Notch acts in the manner of a switch, with *sim* expression turned on in the nucleus depending on whether a minimum threshold of Notch activity is crossed. Once on, sim expression remains stable over time and is unaffected by changes in Notch activity above the threshold. At the tissue-level, an analog mode of regulation is observed, with the level of Notch activity determining both the timing of onset, and the frequency at which individual mesectodermal nuclei express *sim*.

Taken together, the data point towards a model where the Notch receptor integrates noisy, analog signals over time in order to generate a digital switch-like behaviour. Such a manner of regulation could be essential in making certain that all mesectodermal nuclei turn on *sim* before gastrulation begins. During T-cell specification, a similar mode of regulation by Notch has been observed. Changing Notch levels in cultured T-cell progenitors increases the number of cells expressing Notch target Bcl11b, but not the expression levels per cell (Kueh et al., 2016).

Physiologically, such a non-linear mode of regulation where a threshold needs to be reached in order to produce the output, can serve the advantage of making the signalling robust to fluctuating inputs (Mc Mahon et al., 2014)(as described in section 1.2.1). In the early embryo, during the Notch mediated process of mesectoderm specification, there are multiple dynamic morphogenetic events occurring in parallel. Membrane trafficking, changes in plasma membrane composition and precisely timed expression of zygotic factors together regulate cortical actomyosin contractility that drives the process of cellularization (Fabrowski et al., 2013; Krueger et al., 2019).

Furthermore, at the end of cellularization, cells start to undergo a series of cell shape changes at their apical and basal ends resulting in tissue wide coordinated movements that culminate in the process of mesoderm invagination giving rise to the ventral furrow (Sweeton et al., 1991). Both these processes involve dynamic movements of these interconnected cells along all three axes. In this context, one could speculate that adopting such a mode of operation whereby Notch requires to overcome a threshold can help to counter spurious target gene expression resulting from transient cell-cell contacts during these morphogenetic movements.

The molecular mechanism underlying this digital switch-like behaviour is unclear. As introduced in section 1.2.1, such non-linear responses are commonly the manifestation of having either a positive feedback or ultra-sensitivity, where when the threshold is overcome, very small changes in input-signal concentration can result in step changes in activity (Sagner and Briscoe, 2017). With regard to the activation of *sim*, this regulation could potentially be encoded either at the level of architecture of the *sim* promoter/ enhancer, or by the presence of repressors that need to be overcome by a cumulative amount of Notch activity.

The *sim* gene contains two promoters – early and late. The early promoter is active during stage 5 of embryonic development, when Notch signalling occurs. This promoter is positively regulated by activated by Dorsal, Twist and Notch signalling in mesectodermal cells and is inhibited by Snail. The necessity of these upstream regions for *sim* expression has been established by mutagenesis experiments. The *sim* late promoter is only active following stage 8 onwards following mesoderm invagination. From this stage onwards, *sim* expression maintained by the presence of a positive feedback loop, via *sim* autoregulation and this is thought to occur in a Notch independent fashion (Morel and Schweisguth, 2000). Hence as there is currently no

evidence for *sim* autoregulation during stage 5 when the early promoter is active, we can potentially rule out positive regulation as a source of the threshold response.

In the absence of Notch, the DNA binding CSL molecule Suppressor of Hairless (Su(H)) acts as a repressor of Notch target genes by recruiting co-repressor molecules to their regulatory regions. Upon activation, NICD enters the nucleus and converts Su(H) from a repressor to an activator, thus playing the dual role of simultaneously alleviating repression and activating transcription (Morel and Schweisguth, 2000)(Kopan and Ilagan, 2009). The number, affinity and orientation of the Su(H) (CSL in general) binding sites upstream of Notch target genes has been shown to determine their activation (Bailey and Posakony, 1995; Ong et al., 2006). In the *sim* upstream regulatory region, there are 10 binding sites for Su(H), which have been shown to be important for activation of *sim* in mesectodermal cells (Morel and Schweisguth, 2000). Also, looking at the dynamics of NICD and Su(H) in the nucleus using FRAP, a recent study (in *Drosophila* salivary glands) has shown that in the absence of Notch, Su(H) is only transiently bound to DNA (~0.5-2s), and in the presence of NICD, its recruitment and time of residence at promoters of Notch targets is significantly increased (10-15s) (Gomez-Lamarca et al., 2018). Together with these findings, one can hypothesise that in the context of Notch regulation of *sim,* reaching a minimum threshold of Notch receptor activation would be necessary to generate an optimal local concentration of NICD in the nucleus. This could be essential to both increase the residence time of Su(H)-Notch in order to form functional complexes at the regulatory regions and also saturate the Su(H) binding sites. Altering the levels of Su(H) by performing knock down experiments and/or deleting Su(H) binding sites in the *sim* regulatory region could provide insights into its role in this context. In addition Chromatin remodeling, leading to increased enhancer accessibility, was found to be associated with increased Su(H)

occupation time at promoters (Pillidge and Bray, 2019). Whether chromatin modifiers play a limiting role in setting Notch threshold require further experiments. Overall, a better understanding of the principles and mechanisms of Notch target activation in the nucleus will enhance our understanding of how cells interpret dynamic changes in Notch levels during organismal development.

Another observation regarding the activation of *sim* was that once a *sim* spot came on, its intensity remained relatively stable until the initiation of gastrulation movements. This is in contrast with recent studies of transcriptional bursting in the range of 5-10 minutes observed in several signalling genes during nuclear cycle 14 (Bothma et al., 2014)(Fukaya et al., 2016). A comparative study of differences in the architecture of the *sim* enhancer/ promoter with respect to the genes that exhibit bursting activity could provide further insights into this behaviour.

4.2 The role of ligand/ receptor clustering in modulating signalling during development

Using opto-Delta, in this thesis I have demonstrated that light induced clustering of Delta results in inhibition of signalling by interacting with Notch *in cis* rather than *in trans*. Studying the process of cis inhibition *in vivo* has been challenging, and using opto-Delta to generate stable *cis* complexes of Notch and Delta can be a technique to further understand the mechanistic details of the process.

This phenomenon of ligand clustering resulting in signalling inhibition is in contrast to few other signalling pathways involving membrane associated ligands and receptors, where ligand/receptor clustering has been associated with increased signal propagation. Ligand binding triggers Receptor-Tyrosine-Kinase (RTK) dimerization

that allows them to phosphorylate each other and in-turn activate the downstream signalling cascade (Lemmon and Schlessinger, 2010). In T-cells, clustering of the T-cell receptors (TCRs) serves to amplify signalling from the T-cell receptor at the immunological synapse (Davis and Dustin, 2004). In these cases, clustering has been proposed to increase the local concentration of receptors and this could in-turn serve to increase the rate of reaction by increasing chances of interaction with ligands or creating more stable complexes where ligand-receptor interactions are highly dynamic.

With regards to Notch, a potential role of Notch-Delta clustering to distinguish between dynamic modes of signalling in mammalian cells was recently shown (Nandagopal et al., 2018). Their findings indicated that the type of Notch ligand used (mouse DLL1/DLL4) determines whether the signalling elicited is transient or sustained. Ectopic expression of DLL1/DLL4 in chick embryos resulted in distinct cell fates being adopted and further characterization in signal sending cells revealed a significantly more punctate distribution of DLL1-NotchECD vesicles as compared to DLL4-NotchECD which was dispersed. This led them to propose a model where clustering was necessary for the pulsatile activation process mediated by DLL1, although not conclusive.

In the context of *Drosophila*, unpublished data from our lab has demonstrated that activation of Notch signalling in the presumptive mesoderm of the early embryo is associated with formation of clusters of Delta molecules in the plasma membrane. Additionally I have observed that in the pupal notum (16 hrs APF), Delta appears to be distributed in a significantly clustered manner in the plasma membrane across the entire tissue. Immunostaining revealed that these Delta clusters colocalize with the Notch extracellular domain (NECD) (data not shown). While the optogenetic clustering

induced by our system induces *cis* interactions and inhibits signalling, it may not be straightforward to relate this to endogenous Notch-Delta clustering. Whether these rapidly induced optogenetic clusters influence the binding conformation and dynamics of Notch-Delta complexes when compared to an endogenous cluster remains to be explored. Overall, it is tempting to hypothesise that clustering could serve the purpose of regulating signalling dynamics by creating local hubs for either activation of inhibition (via *cis*/ *trans* complexes), and this serves as an exciting question for further investigation.

4.3 Opto-Delta as an endogenously tagged optogenetic tool to control signalling during *Drosophila* development

To my knowledge, opto-Delta is the first optogenetic tool to control endogenous Notch signalling during organismal development. This is a significant addition to a rising number of optogenetic tools that are being developed to perturb/activate and understand principles and mechanisms of signalling pathways in a dynamic fashion *in vivo*. Johnson and colleagues generated an optogentic tool using the iLID heterodimerizing sytem, Opto-SOS to control ERK signalling activation during embryogenesis (Johnson et al., 2017). They discovered that the cumulative amount of signal dictates the switch between endoderm and ectoderm fates, as opposed to the duration or amplitude of signalling. A photoactivable Nodal receptor was created to temporally perturb Nodal signalling and observe the effect on cell fate during zebrafish gastrulation (Sako et al., 2016). Their results demonstrated that the extended duration of signalling in the organizer tissue results in suppression of endodermal cell fate and promotes precordal plate formation. While the above mentioned tools have given rise to novel and significant findings, the expression of the

optogenetically tagged proteins is under the control of inducible/ constitutive promoters or are introduced in the form of mRNA injections. This gives rise to the potentially unfavourable effects of overexpression that can skew our understanding of the developing system in the native context. The opto-Delta tool described in my thesis represents a significant advancement towards addressing this problem; using genome engineering (as described in the Results) both allelic copies of Delta were tagged with CRY2 in their endogenous locus. This ensures that our understanding of the signalling system is as close to the endogenous context as possible and this is especially crucial for a signalling pathway like Notch whose functionality is highly sensitive to the relative levels of ligand/ receptor. As mentioned in section 1.3.3, changing the expression level alone in can bias the directionality of signalling and even the modality of signalling between *cis* and *trans*. Also, this simplifies the genetics by doing away with the need to combine a tissue specific driver in every case. Amongst the few studies that have used optogenetics to manipulate signalling pathways *in vivo*, to my knowledge the only other effort that managed to generate an endogenously tagged optogenetic allele was by Yumerefendi and colleagues where they generated an optogenetically tagged allele of transcription factor Lin-1 with light using CRISPR-Cas9 and controlled its nuclear translocation in vivo (Yumerefendi et al., 2015a).

The clustering/oligomerization feature of CRY2 has been employed by other studies during *Drosophila* embryogenesis to inhibit signalling pathways and understand their temporal features. Huang and colleagues generated a CRY2 tagged allele of the A-P morphogen bicoid and found a positive correlation between the concentration of bicoid and the duration needed to induce target genes in the early embryo (Huang et al., 2017). Kaur and colleagues developed a CRY2-tagged beta catenin to perturb Wnt

signalling and identified that signalling was needed during late embryogenesis to not only initiate and but also maintain patterning (Kaur et al., 2017).

These CRY2-based tools however do not delve into characterizing the mechanism by which inducing clustering of a key pathway component results in inhibitory effects with respect to signalling. In this regard, I have characterized in detail the mode of function of opto-Delta in multiple tissues during development, leading to the conclusion that upon photo-activation, it inhibits Notch by binding *in cis*.

While the ability to rapidly induce clustering of opto-Delta (and in response, Notch) within the timeframe of few seconds (~15 s in a Delta-CRY2 homozygous background) is highly advantageous for acute perturbation of signalling, CRY2 based homo-oligomerization tools have the pitfall of slow reversion kinetics. Once induced by photo-activation, protein-clusters are stable over several minutes (~20 min) before they revert back to their monomeric state. This can be disadvantageous if we intend to perform temporally patterned perturbation (sequential inactivation and activation) of signalling while studying processes that occur in the timeframe of several minutes to an hour. Optogenetic dimerization systems like the iLID system (Guntas et al., 2015) that have shorter reversion kinetics in the range of several seconds ($t_{1/2}$ ~ 20s) can be employed. However, for processes that manifest over several hours, CRY2 oligomerization provides an efficient system for such pulsatile activations.

4.4 Optogenetic tool to activate Notch signalling

I have also presented an attempt to develop a tool to activate Notch signalling by using optogenetics to directly control the release of the Notch intra-cellular domain (NICD). This would potentially serve as a means to orthogonally (independent of the endogenous genetic program) activate the Notch pathway ectopically in competent

tissues during development to gain a dynamic understanding of the necessity and sufficiency of Notch signalling to drive a morphogenetic process. This will also serve as a potential mode to control the activity of other transcription factors during development, and will be a significant addition to the growing number of approaches in the budding field of synthetic morphogenesis.

Unfortunately when I tested the functionality of the tool, there was significant release of NICD into the nucleus already in the dark, necessitating further optimization. This observation is in contrast to the dynamic light vs dark ratio of the LOVTRAP tool observed in cell culture studies (Wang et al., 2016). Recent studies (LINUS/LANS tools) have successfully used the caging/uncaging property of the LOV2 domain to control nuclear localization of proteins in cell culture (Niopek et al., 2014b; Yumerefendi et al., 2015b).In the dark, the NLS is caged, and upon photoactivation, it is exposed, facilitating the nuclear entry of the protein. I decided to mutate the endogenous NLS sequences of NICD and employ the above single-component optogenetic tool to control its activity in *Drosophila* tissues. These experiments have yielded promising results, but as the data is preliminary and the tool is currently still being characterized in different embryonic and larval tissues, it is currently beyond the scope of this thesis.

4.5 Implications for future studies of spatio-temporal dynamics of Notch signalling during development

In this thesis, I have perturbed signalling over the course of nuclear cycle 14 order to explore the dynamic input output relationship of Notch and its target gene *sim* during mesectoderm specification. Notch signalling occurs at different timescales in different

tissue contexts. I have demonstrated that opto-Delta can be used to inhibit signalling in the embryonic neurectoderm where the Notch-dependent process of neuroblast delamination occurs over a period of several minutes post gastrulation. During the development of eye, wing and Notum tissues, Notch signalling occurs over several hours. How signalling is regulated over time in these tissues and the duration for which is required are still open questions to be addressed. In combination with appropriate real-time reporters of signalling, opto-Delta potentially serves as a useful tool to explore dynamic modes of signalling in various tissues during *Drosophila* development.

In addition to temporal perturbation, opto-Delta can also be used to inhibit signalling in defined spatial regions within the tissue as described in section 3.1.6. Increasing number of studies are shedding light on the importance of Notch regulation in space. In the pupal notum, during Notch-mediated SOP lineage decisions, Trilinski and colleagues have demonstrated using photo-convertible fluorescent reporters that the pool of Notch receptors basal to the cell midbody is the one that specifically gets activated (Trylinski et al., 2017). During neuroblast delamination in the embryo, cells in the proneural cluster that donot receive the Notch signal undergo cell shape changes, starting with apical constriction and loss of cell-junctions eventually culminating in delamination. How the lack of Notch signal gets translated into these changes in cell morphology remains an outstanding question (Simões et al., 2017). Optogenetic perturbation of Notch at single cell resolution will contribute to unravelling these processes in greater detail. Recent studies from our lab (Izquierdo et al., 2018; Krueger et al., 2018) have showed that using localized 2-photon based activation and/ or sub-cellular anchors, it is possible to activate optogenetically tagged proteins

specifically at the apical or basal surfaces of epithelial cells. This provides an elegant strategy to target specific pools of Notch in the cell and understand both their intracellular regulation and contributions to signalling at the tissue-level.

5. Materials and Methods

5.1 Methods

5.1.1 Cloning and transgenesis

Endogenous Targeting of the Delta Locus

The following method was written by Aleksander Necakov and is adapted from the submitted manuscript “Optogenetic inhibition of Delta reveals digital Notch signalling output during tissue differentiation” (see Appendix).

Homologous recombination was used to target the endogenous Delta locus following a procedure described(Huang et al., 2009). Briefly, a large portion of the Delta locus between the intron preceding exon 6 to a region downstream of the transcriptional stop site, was replaced with a targeting cassette through knock-in of an attP landing site and a loxP-flanked mini white cassette. As a first step, a transgenic donor line containing the attP-containing targeting cassette on chromosome 2 was established. This targeting cassette carried flanking homology arms including sequences extending ~5.5 kb upstream of the intron immediately upstream of exon 6 (Left Homology arm), and ~3 kb downstream of the transcriptional stop site (Right Homology arm). The transcriptional termination site, along with sites of low sequence conservation at insertion sites were identified using the UCSC Genome browser in order to mitigate any potential detrimental mismatches arising as a consequence of errant recombination events. The Delta-attP targeting cassette was mobilized through a combination of FLP/FRT and Isc1 genomic excision/cleavage, resulting in a linear, double stranded, extra-chromosomal targeting construct. Heterozygous Delta-attP founder lines were identified as red-eyed transformants that exhibited an obvious Delta-wing phenotype resulting from the haploinsufficiency of the Delta-attP loss-of-

function allele. Candidate transformants were fully characterized and validated by PCR and Sanger sequencing, resulting in the identification of a *bona fide* Dealt-attP founder line. The mini-white was subsequently excised from the Delta-attP locus through Cre/Lox mediated recombination. This white-eyed Delta-attP founder line was then used as a substrate to generate Delta::EGFP, Delta::CRY2, Delta::EGFP::CRY2, Delta::TagRFP::CRY2, Delta::TagRFP::CRY2 Olig and Delta::CIBN fly lines through Φ C31-mediated attp/attB recombination. CRY2, CIBN and CRY2 Olig were amplified from existing plasmids (CRY2 and CIBN from (Guglielmi et al., 2015) and CRY2 Olig from Addgene plasmid # 60032,(Taslimi et al., 2014)). An attB vector containing the entire Delta genomic sequence that was removed from upstream of exon 6 to downstream of the transcriptional stop site, was produced for each of these rescue constructs, which were engineered to incorporate the coding sequences of their respective tag as an intramolecular fusion inserted between amino acids 701 and 702 of Delta protein. Transformants were identified by their red-eye colour, and recue of the Delta haploinsufficient wing phenotype, and were subsequently verified by PCR and Sanger sequencing.

sim-MS2 reporter line

The following method was written by me and is adapted from the submitted manuscript "Optogenetic inhibition of Delta reveals digital Notch signalling output during tissue differentiation" (see Appendix).

To generate the *sim*-MS2 line, the *sim* enhancer and promoter region shown below was fused to 24 MS2 stem loop repeats. This line was generated by Emilia Esposito. Cloning was performed identical to the *eve*>MS2 construct described previously (Bothma et al., 2014)

Sim Enhancer (664 bp)

AGCAGAGCTCTTATCGTTGTGGCCCCGGCATATGTTACGCACATTTACAGCGTA
TGGCGATTTTCCGCTTTCCACGGCCACGGCCACAGCTTCCCACCTGATAGGAC
AGCTCGGCAATGTGTGGGAATCGCAGTGAGGTGCCGGTAGGAGTGGCAGGTA
AGCCTGGCCGCCTCGCAAGTTTCTCACACTTCCAGGACATGTGCTGCTTTTTTG
GCCGTTTTTCCCCGACTGGTTATCAATTGGCCGATTGGAAATTCCCCGATGGCG
ATGCGCTAGCGTGAGAACATGAGCTGCGAGCATCGGGTTTTTAGCATATCCATA
CCTGTGGCTCGTCCTGATGGGAAGCGAGAAGCAGCAGGATCGGATGTAGGAT
GCAGGATATAGGGTATAGGCGCTGTTGCGCCTCACCCGCAACACCCACATTAG
CATCGGACCAGCGTCCAGTGTCCTGTTAATTGCTTTATGGACTCTCCACTTTCC
GCTGCGTGGGAATCTTTGCTCATCCTACCTGTTTCCATGCCACACCAACCCATT
CCCACAGCATTGTCCTCCTTATGTGAAACTCTCTAGTTCAAGTTCAGTGTGAATA
TTTGTGTTGACTTTATTTTTAAACTTTTGGCCATTTGTTTTCAGTTTGCTGTTTGC
CTGTAACCAGATTAAGGTC

Sim Promoter (181 bp)

AATCCAGTGCAGCCAATGGCAGGTTGTTTTCTCAGGATCAGGTAACAGATCCTT
TTCGGGATCAGTTGGGAAACTGTTAAAAGTGCTTGTGCCGCTGGAAAGCGGCT
CAGTTGCAAACAGGTGATTGCAGGGATATGAGCAAGTGCTGAGAAGGTGCTCG
CAACAGTCTCAAAGCAGGATC

Cloning

Plasmids for were cloned using a combination of Gibson assembly and Gateway cloning techniques. For Gibson assembly, a custom made master mix (see Materials) was prepared (Gibson et al., 2009). 10 µl aliquot of Gibson master mix was mixed with

a 10 µl mix of DNA fragments (PCR amplified using primers with 5' extensions to contain overlapping regions) to be joined, on ice. Linearized vector and inserts were combined in the ratio 3:1 (total concentration of 0.6 pmol) and incubated for 1 hr at 50°C before transformation into TOP10 *E. coli* cells. PCR, DNA purification, *E. coli* transformation and gateway cloning were done using commercialized procedures (see Materials)

For cloning the opto-Notch constructs mCherry::Zdk1::NICD, NES::mCherry::Zdk1::NICD and Mito::EGFP::LOV2 : NICD was amplified from Drosophila cDNA library; AsLOV2 domain (amino acids 404-546) from PA-Rac1 (Addgene plasmid # 22027,(Wu et al., 2009); Zdk1 peptide (GenBank: KX429612.1) was synthesized (Invitrogen GeneART); Mitochondrial localization sequence (Mito) used was amino acids 1-36 (Kanaji et al., 2000) of *Drosophila* Tom-20 (UniProt ID: Q15RF6); NES used was from Smad 4 (Sequence: GIDLSGLSLQ). The constructs were first cloned into a pENTR entry vector and then sub-cloned into a pPW destination vector (Drosophila Genomics Resource center, Bloomington) using the Gateway cloning system (Thermo Fischer Scientific).

For generating plasmids to be expressed in HeLa cell culture, DLL1::mCherry::CRY2, Notch1::YFP (Extracellular) and Notch1::Myc (Extracellular): full length Mouse DLL1 was amplified from cDNA obtained from Mouse embryo tail-buds (courtesy Alexander Aulehla); Notch-1 was amplified from 2 separate plasmids (Addgene #41728 and Addgene #20183) and the YFP/ c-Myc tag was inserted in-frame with Notch-1 at amino acid position number 20. The constructs were first cloned into a pENTR entry vector and then sub-cloned into a pcDNA-DEST40 destination vector for mammalian expression using the Gateway cloning system (Thermo Fischer Scientific).

5.1.2 Cell culture

HeLa cells were cultured in DMEM (Gibco) supplemented with 10% heat inactivated FBS, 2mM L-glutamine (Gibco), 1mM Sodium Pyruvate at 37 C and 5% CO2. Cells were seeded at 100.000 cells in 2ml glass bottom dishes (MatTek corporation). After 24 hrs plasmid transfection was done using FuGENE HD (Roche) according to the manufacturer's instruction (FuGENE:DNA ratio is 3:1). Cells were live imaged/ fixed 24-48 hrs after transfection.

The methods in the following sections were written by me and are adapted from the submitted manuscript "Optogenetic inhibition of Delta reveals digital Notch signalling output during tissue differentiation" (see Appendix).

5.1.3 Live Imaging and Optogenetic activation

Cages with flies expressing Delta-CRY2 were maintained in the dark. Late stage 4 (Cycle 13) embryos were selected under halocarbon oil and mounted using a standard stereomicroscope with a red-emitting LED as the transmission light source. Mounting for live imaging was carried out as follows: embryos were dechorionated with 100% sodium hypochlorite for 2 min, rinsed with water and mounted immersed in PBS onto a 35 mm glass-bottom dish (MatTek corporation). Embryos were then positioned with their ventro-lateral side facing the cover-slip. Photo-activation and acquisition of movies was done with a spinning disk Ultraview VoX system (Perkin Elmer) using a 40x/NA 1.3 oil immersion objective (Zeiss). Live imaging was performed at 25 °C. Bright field illumination was filtered using a Deep Amber lighting filter (Cabledelight,

Ltd.) in order to locate the embryos. The Microscope was controlled using Volocity software (Perkin Elmer).

For imaging the kinetics of Delta-CRY2 clustering live, embryos heterozygous for Delta::GFP-CRY2 embryos were imaged using fluorescence live imaging (Perkin Elmer Vox, Spinning Disc Confocal, 63x Oil immersion objective). A single plane, 3 microns below the apical surface was imaged (λ=488 nm, laser power out of the objective= 0.6 mW) over six minutes at two-second intervals in three individual embryos (n=100 cells in total).

To image the clustering of Notch Extracellular-YFP in a Delta-CRY2 heterozygous background, at t = 0s, a pre-activation stack was acquired using a 514 nm laser, followed by an immediate cycle of photo-activation (5 s, λ=488 nm, laser power out of the objective= 0.6 mW). Thereafter, a post-activation stack was acquired using the 514 nm laser at t = 60s. The above cycle was repeated till t = 120s. While imaging the clustering of Notch Extracellular-YFP in a Delta-CRY2 homozygous background, there was no time delay between the pre-activation, photo-activation and post-activation stacks. All stacks were 10 µm starting from the most apical plane of the embryo surface with a z-interval of 0.4 µm.

For clonal analysis, Delta-CRY2 pupae were collected at puparium formation and either photo-activated under a white lamp source (20 W) or placed in the dark at 25 °C until 16.5 hrs after puparium formation (APF) for live imaging as described previously(Couturier, trylinski 2014). Imaging was done with a Zeiss LSM 780 confocal microscope with a 63x/NA 1.4 oil immersion objective (Carl Zeiss).

For *sim* expression, virgin females of the line w; MCP (No NLS)-GFP/CyO; Delta-CRY2/” were crossed to males expressing the *sim*-MS2 reporter. Resulting embryos were mounted for imaging and photo-activated after allowing incremental time

intervals (0/5/10/15/20/25 min) of signalling from the onset of cycle 14. Photo-activation was carried out by illumination with a 488 nm laser line (200 ms/slice, laser power out of the objective= 0.6 mW) every minute by gradually increasing the stack size from 20 to 25 to 30 µm (z-interval of 0.8 µm) from the apical surface as cellularization proceeded. *sim* nuclear spots were recorded also using a 488 nm laser at a time resolution of 30 s and a stack size of 25 µm (z-interval of 0.4 µm) until the onset of ventral furrow formation. For controls, female virgins expressing MCP-GFP (without Delta-CRY2) were crossed to males expressing the *sim*-MS2 reporter and photo-activated using the same protocol described above from the onset of cycle 14. For imaging *sim* expression in Notch heterozygous embryos, female virgins expressing one copy of the mutant $Notch^{55e11}$ allele and MCP-GFP, were crossed to males expressing *sim*-MS2. Image acquisition in the resulting embryos and corresponding controls (without $Notch^{55e11}$) was started as soon as *sim* spots began to appear, without any prior photo-activation.

Spatial activation of opto-Delta: Photo-activation in a localized region was carried out by illumination with a 950 nm 2-photon laser (pixel dwell time: 1.3 µs and pixel size: 0.4 µm, laser power = 10 mW) every 45 s by gradually increasing the stack size from 20 to 25 to 30 µm (z-interval of 1 µm) from the apical surface as cellularization proceeded. *sim* nuclear spots (visualized by MCP::mCherry) were recorded also using a 561 nm laser at a time resolution of 30 s and a stack size of ~25 µm (z-interval of 0.5 µm) ~5 mins prior to the onset of ventral furrow. Images were acquired with a Zeiss LSM 780 NLO confocal microscope with a 40x/NA 1.2 water immersion objective (Carl Zeiss)

Neuroblast imaging: Photo-activation (5 s, λ=488 nm, laser power out of the objective= 0.6 mW) in the neurectoderm was started immediately post ventral furrow formation

and was repeated thrice at a time resolution of 20 s. Following this, the membrane marker gap43::mCherry was imaged using the 561 nm laser every 30 s along with a photo-activation stack at a time-resolution of 10 min. All stacks were 10 µm starting from the most apical plane of the embryo surface with a z-interval of 0.4 µm. Images were acquired using a Perkin Elmer Vox, Spinning Disc Confocal, 40x Oil immersion objective.

For live imaging clustering of Delta::mCherry::CRY2 in cell culture: A pre-activation stack was acquired using a 561 nm laser, followed by an immediate cycle of photo-activation (5 s, λ=488 nm, laser power out of the objective= 0.6 mW) which was done at a time-resolution of 20 s for 2 time points. Thereafter, a post-activation stack was acquired using the 561 nm laser at t = 30s. All stacks were 10 µm starting from the most apical plane of the embryo surface with a z-interval of 0.4 µm. Images were acquired using a Perkin Elmer Vox, Spinning Disc Confocal, 100x Oil immersion objective.

Imaging of opto-Notch activation in the early embryo during the mitotic phase was done as follows: A pre-activation stack was acquired using a 561 nm laser, followed by an immediate cycle of photo-activation (4 s, λ=488 nm, laser power out of the objective= 0.6 mW) which was done at a time-resolution of 10 s for 3 time points. Thereafter, a post-activation stack was acquired using the 561 nm laser at t = 30s. All stacks were 15 µm starting from the most apical plane of the embryo surface with a z-interval of 0.4 µm. Images were acquired using a Perkin Elmer Vox, Spinning Disc Confocal, 63x Oil immersion objective.

Optogenetic inhibition of Notch signaling during development and analysis of mutant phenotypes

Flies homozygous for Delta::CRY2, which are viable and fertile in the dark, were reared on standard German food (Bloomington *Drosophila* stock center recipe) in standard acrylic fly vials, and exposed to ambient light from larval stages until eclosion. These adults, along with their counterparts reared in the dark, were imaged on a Zeiss stereo-dissection microscope in order to characterize variations in wing, notum, and eye morphology. For embryonic analysis, homozygous Delta::CRY2 embryos were collected for two hours on apple-juice agar plates in acrylic cages maintained either in the dark, or exposed to ambient light for 24 hours at 25 °C. Cuticle preparations of collected embryos were made using Hoyer's medium, and imaged on a Zeiss stereo-dissection microscope. For Delta-CRY2 adult nota and eyes, the following protocol was used: pupae were collected at the puparium formation stage and illuminated under a white lamp source (20 W) or placed in the dark at 25 ºC until they hatched. Adults were frozen at -20 ºC for 15 minutes and then immediately prepared for bright-field imaging using a Zeiss AxioZoom V16 macroscope.

5.1.4 Image analysis

To quantify Delta::GFP::CRY2 clustering kinetics, a data pipeline was developed in Cell Profiler to automatically identify and segment individual Delta::GFP::CRY2 clusters in a series of individual confocal images. Segmentation serves to first map the positional coordinates for each cluster, allowing for automatic quantification of the number of clusters in each image. Delta protein abundance in individual clusters was then automatically quantified by integrating fluorescence intensity across the total area of each cluster as identified through segmentation. Data normalization was performed

through the following formula: (Total Number of Clusters x Mean Intensity of Clusters) ÷ Total Intensity of Image. This approach to normalization provides a quantitative measure of the total amount of Delta protein (Delta::GFP:CRY2 locked into clusters), and the resulting data were plotted as the relative intensity of Delta clusters over time plus or minus standard deviation over time. This image analysis pipeline automatically identifies and segments individual Delta-GFP-CRY2 clusters in a series of individual images collected using spinning-disk confocal microscopy. Segmentation serves to first map the positional coordinates for each cluster, allowing for automatic quantification of the number of clusters in each image. Delta protein abundance in individual clusters is then automatically quantified by integrating fluorescence intensity across the total area of each cluster as identified through segmentation.

For the quantification of Notch protein levels at the plasma membrane, confocal images were processed using Fiji and analyzed using MATLAB-R2017b (MathWorks). A sum-of-slice projection of 10 focal planes was used to segment line profiles with a line width of 7 pixels which were drawn across approximately 30 interfaces in both ectoderm and mesoderm of each embryo, and the corresponding intensity profiles were extracted in Fiji. This data was then input into a customized MATLAB pipeline. Peak values in the intensity profile were identified using the findpeaks function in MATLAB and the integrated intensity across individual interfaces was calculated by choosing an interval of 0.78 µm centered at the peak.

For the clonal analysis, the total number of sensory organ precursor cells (SOPs, marked by neur-iRFPnls) at the border of wild-type and Delta-CRY2 clones were counted manually and scored for their presence on the side of either the wild-type or Delta-CRY2 homozygous clone. The number of SOPs on the side of the Delta-CRY2

clone were then plotted as a percentage of total number of SOPs at the border in both the photo-activated and dark conditions.

For the analysis and quantification of *sim* expression using the MS2-MCP system the numbers of spots and associated intensity was quantified under different photo-activation regimes. In order to remove noise, individual images from stacks were median-filtered with a 3x3 pixel neighborhood. A mean-filter over a 100x100 pixel neighborhood was used to determine the background and subtracted to the median-filtered image. We then computed the maximum projection. We subtracted to the maximum projection image its median-filtered image with a 30x30 pixel neighborhood. The resulting image was Gaussian-filtered with a standard deviation of 3 pixels (corresponding to the size of a diffraction-limited spot under our imaging conditions). The segmented image was built from the zero crossings of the Laplacian of the filtered maximum projection. Segmentation of background was rejected based on blob size and intensity. The final segmented image was manually curated. The segmented image was used as mask to extract the intensity of individual *sim* puncta.

For the quantification of *sim* expression using FISH, nascent *sim* transcribing spots in the nucleus were segmented, and their intensities were quantified in fixed embryos using a similar methodology as described above. In nuclei containing two visible transcriptional foci, both of them were used for quantification. The staging of embryos as early, middle and late during the course of cellularization was done as follows: The Early group was identified as having detectable levels of Sim expression, and as where the cellularization furrow was measured to be at least 12 µm deep from the vitelline membrane but still positioned apical to the base of the cortical nuclei. The Middle group was identified as having detectable levels of Sim expression, and as where the cellularization furrow was positioned anywhere between the base of the

cortical nuclei and three microns basal to the nuclei. The Late group was identified as having detectable levels of Sim expression, and as where the cellularization furrow was positioned at least 5 microns below the base of the cortical nuclei and including cephalic furrow formation, but prior to ventral furrow formation.

To quantify Delta protein content at the plasma membrane, cell outlines were segmented based on the E-cadherin signal co-stained with Delta using Embryo Development Geometry Explorer (EDGE) software (Gelbart et al., 2012) provided via GitHub (https://github.com/mgelbart/embryo-development-geometry-explorer). Image stacks spanning 3.5 µm were projected in 2-D using the sum-of-slices. The membrane-bound Delta signal was measured in a 0.3 µm thick region lining the segmented membrane and for each embryo the mean intensity value of the ectoderm and of the mesoderm was calculated. To quantify the membrane-to-cytoplasmic ratio of the Delta signal in the mesoderm, for individual cells the central (cytoplasmic) signal was derived from the inverted mask of the segmented membrane and divided by the Delta signal measured at the surrounding cell edges. An average membrane-to-cytoplasmic ratio was calculated from ~40 cells per embryo.

To analyze the co-localization of Delta and Rab5 in the mesoderm, vesicles were detected in a 7-µm-spanning image stack using the Fiji “Spots colocalization” plugin ComDet v.0.4.1 provided via GitHub (https://github.com/ekatrukha/ComDet). Identified Delta particles were binary classified for an overlap with Rab5 particles in at least 1 pixel. The percentage of Rab5-positve Delta particle was calculated per embryo.

For measuring neuroblast apical cell surface area over time, a pipeline adapted from Izquierdo et al. 2018 was used.

Estimation of activation rates

The temporal evolution of transcription spot numbers was adjusted by N_{max} (1-exp(-*k* (t-t_0)) where N_{max} is the maximum number of spots that can be activated (i.e. the number of nuclei in the mesectoderm), *k* is the activation rate and t_0.the delay to activation. N_{max} was taken as constant and only two parameters *k* and t_0 were adjusted for each embryo.

5.1.5 Immunostaining

Delta-CRY2 embryos enriched in stage 4 and 5 were collected, dechorionated in bleach for 2 min, covered in PBS and photo-activated with the following illumination protocol: 2 min under blue light from a fluorescence lamp source (Olympus X-Cite 120 W, 470/40 bandpass filter. Light power out of the objective= 1.8 mW) 5 min under a white light source (HAL-100 Zeiss) and 3 min with no illumination. This protocol was repeated 6 times to ensure a total photo-activation period of 1 hour. Thereafter, embryos were immediately fixed in 4% Paraformaldehyde (Electron Microscopy Sciences) and Heptane (Sigma) for 20 min after which they were devitellinized and stored in methanol at -20 °C.

For Immunostaining, fixed embryos were blocked in 10% Bovine Serum Albumin(BSA) in PBS 0.1% Triton-X (Sigma) for 1 hour, following which they were incubated overnight in the primary antibody diluted in PBS containing 5% BSA and 0.1% Triton-X. The embryos were then washed and incubated in the secondary antibody for 45 min at room temperature. After another round of washing, embryos were mounted on glass slides using aqua-poly/mount (Polysciences Inc.). For the non-photo-activated control, embryos were collected under Deep Amber filtered light (as mentioned

previously) and fixed in the dark prior to immunostaining. Images were acquired with a Zeiss LSM 780 NLO confocal microscope with a 63x/NA 1.2 water immersion objective (Carl Zeiss).

For HeLa cell culture immunostainings, a protocol to fix and stain cells without permeablization was adapted from (Hinners et al., 1999) in order to visualize only the plasma membrane pool of Notch. PBS was replaced by Sodium Phosphate buffer (NaPi) in all steps. After aspiration of cell culture media, cells were rinsed twice in NaPi containing 0.9mM $CaCl_2$ and 0.5mM $MgCl_2$. Fixation was performed either In the dark or after blue light photo-activation with a fluorescence lamp source (as described in the previous section) for ~3 min., scanning the entire dish. Cells were fixed using 3% PFA for 30 min. at room temperature (RT). Fixation was stopped by quenching in 50mM NH4Cl for 10 min. Cells were blocked in 10% BSA in NaPi for 30 min following which the primary antibody diluted in 5% BSA was added and cells were incubated for 1.5 hrs at RT. After washes with NaPi, the secondary antibody was added (and washed off post 1 hr at RT) and cells were stored in a light protected manner at 4 C. Cells were imaged with a Perkin Elmer Vox, Spinning Disc Confocal, 63x Oil immersion objective.

5.1.6 In-situ hybridization (ISH)/ Fluorescent in-situ hybridization (FISH)

Fixed embryos stored at -20º C in methanol were transferred to xylene and washed on the rocker for 20 min. in order to clear the yolk. Embryos were then transferred back to methanol, and following a quick rinse, were washed 3x with $PTw_{0.1\%}$. Embryos were incubated in PBTK for 30 min. at RT; Proteinase-K digestion was stopped by washing twice in PBTG. Following a rinse in $PTw_{0.1\%.}$ embryos were post-fixed at RT for 20 min with PBTF. To remove all traces of fixative, 5x washes with $PTw_{0.1\%.}$ were

performed. A 1:1 mixture of hybridization buffer: $PTw_{0.1\%}$ was prepared and embryos were rinsed. This was replaced with 100% hybridization buffer at 65º C. Prehybridization buffer was prepared by boiling hybridization buffer for 5 minutes at 100 C and then coolng on ice for 5 minutes. Samples were then incubated in prehybridization solution for ~ 2 hours at 65º C. Probe solution was prepared by adding ~50-100ng of probe (or as desired) in ~ 100 uL of hybridization buffer plus 5% dextran and samples were incubated in this overnight (15 h) at 65º C. Embryos were washed 5x for 10 minutes each in 100% hybdridization buffer at 65 ºC. After this, 15 min washes were performed with serial dilutions of the hybridization buffer in $PTw_{0.1\%}$ (3:1, 1:1, and 1:3). With 5 final washes with $PTw_{0.1\%}$,embryos were cooled to RT and blocked in 5% BSA for 1 hr. For FISH, 1% skim milk was used in the blocking solution instead of 5% BSA. Embryos were incubated for 2hrs at RT or overnight at 4º C in the primary antibody solution (Anti-Dig-AP, AP (Alkaline Phosphatase) conjugated for ISH and Anti-Dig without AP for FISH).

For ISH, after several washes with $PTw_{0.1\%,}$ embryos were rinsed 3 x 5 minutes in fresh AP-wash buffer. The substrate NBT/BCIP was diluted 1:50 in AP-colour buffer and added to the samples on a 24 well plate. The color develops between 20-40 minutes and the reaction is stopped by washing in $PTw_{0.1\%}$ or through an ethanol series to reduce background.

For FISH, after several washes with $PTw_{0.1\%}$, embryos were incubated in secondary antibody and following another round of washing, were mounted on slides using aqua-poly/mount (Polysciences Inc.) after 10 min. incubation in DAPI to visualize nuclei.

Imaging conditions for visualizing nascent *sim* transcripts by Fluorescent in-situ hybridization (FISH) in wild-type (w1118) embryos was identical to that used for the MS2-MCP system, except that a 63x Oil immersion objective was used instead of 40x.

5.1.7 *Drosophila* strains and genetics

In order to induce clones in the pupal notum:

w; Ubx-FLP neur-iRFP670nls/+; FRT82B ubi-RFPnls/ FRT82B Delta::CRY2.

Clones were detected by the loss of nuclear-RFP.

In order to visualize sequestration and optogenetic release of NICD:

w[*]; P[w+, UASp>mCherry::Zdk1::NICD]/ P[w+, Mat.tubulin>Gal4::VP16]; P[w+, UASp>Mito-EGFP::LOV2]/ P[w+, Mat.tubulin>Gal4::VP16]

5.1.8 *Drosophila* stocks

All stocks were maintained by standard methods at 22°C, unless otherwise specified and lines carrying the optogenetic CRY2 tag were stored in the dark.

Fly Stock	**Description**
w[*]; ; Delta::EGFP/ ”	Endogenous Delta tagged intracellularly with EGFP
w[*]; ; Delta::CRY2/ ”	Endogenous Delta tagged intracellularly with CRY2
w[*]; ; Delta::EGFP::CRY2/ TM6B,Tb	Endogenous Delta tagged intracellularly with EGFP and CRY2
w[*]; ; Delta::TAGRFP::CRY2/ TM6B,Tb	Endogenous Delta tagged intracellularly with TAGRFP and CRY2

w[*]; ; Delta::TAGRFP::CRY2-olig/ TM6B,Tb	Endogenous Delta tagged intracellularly with TAGRFP and CRY2-olig (increased clustering variant of CRY2)
w[*]; ; Delta::CIBN/ ”	Endogenous Delta tagged intracellularly with CRY2 dimerizing partner CIBN
Notch-Extra::YFP/Y	Endogenous Notch tagged extracellularly with YFP at amino acid 55. (DGRC-Kyoto Line 115544)
Notch-Extra::YFP/ Y; ; Delta::CRY2/ ”	Endogenous Notch tagged extracellularly with YFP combined with Delta::CRY2
yw[*]; P[w+, nosP> MCP-no nls::GFP]; +/ +	MCP with nuclear localization sequence removed and tagged with GFP, driven by the Nanos promoter (from Thomas Gregor)
w[*]; P[w+, nosP> MCP-no nls::GFP]/ CyO; MKRS/ TM3,Ser	“ (Single copy of MCP-no nls::GFP, used for control experiments)
w; P[w+, nosP> MCP-no nls::GFP]/ CyO; Delta::CRY2/ ”	MCP with nuclear localization sequence removed and tagged with GFP, combined with Delta::CRY2
w[*]; P[w+, nosP> MCP-no nls::mCherry]/ CyO; P[w+, nosP> MCP-no nls::mCherry]/ TM3,Sb.	MCP with nuclear localization sequence removed and tagged with mCherry, driven by the Nanos promoter (Bothma et al., 2018)

w[*]; P[w+, nosP> MCP-no nls::mCherry]/ CyO; Delta::CRY2/ ”	MCP with nuclear localization sequence removed and tagged with mCherry, combined with Delta::CRY2
yw[*]; ; Sim-MS2/ ”	Sim enhancer and promoter fused to MS2 stem loops (from Emilia Esposito/ Michael Levine)
w[*]; P[w+, sqhp>Gap43::mCherry]/CyO; Delta::CRY2/ ”	Gap43 membrane marker tagged with mCherry and driven by the Spaghetti-squash promoter and combined with Delta::CRY2
w[*]; ; FRT82B Delta::CRY2/ ”	FRT82B recombined with Delta::CRY2 on the 3rd chromosome for clonal analysis
w[*]; Ubx-FLP neur-iRFP670nls/ CyOGFP; FRT82B ubi-RFPnls	Line expressing Flippase driven by the Ultrabithorax promoter recombined with a fluorescent SOP marker driven by the Neuralized promoter; FRT82B recombined with ubi-RFPnls in order to visualize clones in the tissue (from Francois Schweisguth, Corturier et al, 2014)
yw[*]; EGFP::Rab5/CyO	Endogenous GFP-tagged early endosome marker Rab5, (Fabrowski et al., 2013)

yw[*] FRT19A Notch^{55e11}/ FM7c	Notch loss-of-function mutation (from Eric Wieschaus)
w[*]; ; Df(3R)BSC850/TM6C, Sb cu	(Bloomington Stock BL-27922), Chromosomal defeciency in 3R lacking Delta
w[*]; If/CyO; P[w+, UASp>Mito-EGFP::LOV2]/TM6B, Tb	UASp driven LOV2 domain fused to a mitochondrial localization sequence and tagged with EGFP
w[*]; P[w+, UASp>mCherry::Zdk1::NICD]/CyO; MKRS/ TM6B, Tb	UASp driven NICD fused to the Zdk1 peptide and tagged with mCherry
w[*]; P[w+, mat.tub > Gal4::VP16]; P[w+, mat.tub > Gal4::VP16]	Maternal tubulin promoter driven Gal4 (Bloomington Stock 7062-7063)

5.2 Materials

5.2.1 Kits

Phusion Flash High-Fidelity PCR Master Mix	Thermo Scientific
QIAprep Spin Miniprep Kit	Qiagen
Plasmid Midiprep Kit	Qiagen
QIAquick Gel Extraction Kit	Qiagen
QIAquick PCR Purification Kit	Qiagen
pENTR/D-TOPO Cloning Kit	Thermo Fisher

5.2.2 Chemicals/ reagents

Ampicillin	Applichem
Kanamycin	Roth
Dulbecco's Modified Eagle Medium (DMEM)	Gibco
Fetal Bovine Serum (FBS) Gold	PAA Laboratory Gmbh.
FuGENE HD	Roche
L-Glutamine	Gibco
Sodium Pyruvate	Gibco
OptiMEM cell culture medium	Gibco
Halocarbon oil 27	Sigma Aldrich
n-Heptane	Sigma Aldrich

Methanol	Sigma Aldrich
Xylene	Sigma Aldrich
Paraformaldehyde (PFA)	Electron Microscopy Sciences
DAPI	Thermo Scientific
NBT/ BCIP (substrate for ISH)	Roche
Dextran sulphate	Sigma Aldrich

5.2.3 Buffers/ solutions

LB (Luria Bertani broth) medium	In 1 L H_20 10 g Tryptone 5g Yeast extract 10g NaCl
TB (terrific broth)medium	In 1 L H_20 20g Tryptone 24g Yeast extract 0.017 KH_2PO_4 0.072 K_2HPO_4
Isothermal reaction buffer	500 mM Tris-HCl (pH 7.5) 25% PEG-8000 50 mM MgCl2 50 mM DTT 5 mM NAD

Gibson assembly mix	1x Isothermal reaction buffer 10 U/µl T5 exonuclease (New England Biolabs) 2 U/µl Phusion DNA polymerase (New England Biolabs) 40 U/µl Taq ligase (Epicentre)
TAE buffer (50x)	2 M Tris 1 M acetic acid 50 mM EDTA
PBS	2.7 mM KCl 137 mM NaCl 10 mM Na_2HPO_4 2 mM KH_2PO_4
$PBS_{Tr0.1\%}$	0.1% Triton-X in PBS
$PBS_{Tw0.1\%}$	0.1% Tween 20 in PBS
Blocking solution	For IF, 10% Bovine serum albumin (BSA) in $PBS_{Tr0.1\%}$ For ISH, 5% Bovine serum albumin (BSA) in $PBS_{Tw0.1\%}$
PBTK	3 µg/ml Proteinase K (Thermo Fisher Scientific) in $PBS_{Tw0.1\%}$
PBTG	2 mg/ml Glycine (Sigma) in $PBS_{Tw0.1\%}$
PBTF	20% PFA in $PBS_{Tw0.1\%}$
In situ hybridization buffer	For 100 ml, 1g blocking reagent (Roche)

	0.1g Chaps (Sigma) 50 ml Formamide 25 ml 20x SSC buffer 2 ml 50x Denharts 0.1% yeast tRNA 0.01% Heparin 0.1% Tween 20 DNAase RNAase free H2O to 100 ml
AP wash buffer	0.1 M Tris-HCl (pH 9.5) 0.1 M NaCl 50 mM MgCl2 Tetramisol 1 mM 0.1% Tween 20
AP colour buffer	0.1 M Tris-HCl (pH 9.5) 0.1 M NaCl 0.1% Tween 20

5.2.4 Bacteria/ Mammalian cells

One Shot TOP10 Chemically Competent *E. coli*	Thermo Fisher Scientific
HeLa Kyoto human cell line	From S. Narumiya, Kyoto University

5.2.5 Antibodies (for immunofluorescence)

Antibody	Species	Dilution	Source
anti-extracellular Notch EGF repeats-12-20	Mouse	1:20	C458.2H Developmental Studies Hybridoma bank, DSHB
anti-Delta	Mouse	1:100	C594.9B, DSHB
anti-intracellular Notch	Mouse	1:20	C17.9C6, DSHB
anti-Tom	Rat	1:100	Home-made
anti-E-Cadherin	Rabbit	1:100	sc-33743, Santa Cruz Biotech.
anti-c-Myc (9E10)	Mouse	1:400	sc-40, Santa Cruz Biotech.
anti-DIG-AP	Sheep	1:500	Roche
Anti-DIG	Sheep	1:500	Roche
Anti-GFP	Rabbit	1:1000	Abcam
anti-mouse Alexa 488	Goat	1:500	Thermo Scientific
anti-mouse Alexa 647	Goat	1:500	Thermo Scientific
anti-rat Alexa 647	Goat	1:500	Thermo Scientific

anti-rabbit Alexa 488	Goat	1:500	Thermo Scientific
anti-Sheep Alexa 488	Donkey	1:500	Thermo Scientific

6. References

del Álamo, D., Rouault, H., and Schweisguth, F. (2011). Mechanism and Significance of cis-Inhibition in Notch Signalling. Curr. Biol. *21*, R40–R47.

An, Y., Xue, G., Shaobo, Y., Mingxi, D., Zhou, X., Yu, W., Ishibashi, T., Zhang, L., and Yan, Y. (2017). Apical constriction is driven by a pulsatile apical myosin network in delaminating Drosophila neuroblasts. Development *144*, 2153–2164.

Artavanis-Tsakonas, S., Rand, M.D., and Lake, R.J. (1999). Notch signaling: Cell fate control and signal integration in development. Science (80-.). *284*, 770–776.

Arvanitis, D., and Davy, A. (2008). Eph/ephrin signaling: Networks. Genes Dev. *22*, 416–429.

Bailey, A.M., and Posakony, J.W. (1995). Suppressor of hairless directly activates transcription of enhancer of split complex genes in response to Notch receptor activity. Genes Dev. *9*, 2609–2622.

Balaskas, N., Ribeiro, A., Panovska, J., Dessaud, E., Sasai, N., Page, K.M., Briscoe, J., and Ribes, V. (2012). Gene regulatory logic for reading the Sonic Hedgehog signaling gradient in the vertebrate neural tube. Cell *148*, 273–284.

Bardin, A.J., and Schweisguth, F. (2006). Bearded Family Members Inhibit Neuralized-Mediated Endocytosis and Signaling Activity of Delta in Drosophila. Dev. Cell *10*, 245–255.

Batchelor, E., Mock, C.S., Bhan, I., Loewer, A., and Lahav, G. (2008). Recurrent Initiation: A Mechanism for Triggering p53 Pulses in Response to DNA Damage. Mol. Cell *30*, 277–289.

Becam, I., and Milán, M. (2008). A permissive role of Notch in maintaining the DV affinity boundary of the Drosophila wing. Dev. Biol. *322*, 190–198.

Becam, I., Fiuza, U.M., Arias, A.M., and Milán, M. (2010). A Role of Receptor Notch in Ligand cis-Inhibition in Drosophila. Curr. Biol. *20*, 554–560.

Benoit, B., He, C.H., Zhang, F., Votruba, S.M., Tadros, W., Westwood, J.T., Smibert, C.A., Lipshitz, H.D., and Theurkauf, W.E. (2009). An essential role for the RNA-binding protein Smaug during the Drosophila maternal-to-zygotic transition. Development *136*, 923–932.

Bollenbach, T., Pantazis, P., Kicheva, A., Bökel, C., González-Gaitán, M., and Jülicher, F. (2008). Precision of the Dpp gradient. Development *135*, 1137–1146.

Bothma, J.P., Garcia, H.G., Esposito, E., Schlissel, G., Gregor, T., and Levine, M. (2014). Dynamic regulation of eve stripe 2 expression reveals transcriptional bursts in living Drosophila embryos. Proc.

Natl. Acad. Sci. U. S. A. *111*, 10598–10603.

Bothma, J.P., Garcia, H.G., Ng, S., Perry, M.W., Gregor, T., and Levine, M. (2015). Enhancer additivity and non-additivity are determined by enhancer strength in the Drosophila embryo. Elife *4*.

Bothma, J.P., Norstad, M.R., Alamos, S., Correspondence, H.G.G., and Garcia, H.G. (2018). LlamaTags: A Versatile Tool to Image Transcription Factor Dynamics in Live Embryos In Brief LlamaTags: A Versatile Tool to Image Transcription Factor Dynamics in Live Embryos. Cell *173*, 1810–1822.

Boyden, E.S., Zhang, F., Bamberg, E., Nagel, G., and Deisseroth, K. (2005). Millisecond-timescale, genetically targeted optical control of neural activity. Nat. Neurosci. *8*, 1263–1268.

Bray, S.J. (2006). Notch signalling: a simple pathway becomes complex. Nat. Rev. Mol. Cell Biol. *7*, 678–689.

Bray, S.J., and Gomez-Lamarca, M. (2018). Notch after cleavage. Curr. Opin. Cell Biol. *51*, 103–109.

Brenner, S. (1974). The genetics of C.elegans. Methods *77*, 71–94.

Bugaj, L.J., Choksi, A.T., Mesuda, C.K., Kane, R.S., and Schaffer, D. V (2013). Optogenetic protein clustering and signaling activation in mammalian cells. Nat. Methods *10*, 249–252.

Cagan, R.L., and Ready, D.F. (1989). Notch is required for successive cell decisions in the developing Drosophila retina. Genes Dev. *3*, 1099–1112.

Chitnis, A. (2006). Why is delta endocytosis required for effective activation of Notch? Dev. Dyn. *235*, 886–894.

Corson, F., Couturier, L., Rouault, H., Mazouni, K., and Schweisguth, F. (2017). Self-organized Notch dynamics generate stereotyped sensory organ patterns in Drosophila. Science (80-.). *356*.

Couturier, L., Vodovar, N., and Schweisguth, F. (2012). Endocytosis by Numb breaks Notch symmetry at cytokinesis. Nat. Cell Biol. *14*, 131–139.

Cowden, J., and Levine, M. (2002). The Snail repressor positions Notch signaling in the Drosophila embryo. Development *129*, 1785–1793.

Crossley, P.H., Minowada, G., MacArthur, C.A., and Martin, G.R. (1996). Roles for FGF8 in the induction, initiation, and maintenance of chick limb development. Cell *84*, 127–136.

Dallas, M.H., Varnum-Finney, B., Delaney, C., Kato, K., and Bernstein, I.D. (2005). Density of the Notch ligand Delta1 determines generation of B and T cell precursors from hematopoietic stem cells. J. Exp. Med. *201*, 1361–1366.

Davis, D.M., and Dustin, M.L. (2004). What is the importance of the immunological synapse? Trends Immunol. *25*, 323–327.

Dessaud, E., McMahon, A.P., and Briscoe, J. (2008). Pattern formation in the vertebrate neural tube: A sonic hedgehog morphogen-regulated transcriptional network. Development *135*, 2489–2503.

Dictenberg, J. (2012). Genetic encoding of fluorescent RNA ensures a bright future for visualizing nucleic acid dynamics. Trends Biotechnol. *30*, 621–626.

Dinkel, H., Van Roey, K., Michael, S., Kumar, M., Uyar, B., Altenberg, B., Milchevskaya, V., Schneider, M., Kühn, H., Behrendt, A., et al. (2016). ELM 2016--data update and new functionality of the eukaryotic linear motif resource. Nucleic Acids Res. *44*, D294-300.

Doupé, D.P., and Perrimon, N. (2014). Techniques: Visualizing and manipulating temporal signalling dynamics with fluorescence-based tools. Sci. Signal. *7*.

Duffy, J.B. (2002). GAL4 system in Drosophila: A fly geneticist's Swiss army knife. Genesis *34*, 1–15.

van Eeden, F., and St Johnston, D. (1999). The polarisation of the anterior-posterior and dorsal-ventral axes during Drosophila oogenesis. Curr. Opin. Genet. Dev. *9*, 396–404.

Fabrowski, P., Necakov, A.S., Mumbauer, S., Loeser, E., Reversi, A., Streichan, S., Briggs, J.A.G., and De Renzis, S. (2013). Tubular endocytosis drives remodelling of the apical surface during epithelial morphogenesis in Drosophila. Nat. Commun. *4*.

Foe, V.E., and Alberts, B.M. (1983). Studies of nuclear and cytoplasmic behaviour during the five mitotic cycles that precede gastrulation in Drosophila embryogenesis. J. Cell Sci. *61*, 31–70.

Franklin, J.L., Berechid, B.E., Cutting, F.B., Presente, A., Chambers, C.B., Foltz, D.R., Ferreira, A., and Nye, J.S. Autonomous and non-autonomous regulation of mammalian neurite development by Notch1 and Delta1. Curr. Biol. *9*, 1448–1457.

Fukaya, T., Lim, B., and Levine, M. (2016). Enhancer Control of Transcriptional Bursting. Cell *166*, 358–368.

Garcia, H.G., Tikhonov, M., Lin, A., Gregor, T., and Author, C.B. (2013). Quantitative live imaging of transcription in Drosophila embryos links polymerase activity to macroscopic patterns NIH Public Access Author Manuscript. Curr Biol *23*.

Gaspar, I., and Ephrussi, A. Strength in numbers: quantitative single-molecule RNA detection assays. Wiley Interdiscip. Rev. Dev. Biol. *4*, 135–150.

Gelbart, M.A., He, B., Martin, A.C., Thiberge, S.Y., Wieschaus, E.F., and Kaschube, M. (2012).

Volume conservation principle involved in cell lengthening and nucleus movement during tissue morphogenesis. Proc. Natl. Acad. Sci. U. S. A. *109*, 19298–19303.

Gomez-Lamarca, M.J., Falo-Sanjuan, J., Stojnic, R., Abdul Rehman, S., Muresan, L., Jones, M.L., Pillidge, Z., Cerda-Moya, G., Yuan, Z., Baloul, S., et al. (2018). Activation of the Notch Signaling Pathway In Vivo Elicits Changes in CSL Nuclear Dynamics. Dev. Cell *44*, 611-623.e7.

Gordon, W.R., Zimmerman, B., He, L., Miles, L.J., Huang, J., Tiyanont, K., McArthur, D.G., Aster, J.C., Perrimon, N., Loparo, J.J., et al. (2015). Mechanical Allostery: Evidence for a Force Requirement in the Proteolytic Activation of Notch. Dev. Cell *33*, 729–736.

Guglielmi, G., Barry, J.D., Huber, W., and De Renzis, S. (2015). An Optogenetic Method to Modulate Cell Contractility during Tissue Morphogenesis. Dev. Cell *35*, 646–660.

Guglielmi, G., Falk, H.J., and De Renzis, S. (2016). Optogenetic Control of Protein Function: From Intracellular Processes to Tissue Morphogenesis. Trends Cell Biol. *26*, 864–874.

Guntas, G., Hallett, R.A., Zimmerman, S.P., Williams, T., Yumerefendi, H., Bear, J.E., and Kuhlman, B. (2015). Engineering an improved light-induced dimer (iLID) for controlling the localization and activity of signaling proteins. Proc. Natl. Acad. Sci. U. S. A. *112*, 112–117.

Halstead, J.M., Lionnet, T., Wilbertz, J.H., Wippich, F., Ephrussi, A., Singer, R.H., and Chao, J.A. (2015). An RNA biosensor for imaging the first round of translation from single cells to living animals. Science (80-.). *347*, 1367–1370.

Harrison, M.M., Li, X.Y., Kaplan, T., Botchan, M.R., and Eisen, M.B. (2011). Zelda binding in the early Drosophila melanogaster embryo marks regions subsequently activated at the maternal-to-zygotic transition. PLoS Genet. *7*.

Hartenstein, V., and Campos-Ortega, J.A. (1984). Early neurogenesis in wild-type Drosophila melanogaster. Wilhelm Roux's Arch. Dev. Biol. *193*, 308–325.

Heitzler, P., and Simpson, P. (1991). The choice of cell fate in the epidermis of Drosophila. Cell *64*, 1083–1092.

Henrique, D., and Schweisguth, F. (2019). Mechanisms of notch signaling: A simple logic deployed in time and space. Dev. *146*.

Hinners, I., Moschner, J., Nolte, N., and Hille-Rehfeld, A. (1999). The orientation of membrane proteins determined in situ by immunofluorescence staining. Anal. Biochem. *276*, 1–7.

Hirokawa, N., Tanaka, Y., Okada, Y., and Takeda, S. (2006). Nodal Flow and the Generation of Left-

Right Asymmetry. Cell *125*, 33–45.

Hogan, B.L. (1996). Bone morphogenetic proteins: multifunctional regulators of vertebrate development. Genes Dev. *10*, 1580–1594.

Housden, B.E., Fu, A.Q., Krejci, A., Bernard, F., Fischer, B., Tavaré, S., Russell, S., and Bray, S.J. (2013). Transcriptional Dynamics Elicited by a Short Pulse of Notch Activation Involves Feed-Forward Regulation by E(spl)/Hes Genes. PLoS Genet. *9*, e1003162.

Huang, A., Amourda, C., Zhang, S., Tolwinski, N.S., and Saunders, T.E. (2017). Decoding temporal interpretation of the morphogen bicoid in the early drosophila embryo. Elife *6*.

Huang, J., Zhou, W., Dong, W., Watson, A.M., and Hong, Y. (2009). Directed, efficient, and versatile modifications of the Drosophila genome by genomic engineering. Proc. Natl. Acad. Sci. U. S. A. *106*, 8284–8289.

Ilagan, M.X.G., Lim, S., Fulbright, M., Piwnica-Worms, D., and Kopan, R. (2011). Real-time imaging of notch activation with a luciferase complementation-based reporter. Sci. Signal. *4*, rs7.

Ip, Y.T., Park, R.E., Kosman, D., Yazdanbakhsh, K., and Levine, M. (1992). dorsal-twist interactions establish snail expression in the presumptive mesoderm of the Drosophila embryo. Genes Dev. *6*, 1518–1530.

Itoh, M., Kim, C.-H., Palardy, G., Oda, T., Jiang, Y.-J., Maust, D., Yeo, S.-Y., Lorick, K., Wright, G.J., Ariza-McNaughton, L., et al. (2003). Mind bomb is a ubiquitin ligase that is essential for efficient activation of Notch signaling by Delta. Dev. Cell *4*, 67–82.

Izquierdo, E., Quinkler, T., and De Renzis, S. (2018). Guided morphogenesis through optogenetic activation of Rho signalling during early Drosophila embryogenesis. Nat. Commun. *9*.

Johnson, H.E., Goyal, Y., Pannucci, N.L., Schüpbach, T., Shvartsman, S.Y., and Toettcher, J.E. (2017). The Spatiotemporal Limits of Developmental Erk Signaling. Dev. Cell *40*, 185–192.

Jongbloets, B.C., and Jeroen Pasterkamp, R. (2014). Semaphorin signalling during development. Dev. *141*, 3292–3297.

Kanaji, S., Iwahashi, J., Kida, Y., Sakaguchi, M., and Mihara, K. (2000). Characterization of the signal that directs Tom20 to the mitochondrial outer membrane. J. Cell Biol. *151*, 277–288.

Kasai, Y., Stahl, S., and Crews, S. (1998). Specification of the Drosophila CNS midline cell lineage: direct control of single-minded transcription by dorsal/ventral patterning genes. Gene Expr. *7*, 171–189.

Kaur, P., Saunders, T.E., and Tolwinski, N.S. (2017). Coupling optogenetics and light-sheet microscopy, a method to study Wnt signaling during embryogenesis. Sci. Rep. *7*.

Kawahashi, K., and Hayashi, S. (2010). Dynamic intracellular distribution of Notch during activation and asymmetric cell division revealed by functional fluorescent fusion proteins. Genes to Cells *15*, 749–759.

Kennedy, M.J., Hughes, R.M., Peteya, L.A., Schwartz, J.W., Ehlers, M.D., and Tucker, C.L. (2010). Rapid blue-light-mediated induction of protein interactions in living cells. Nat. Methods *7*, 973–975.

Kiecker, C., and Niehrs, C. (2001). AP neural patterning by a Wnt gradient.

Klein, T., and Arias, A.M. (1998). Interactions among Delta, Serrate and Fringe modulate Notch activity during Drosophila wing development. Development *125*.

Kolar, K., Knobloch, C., Stork, H., Žnidarič, M., and Weber, W. (2018). OptoBase: A Web Platform for Molecular Optogenetics. ACS Synth. Biol. *7*, 1825–1828.

Kopan, R., and Ilagan, M.X.G. (2009). The canonical Notch signaling pathway: unfolding the activation mechanism. Cell *137*, 216–233.

Krueger, D., Tardivo, P., Nguyen, C., and De Renzis, S. (2018). Downregulation of basal myosin- II is required for cell shape changes and tissue invagination . EMBO J. *37*.

Krueger, D., Quinkler, T., Mortensen, S.A., Sachse, C., and De Renzis, S. (2019). Cross-linker–mediated regulation of actin network organization controls tissue morphogenesis. J. Cell Biol. *218*, 2743–2761.

Kueh, H.Y., Yui, M.A., Ng, K.K.H., Pease, S.S., Zhang, J.A., Damle, S.S., Freedman, G., Siu, S., Bernstein, I.D., Elowitz, M.B., et al. (2016). Asynchronous combinatorial action of four regulatory factors activates Bcl11b for T cell commitment. Nat. Immunol. *17*, 956–965.

Langridge, P.D., and Struhl, G. (2017). Epsin-Dependent Ligand Endocytosis Activates Notch by Force. Cell *171*, 1383-1396.e12.

Le, B.R. (2006). Regulation of Notch signalling by endocytosis and endosomal sorting. Curr. Opin. Cell Biol. *18*, 213–222.

LeBon, L., Lee, T. V, Sprinzak, D., Jafar-Nejad, H., and Elowitz, M.B. (2014). Fringe proteins modulate Notch-ligand cis and trans interactions to specify signaling states. Elife *3*, e02950.

Lecourtois, M., and Schweisguth, F. (1995). The neurogenic suppressor of hairless DNA-binding protein mediates the transcriptional activation of the enhancer of split complex genes triggered by

Notch signaling. Genes Dev. *9*, 2598–2608.

Lemmon, M.A., and Schlessinger, J. (2010). Cell signaling by receptor tyrosine kinases. Cell *141*, 1117–1134.

Leptin, M. (1991). twist and snail as positive and negative regulators during Drosophila mesoderm development. Genes Dev. *5*, 1568–1576.

López-Schier, H., and St. Johnston, D. (2001). Delta signaling from the germ line controls the proliferation and differentiation of the somatic follicle cells during Drosophila oogenesis. Genes Dev. *15*, 1393–1405.

Luca, V.C., Kim, B.C., Ge, C., Kakuda, S., Wu, D., Roein-Peikar, M., Haltiwanger, R.S., Zhu, C., Ha, T., and Garcia, K.C. (2017). Notch-Jagged complex structure implicates a catch bond in tuning ligand sensitivity. Science *355*, 1320–1324.

Masamizu, Y., Ohtsuka, T., Takashima, Y., Nagahara, H., Takenaka, Y., Yoshikawa, K., Okamura, H., and Kageyama, R. (2006). Real-time imaging of the somite segmentation clock: revelation of unstable oscillators in the individual presomitic mesoderm cells. Proc. Natl. Acad. Sci. U. S. A. *103*, 1313–1318.

Mazumdar, A., and Mazumdar, M. (2002). How one becomes many: Blastoderm cellularization in Drosophila melanogaster. BioEssays *24*, 1012–1022.

Mc Mahon, S.S., Sim, A., Filippi, S., Johnson, R., Liepe, J., Smith, D., and Stumpf, M.P.H. (2014). Information theory and signal transduction systems: From molecular information processing to network inference. Semin. Cell Dev. Biol. *35*, 98–108.

Melen, G.J., Levy, S., Barkai, N., and Shilo, B.-Z. (2005). Threshold responses to morphogen gradients by zero-order ultrasensitivity. Mol. Syst. Biol. *1*, 2005.0028.

Micchelli, C.A., Rulifson, E.J., and Blair, S.S. (1997). The function and regulation of cut expression on the wing margin of Drosophila: Notch, Wingless and a dominant negative role for Delta and Serrate. Development *124*, 1485–1495.

Miller, A.C., Lyons, E.L., and Herman, T.G. (2009). cis-Inhibition of Notch by endogenous Delta biases the outcome of lateral inhibition. Curr. Biol. *19*, 1378–1383.

Morel, V., and Schweisguth, F. (2000). Repression by suppressor of hairless and activation by Notch are required to define a single row of single-minded expressing cells in the Drosophila embryo. Genes Dev. *14*, 377–388.

Morel, V., Le Borgne, R., and Schweisguth, F. (2003). Snail is required for Delta endocytosis and Notch-dependent activation of single-minded expression. Dev. Genes Evol. *213*, 65–72.

Morisato, D., and Anderson, K. V (1995). OF THE DROSOPHILA EMBRYO.

Mummery-Widmer, J.L., Yamazaki, M., Stoeger, T., Novatchkova, M., Bhalerao, S., Chen, D., Dietzl, G., Dickson, B.J., and Knoblich, J.A. (2009). Genome-wide analysis of Notch signalling in Drosophila by transgenic RNAi. Nature *458*, 987–992.

Nandagopal, N., Santat, L.A., Lebon, L., Sprinzak, D., Bronner, M.E., and Elowitz, M.B. (2018). Dynamic Ligand Discrimination in the Notch Signaling Pathway. Cell *172*, 1–12.

Niopek, D., Benzinger, D., Roensch, J., Draebing, T., Wehler, P., Eils, R., and Di Ventura, B. (2014a). Engineering light-inducible nuclear localization signals for precise spatiotemporal control of protein dynamics in living cells. Nat. Commun. *5*.

Niopek, D., Benzinger, D., Roensch, J., Draebing, T., Wehler, P., Eils, R., and Di Ventura, B. (2014b). Engineering light-inducible nuclear localization signals for precise spatiotemporal control of protein dynamics in living cells. Nat. Commun. *5*, 4404.

Nüsslein-volhard, C., and Wieschaus, E. (1980). Mutations affecting segment number and polarity in drosophila. Nature *287*, 795–801.

Ohlstein, B., and Spradling, A. (2007). Multipotent Drosophila intestinal stem cells specify daughter cell fates by differential notch signaling. Science *315*, 988–992.

Ong, C.-T., Cheng, H.-T., Chang, L.-W., Ohtsuka, T., Kageyama, R., Stormo, G.D., and Kopan, R. (2006). Target selectivity of vertebrate notch proteins. Collaboration between discrete domains and CSL-binding site architecture determines activation probability. J. Biol. Chem. *281*, 5106–5119.

Perrimon, N., Pitsouli, C., and Shilo, B.-Z. (2012). Signaling mechanisms controlling cell fate and embryonic patterning. Cold Spring Harb. Perspect. Biol. *4*, a005975.

Pillidge, Z., and Bray, S.J. (2019). SWI/SNF chromatin remodeling controls Notch-responsive enhancer accessibility. EMBO Rep. *20*.

Poulson, D.F. (1937). Chromosomal Deficiencies and the Embryonic Development of Drosophila Melanogaster. Proc. Natl. Acad. Sci. *23*, 133–137.

Poulson, D.F. (1940). The effects of certain X-chromosome deficiencies on the embryonic development of Drosophila melanogaster. J. Exp. Zool. *83*, 271–325.

Pudasaini, A., El-Arab, K.K., and Zoltowski, B.D. (2015). LOV-based optogenetic devices: light-driven

modules to impart photoregulated control of cellular signaling. Front. Mol. Biosci. *2*, 18.

Purvis, J.E., and Lahav, G. (2013). Encoding and decoding cellular information through signaling dynamics. Cell *152*, 945–956.

Reeves, G.T., and Stathopoulos, A. (2009). Graded dorsal and differential gene regulation in the Drosophila embryo. Cold Spring Harb. Perspect. Biol. *1*, a000836.

De Renzis, S., Yu, J., Zinzen, R., and Wieschaus, E. (2006). Dorsal-Ventral Pattern of Delta Trafficking Is Established by a Snail-Tom-Neuralized Pathway. Dev. Cell *10*, 257–264.

De Renzis, S., Elemento, O., Tavazoie, S., and Wieschaus, E.F. (2007). Unmasking activation of the zygotic genome using chromosomal deletions in the Drosophila embryo. PLoS Biol. *5*, 1036–1051.

Riddle, R.D., Johnson, R.L., Laufer, E., and Tabin, C. (1993). Sonic hedgehog mediates the polarizing activity of the ZPA. Cell *75*, 1401–1416.

Sagner, A., and Briscoe, J. (2017). Morphogen interpretation: concentration, time, competence, and signaling dynamics. Wiley Interdiscip. Rev. Dev. Biol. *6*.

Sako, K., Pradhan, S.J., Barone, V., Inglés-Prieto, Á., Müller, P., Ruprecht, V., Čapek, D., Galande, S., Janovjak, H., and Heisenberg, C.P. (2016). Optogenetic Control of Nodal Signaling Reveals a Temporal Pattern of Nodal Signaling Regulating Cell Fate Specification during Gastrulation. Cell Rep. *16*, 866–877.

Schweisguth, F. (2015). Asymmetric cell division in the *Drosophila* bristle lineage: from the polarization of sensory organ precursor cells to Notch-mediated binary fate decision. Wiley Interdiscip. Rev. Dev. Biol. *4*, 299–309.

Shimizu, K., and Gurdon, J.B. (1999). A quantitative analysis of signal transduction from activin receptor to nucleus and its relevance to morphogen gradient interpretation. Proc. Natl. Acad. Sci. U. S. A. *96*, 6791–6796.

Simões, S., Oh, Y., Wang, M.F.Z., Fernandez-Gonzalez, R., and Tepass, U. (2017). Myosin II promotes the anisotropic loss of the apical domain during *Drosophila* neuroblast ingression. J. Cell Biol. *216*, 1387–1404.

Sonnen, K.F., and Aulehla, A. (2014). Dynamic signal encoding—From cells to organisms. Semin. Cell Dev. Biol. *34*, 91–98.

Sonnen, K.F., Lauschke, V.M., Uraji, J., Falk, H.J., Petersen, Y., Funk, M.C., Beaupeux, M., François, P., Merten, C.A., and Aulehla, A. (2018). Modulation of Phase Shift between Wnt and Notch Signaling

Oscillations Controls Mesoderm Segmentation. Cell *172*, 1079-1090.e12.

Sorre, B., Warmflash, A., Brivanlou, A.H., and Siggia, E.D. (2014). Encoding of temporal signals by the TGF-β pathway and implications for embryonic patterning. Dev. Cell *30*, 334–342.

Sprinzak, D., Lakhanpal, A., LeBon, L., Santat, L.A., Fontes, M.E., Anderson, G.A., Garcia-Ojalvo, J., and Elowitz, M.B. (2010). Cis-interactions between Notch and Delta generate mutually exclusive signalling states. Nature *465*, 86–90.

Strickland, D., Lin, Y., Wagner, E., Hope, C.M., Zayner, J., Antoniou, C., Sosnick, T.R., Weiss, E.L., and Glotzer, M. (2012). Light controlling protein aggregation. Nat Methods *9*, 379–384.

Strigini, M., and Cohen, S.M. (1997). A Hedgehog activity gradient contributes to AP axial patterning of the Drosophila wing. Development *124*.

Sutherland, D., Samakovlis, C., and Krasnow, M. a (1996). branchless Encodes a Drosophila FGF Homolog That Controls Tracheal Cell Migration and the Pattern of Branching 10.1016/S0092-8674(00)81803-6 : Cell | ScienceDirect.com.

Sweeton, D., Parks, S., Costa, M., and Wieschaus, E. (1991). Gastrulation in Drosophila: the formation of the ventral furrow and posterior midgut invaginations. Development *112*.

Taslimi, A., Vrana, J.D., Chen, D., Borinskaya, S., Mayer, B.J., Kennedy, M.J., and Tucker, C.L. (2014). An optimized optogenetic clustering tool for probing protein interaction and function. Nat. Commun. *5*, 4925.

Toettcher, J.E., Weiner, O.D., and Lim, W.A. (2013). Using Optogenetics to Interrogate the Dynamic Control of Signal Transmission by the Ras/Erk Module. Cell *155*, 1422–1434.

Trylinski, M., Mazouni, K., and Schweisguth, F. (2017). Intra-lineage Fate Decisions Involve Activation of Notch Receptors Basal to the Midbody in Drosophila Sensory Organ Precursor Cells. Curr. Biol. *27*, 2239-2247.e3.

Wang, H., Vilela, M., Winkler, A., Tarnawski, M., Schlichting, I., Yumerefendi, H., Kuhlman, B., Liu, R., Danuser, G., and Hahn, K.M. (2016). LOVTRAP: an optogenetic system for photoinduced protein dissociation. Nat. Methods *13*, 755–758.

Warmflash, A., Zhang, Q., Sorre, B., Vonica, A., Siggia, E.D., and Brivanlou, A.H. (2012). Dynamics of TGF- signaling reveal adaptive and pulsatile behaviors reflected in the nuclear localization of transcription factor Smad4. Proc. Natl. Acad. Sci. *109*, E1947–E1956.

Wartlick, O., Mumcu, P., Kicheva, A., Bittig, T., Seum, C., Jülicher, F., and González-Gaitán, M.

(2011). Dynamics of Dpp signaling and proliferation control. Science (80-.). *331*, 1154–1159.

Weil, T.T., Parton, R.M., and Davis, I. (2010). Making the message clear: visualizing mRNA localization. Trends Cell Biol. *20*, 380–390.

Wu, Y.I., Frey, D., Lungu, O.I., Jaehrig, A., Schlichting, I., Kuhlman, B., and Hahn, K.M. (2009). A genetically encoded photoactivatable Rac controls the motility of living cells. Nature *461*, 104–108.

Yumerefendi, H., Dickinson, D.J., Wang, H., Zimmerman, S.P., Bear, J.E., Goldstein, B., Hahn, K., and Kuhlman, B. (2015a). Control of Protein Activity and Cell Fate Specification via Light-Mediated Nuclear Translocation. PLoS One *10*, e0128443.

Yumerefendi, H., Dickinson, D.J., Wang, H., Zimmerman, S.P., Bear, J.E., Goldstein, B., Hahn, K., and Kuhlman, B. (2015b). Control of protein activity and cell fate specification via light-mediated nuclear translocation. PLoS One *10*.

Zhang, Y., Alexander, P.B., and Wang, X.F. (2017). TGF-β family signaling in the control of cell proliferation and survival. Cold Spring Harb. Perspect. Biol. *9*.

Books

Gilbert, S.F., *Developmental Biology.* 10th edition. Sinauer associates; 2014

Lim, W., Mayer, B., Pawson, T., *Cell Signaling – principles and mechanisms.* Garland Science; 2015.

Hancock, J., *Cell Signalling.* 3rd edition. Oxford university press; 2010

7. Appendix

A part of the results presented in this thesis is adapted from the submitted manuscript: Viswanathan, R., Necakov, A., Trylinski, M., Harish, R.K., Krueger, D., Esposito, E., Schweisguth, F., Neveu, P., and De Renzis, S. Optogenetic inhibition of Delta reveals digital Notch signalling output during tissue differentiation.

bioRxiv: http://dx.doi.org/10.1101/738039.

Permissions for figures

Fig. no.	Title	License ID	Publisher
1	Encoding and decoding of signaling dynamics	4660870487389	Elsevier
2	Examples of signalling dynamics during development	4660860438337	Science
3	Notch signalling mechanism and modes of activation	4663541374866 4660860156571	Company of Biologists Springer Nature
4	Notch-Delta interactions – trans	4660841412491	Springer Nature

	activation and cis inhibition		
6	Notch activation in the mesoderm and restriction of sim to single-cell wide mesectoderm	4660831281154 4660831085513	Elsevier Elsevier
8	Real time quantitative transcriptional reporter	4660830541253	Elsevier

Acknowledgement

In pursuit of my PhD, the last four years at EMBL were filled with experiences that have positively influenced me, both personally and scientifically. There are a number of people who have motivated me through this journey and who have contributed to the work presented in this thesis.

First, I would like to thank my supervisor, Stefano De Renzis for his mentoring, constant support, for pushing me out of my comfort zone, and for honing my critical thinking and flow of ideas. His inputs and guidance while troubleshooting experiments and have been extremely valuable.

I thank Sasha (Aleksander Necakov) with whom I collaborated in the early stages of the project - for introducing me to the world of Notch and optogenetics, for his patient training and encouragement, and for help with several experiments presented in this thesis.

I acknowledge the suggestions and guidance of my Thesis advisory committee (TAC) members – Alexander Aulehla, Ingrid Lohmann and Pierre Neveu. I also thank Lazaro Centanin for agreeing to be part of my defence committee.

I especially thank Pierre for all his help with the quantification of the *sim* transcription live imaging data and for useful discussions leading to the interpretation of the data.

I thank Francois Schweisguth for his idea of the clonal analysis experiment, for hosting me in his lab, and also Mateusz Trilinski, for his time and effort, that ensured the success of the experiment in a short duration of 10 days.

I am grateful to my fellow lab members (both current and past) for timely assistance and advice during various stages of my project, and for creating an ever-cheerful environment in the lab.

I thank Daniel for his help with image analysis and quantification, and especially for aesthetically improving several figures presented in this thesis. I also thank Emiliano for advice on image analysis, Cristina for taking charge of experiments during the thesis writing period, and both Cristina and Theresa for invaluable assistance with cloning and crosses. Thanks to Rohit for introducing me to fly work and helping with the characterization of opto-Delta, to Pietro for useful discussions and being great company, and to Justin and Thijs for not making me feel the youngest in the lab anymore :). I cherish all the fun times that we had as a lab – ranging from crazy lab day activities, lab dinners to a memorable lab retreat.

I acknowledge the support of the Advanced Light Microscopy Facility (ALMF) at EMBL for prompt and efficient assistance, and the Developmental Biology unit for being extremely collaborative and supportive.

Finally, but importantly, I would like to thank my family back in Chennai, India (my parents, Viswanathan and Jayanthi and brother, Rohit) for their love and constant support through these years, and giving me the freedom to pursue what I love. I also want to express my gratitude to all my teachers from school and university who ignited my interest in science that has led me to this point.